

**The functional significance of alternative
photorespiratory pathways in
*Arabidopsis thaliana***

**Von der naturwissenschaftlichen Fakultät
der Gottfried Wilhelm Leibniz Universität Hannover
zur Erlangung des Grades
Doktorin der Naturwissenschaften
Dr. rer. nat.**

**Genehmigte Dissertation
Von
Diplom-Biologin Katrin Krause
Geboren am 24.02.1984 in Rostock**

Referent: Prof. Dr. Christoph Peterhänsel
Korreferent: Prof. Dr. Bernhard Huchzermeyer
Vorsitz: Prof. Dr. Hans Peter Braun
Tag der Promotion: 23.09.2013

Abstract

Photorespiration is a complex pathway that detoxifies P-glycolate produced by the oxygenase reaction of RubisCO. This process was known as a wasteful pathway, because it requires energy and reducing equivalents and releases CO₂ and NH₃, which has to be re-fixed. In the last years, the negative view on the function of photorespiration was questioned. Evidence was provided that photorespiration has important functions such as providing an energy sink, protecting plants against photoinhibition and preventing the overreduction of the electron transport chain. The major photorespiratory pathway is distributed over three different compartments: chloroplast, peroxisome and mitochondria. There is evidence that side pathways exist that are directly connected with the major pathway (mitochondria side pathway) or involved in CO₂ release near to RubisCO (chloroplastid side pathway).

In this study, the impact of the side pathways on the major pathway was investigated. In order to boost the chloroplastid side pathway, two different glycolate dehydrogenases (GlcDH) from *Escherichia coli* (*EcGlcDH*) or from *Chlamydomonas reinhardtii* (*CrGlcDH*), respectively, were overexpressed and targeted to the chloroplast. Each GlcDH converts glycolate to glyoxylate that is further oxidized to CO₂ in the vicinity of RubisCO. The impact of the GlcDH transgene was investigated in a photorespiratory mutant background (catalase 2 knock-out mutant, Δ Cat2) as well as in the wild type background (WT) of *Arabidopsis thaliana* Col-0. In the Δ Cat2 background, transgenic lines showed reduced H₂O₂ production under photorespiratory conditions. This resulted in a lower negative impact of H₂O₂ on protein content, chlorophyll content and a reduced response to oxidative stress. The double mutant Δ Cat2/35S-*CrGlcDH* was characterized by higher quantum efficiency (F_v/F_m) and higher photosynthetic capacity ($Y(II)$) at low CO₂ concentrations compared to the single Δ Cat2 mutant. Accordingly, H₂O₂-inducible genes like *GstF8* and *Gpx6* were less expressed in Δ Cat2/35S-*CrGlcDH* than the corresponding Δ Cat2. However, no differences in metabolic intermediates related to photorespiration were found. Furthermore, no significant differences were found between *CrGlcDH* overexpressors and azygous siblings.

The importance of the mitochondrial side pathway was investigated by crossing Cat2 with a knock-out mutant in this pathway (Δ AtGlcDH). Single mutants were viable under ambient CO₂ concentrations. Δ Cat2 mutants showed a visible phenotype: reduced growth and yellowish to light green leaves compared to WT, whereas Δ AtGlcDH mutants did not show any visible differences compared to WT. The double knock-out mutant was not viable at ambient CO₂ concentrations, but could be rescued by high CO₂ concentrations, indicating that the mitochondrial side pathway contributes to photorespiration.

The results from this study indicate, that the chloroplastid and the mitochondrial side pathways play a minor role in WT plants under normal growth conditions, but are important under conditions of high photorespiratory flux and in mutants of the major pathway.

Zusammenfassung

Durch die Oxygenase Funktion der Ribulose-1,5-bisphosphat-carboxylase/-oxygenase (RubisCO) wird Phospho-glycolat gebildet. Dieses ist toxisch und wird durch die Photorespiration in P-Glycerat umgewandelt, welches in den Calvin-Zyklus eingespeist werden kann. Die Photorespiration galt lange Zeit als ein energieverbrauchender und verschwenderischer Prozess. Von dieser negativen Auffassung wird mittlerweile Abstand genommen, da der Photorespiration nun auch eine Funktion in der Photoinhibition und Photoprotektion zugesprochen wird und diese somit zum Schutz der Pflanzen vor hohem Lichteinfall und Temperaturen dient. Der photorespiratorische Hauptzyklus ist über drei verschiedene Kompartimente verteilt: Chloroplast, Mitochondrium und Peroxisom, wobei die Beteiligung von möglichen Seitenwegen in den einzelnen Kompartimenten weitestgehend unbekannt ist. In den letzten Jahren wurden verschiedene Hinweise gefunden, die auf einen möglichen chloroplastidären Seitenweg hindeuten. Ein weiterer anderer Seitenweg wurde in den Mitochondrien identifiziert: Glycolat wird in zwei Reaktionen zu Glycin umgewandelt, welches in den Hauptstoffwechselweg zurück gespeist werden kann. Ziel dieser Arbeit war es, den Einfluss des chloroplastidären und des mitochondrialen Seitenweges auf den Hauptweg der Photorespiration zu untersuchen. Da der chloroplastidäre Seitenweg nicht vollständig identifiziert ist, wurden zwei transgene Glykolat-Dehydrogenasen (GlcDH) in Chloroplasten unabhängig voneinander überexprimiert. Die transgene GlcDH wandelt Glycolat zu Glyoxylat um, welches weiter zu CO_2 verstoffwechselt wird. Das entstandene CO_2 wird in der näheren Umgebung von RubisCO freigesetzt und führt zu einer Steigerung der Photosynthese und zu einer Reduzierung der Photorespiration. Um den Einfluss der GlcDH auf den Hauptweg besser untersuchen zu können, wurden diese mit einer knock-out Mutante des Hauptweges ($\Delta\text{Cat}2$) wie auch mit dem Wild-Typen (WT) kombiniert. Die überexprimierte GlcDH aus *Chlamydomonas reinhardtii* (CrGlcDH) zeichnete sich durch einen positiven Einfluss in der $\Delta\text{Cat}2$ Mutante aus. CrGlcDH reduzierte den Fluss durch den Hauptstoffwechselweg der Photorespiration in der $\Delta\text{Cat}2$ Mutante, was durch eine erhöhte Quantum Effizienz der Photosynthese, eine erhöhte photosynthetische Kapazität und einer reduzierten Geneexpression H_2O_2 induzierter Gene wie *GstF8* und *Gpx6* sowohl bei ambienten als auch bei reduzierten atmosphärischen CO_2 Konzentrationen gekennzeichnet wurde. Ein positiver Einfluss der CrGlcDH im WT-Hintergrund konnte jedoch nicht detektiert werden. Neben dem chloroplastidären Seitenweg wurde auch der mitochondriale Seitenweg untersucht. Dazu wurde die $\Delta\text{Cat}2$ -Mutation mit einer Mutante des mitochondrialen Seitenweges ($\Delta\text{AtGlcDH}$) verwendet. Während die $\Delta\text{Cat}2$ Einzel-Mutante durch gelbliche Blätter und kleineren Durchmesser (Rosettendiameter) unter ambienten Anzuchtbedingungen auffiel, zeigte die $\Delta\text{AtGlcDH}$ Einzel-Mutante keinen Unterschied im Phänotypen im Vergleich zum WT. Die Doppel-knock-out Mutante hingegen war unter

ambienten CO₂ Konzentrationen nicht lebensfähig, konnte jedoch durch Umsetzen in erhöhte CO₂ Konzentrationen gerettet werden. Dieses Ergebnis führte zur der Vermutung, dass der mitochondriale Seitenweg für das Überleben der Δ Cat2 Mutante unter ambienten Bedingungen notwendig ist.

Zusammenfassend zeigen die Analysen dieser Arbeit, dass beide Seitenwege eine untergeordnete Rolle im WT unter ambienten Anzuchtbedingungen spielen, aber eine wichtige Rolle unter niedrigen CO₂ Konzentrationen und im Mutanten-Hintergrund, da sie den Fluss durch den Hauptweg reduzieren und somit die Produktion von toxischen Intermediaten verringern.

Schlagwörter: Photorespiration; Katalase 2 (Cat2); Glykolat-Dehydrogenase (GlcDH);
Photorespiratorischer Stress

Keywords: photorespiration; catalase 2 (Cat2); glycolate dehydrogenase (GlcDH);
photorespiratory stress

Table of contents

Abstract.....	3
Zusammenfassung.....	4
1 Introduction.....	9
1.1 Photosynthesis.....	9
1.2 Function of ribulose-1,5-bisphosphate carboxylase/oxygenase.....	10
1.3 Photorespiration.....	11
1.4 Photorespiratory mutants in the major pathway.....	14
1.4.1 Catalase 2 knock-out mutant.....	15
1.4.2 Glutamate:glyoxylate aminotransferase mutant.....	16
1.5 Alternative photorespiratory pathways.....	17
1.5.1 Knock-out mutant of the alternative mitochondrial pathway.....	20
1.6 Glycolate metabolism in <i>Escherichia coli</i>	20
1.7 Glycolate metabolism in cyanobacteria.....	21
1.8 Glycolate metabolism in green algae.....	22
1.9 Gene technology towards reduction of photorespiration.....	23
1.10 Aim of this study.....	25
2 Materials and Methods.....	27
2.1 Materials.....	27
2.1.1 Chemicals and consumables.....	27
2.1.2 Instruments.....	27
2.1.3 Software and internet-programs.....	29
2.1.4 Markers.....	30
2.1.5 Reaction kits.....	30
2.1.6 Enzymes.....	31
2.1.7 Specific chemicals.....	32
2.1.8 Material and chemicals for GC-MS analysis.....	32
2.1.9 Oligonucleotides.....	33

Table of content

2.1.10	Plasmids.....	37
2.1.11	<i>Escherichia coli</i> strains.....	38
2.1.12	<i>Agrobacterium tumefaciens</i> strains.....	39
2.1.13	Plant material and growth conditions.....	40
2.2.	Methods.....	41
2.2	Molecular Methods.....	41
2.2.2	Microbiological Methods.....	47
2.2.3	Biochemical methods.....	50
2.2.4	Physiological Methods.....	53
3	Results.....	56
3.1.	Characterization of photorespiratory mutants.....	56
3.2	The importance of the chloroplastidal side-pathway.....	64
3.2.1	Crossing of main photorespiratory mutants with overexpressors of a chloroplastidal glycolate dehydrogenase.....	65
3.3	The importance of the mitochondrial side-pathway.....	82
3.2.1	Crossing of two photorespiratory knock-out mutants.....	82
3.2.2	Overexpression of the mitochondrial side pathway.....	87
4.	Discussion.....	90
4.1	Using <i>catalase 2</i> mutants for the investigation.....	90
4.2	Chlorophyll fluorescence.....	92
4.3	Gene expression of H ₂ O ₂ -inducible genes.....	95
4.4	Metabolites.....	99
4.5	Importance of the mitochondrial side-pathway.....	103
5	Conclusion.....	105
6	Appendix.....	106
6.1	Supplemental Figures.....	106
6.2	List of figures.....	112
6.3	List of tables.....	115
6.4	List of abbreviations.....	117

Table of content

6.5 References	121
6.6 Lebenslauf	138
6.7 Publikationen	139
6.9 Eidstattliche Erklärung	140
Danksagung	141

1 Introduction

1.1 Photosynthesis

The evolution of oxygenic photosynthesis was a key developmental step in natural history. The pathway does not only provide carbon for the growth of algae and plants, but also molecular oxygen as a by-product that is used by all aerobic organisms, including animals and humans, as a terminal electron acceptor in respiration.

Photosynthesis is the conversion of light energy into chemical energy and can be divided into primary and secondary reactions. The primary reaction (light reaction) occurs in the thylakoid membrane of chloroplasts and converts light energy into chemical energy (ATP) and reducing equivalents (NADPH) (Hipkins & Baker, 1986). Different pigments, with the chlorophylls being the most important of them, can absorb different wave length of sun light and pass the energy into the photosynthetic apparatus (Duysens et al., 1961). These pigments are arranged in protein complexes and form a network for the photosynthetic electron chain transport inside the thylakoid membrane (Hipkins & Baker, 1986). The electron transport chain starts with capturing light energy by chlorophylls, which transfer the energy to the reaction centers. Two types of reactions centers are known: the photosystem I (PS I) and photosystem II (PS II). The oxidation of water (H_2O) and consequently the starting point of electron transfer take place at PS II. The electrons from water are transported via the electron transport chain to PS I, there $NADP^+$ is reduced. During this process a proton gradient is built, which is important to produce ATP. No CO_2 assimilation takes place during the light reaction, but high rates of light-dependent oxygen evolution were observed (Hipkins & Baker, 1986), because H_2O is split into O_2 , protons and electrons. The second reaction (dark reaction) consumes ATP and NADPH for carbon dioxide assimilation to produce sugars (Lawlor, 2001). The resulting ADP and $NADP^+$ are used in the next light reaction as proton and electron acceptors. The cycle between light and dark reaction is closed.

The majority of photosynthetic organism assimilates CO_2 via C_3 photosynthesis and these organisms are so called C_3 organisms (Ku et al., 1996; Raines, 2006; Raines, 2011). The C_3 cycle utilizes ATP and NADPH, the products of the photosynthetic light reaction, to fix CO_2 into the carbon skeleton of sugars, as previously described. The use of CO_2 and the formation of the carbon skeleton are called the light independent reaction or Calvin-Benson Cycle. The Calvin-Benson Cycle is initiated by the carboxylation of the CO_2 acceptor molecule ribulose-1,5-bisphosphate (RuBP) via ribulose-1,5-bisphosphate carboxylase /oxygenase (RubisCO). The resulting C_6 molecule is instable and immediately breaks down

to two C_3 molecules. The product glycerate-3-phosphate (3PGA) is used to form glyceraldehyde phosphate (G3P) and dihydroxyacetone phosphate via two reactions, that consume the chemical energy and the reducing power produced in the primary reactions (light reactions). Most of the formed G3P is used to regenerate the CO_2 acceptor molecule RuBP, which permits the cycle to continue. The recycling includes a series of reactions. Ten molecules of G3P are necessary to synthesize six molecules of ribulose phosphate (RuP). Each RuP molecule becomes phosphorylated by a hydrolysis of ATP to form the starting compound RuBP. The remaining G3P molecules are used to produce glucose and other sugars. The produced sugars can then be used for metabolic reactions such as the production of amino acids and lipids.

1.2 Function of ribulose-1,5-bisphosphate carboxylase/oxygenase

RubisCO is an abundant enzyme in all photoautotrophic organisms (Ellis, 1979; Raven, 2013). Up to 50% of the protein in a leaf is RubisCO (Tolbert, 1981). This enzyme is a protein complex consisting of eight large subunits and eight small subunits (Andersson, 2007), which is activated in the light. A lysine residue of the active site is carbamylated, followed by binding of Mg^{2+} and the activation of RubisCO (Salvucci and Ogren, 1996). The carbamylation of the lysine residue is limited by two factors. The first factor is the speed of the carbamylation reaction itself and the second factor is that RubisCO can be inhibited by already bound sugars at the active site of the enzyme. The light-activated RubisCO activase counteracts with the latter limitation step (Portis et al., 1986; Wang and Portis, 1992).

In C_3 plants, the initial CO_2 fixation reaction involves the enzyme RubisCO. This enzyme can reduce both carbon dioxide (CO_2) and oxygen (O_2), which leads to photosynthesis or to photorespiration (Figure 1).

The relative rate of the reaction of RubisCO with CO_2 or O_2 depends on different factors. For example, oxygenase activity of RubisCO increases with temperature, because the solubility of CO_2 declines faster than the solubility of oxygen with increasing temperatures resulting in a relative reduction in the CO_2 availability in the vicinity of RubisCO (Jordan and Ogren, 1984; Brooks and Farquhar, 1985). This leads to a higher photorespiration, which can result in a loss of between 30-50% of fixed carbon (Raines, 2006). Drought stress has a similar effect on the carboxylase activity of RubisCO, because plants close stomata, resulting in a reduction of CO_2 supply to the active site of RubisCO (Raines, 2011). Due to the closure of the stomata a second aspect influences the CO_2 and O_2 ratio near to RubisCO. Atmospheric CO_2 cannot enter the leaf and O_2 produced by photosynthesis accumulates in the vicinity of RubisCO (Brooks and Farquhar, 1985).

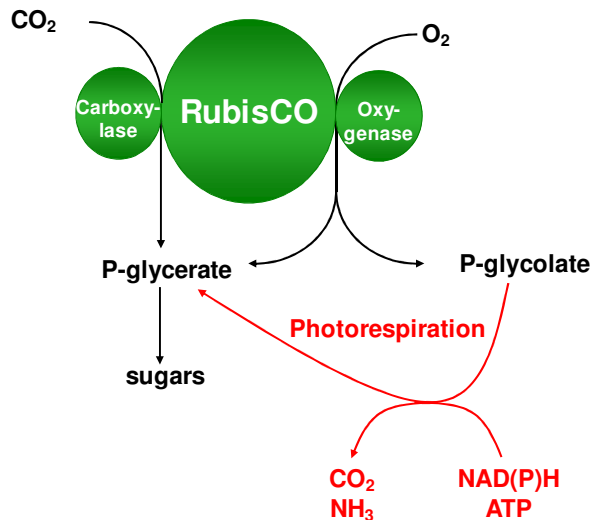


Figure 1: Carboxylase- and oxygenase- reaction of RubisCO in green leaves of higher plants, which also contains photorespiration (Peterhänsel et al., 2010).

The affinity of RubisCO for CO_2 depends also on temperature; increasing temperatures reduce the affinity for CO_2 (Laing et al., 1974). Under ambient air conditions and normal temperatures (25°C) the carboxylation and oxygenation reaction ratio of RubisCO is four to one. This means RubisCO binds four CO_2 molecules for each O_2 molecule.

To conclude, the ratio of carboxylation and oxygenation of RuBP by RubisCO is dependent on CO_2 and O_2 concentrations at the fixation site (Wingler et al., 2000), which are influenced by different stresses. A reduced CO_2 concentration near to RubisCO leads to high rates of oxygenase reaction and with photorespiration as a consequence, which is a wasteful process.

1.3 Photorespiration

The main photorespiratory metabolism is distributed over three different compartments in higher plants (Figure 2). These compartments are the chloroplast, the mitochondrion and the peroxisome (Sharkey, 2001). The initial reaction of photorespiration is the oxygenase reaction of RubisCO forming one molecule 3PG and one molecule phosphoglycolate (2PG) (Wingler et al., 1999) (Figure 2). Phosphoglycerate can directly be used in the Calvin-Benson Cycle to assimilate CO_2 . The toxic phosphoglycolate has to be recycled to phosphoglycerate via photorespiration (Leegood et al., 1995). In the chloroplast phosphoglycolate is dephosphorylated to glycolate by phosphoglycolate phosphatase (PGLP). The product glycolate is transported to the peroxisomes and oxidized to glyoxylate by glycolate oxidase (GO). During this reaction, H_2O_2 is produced and further converted into water and oxygen by catalase (CAT). The transamination of glyoxylate to glycine is catalyzed by glutamate:glyoxylate aminotransferase (GGAT) as well as by serine:glyoxylate

aminotransferase (SGAT) (Prabhu et al., 1996; Wingler et al., 2000). The synthesized glycine is transported into the mitochondria where CO₂ release and NH₃ release take place (Figure 2).

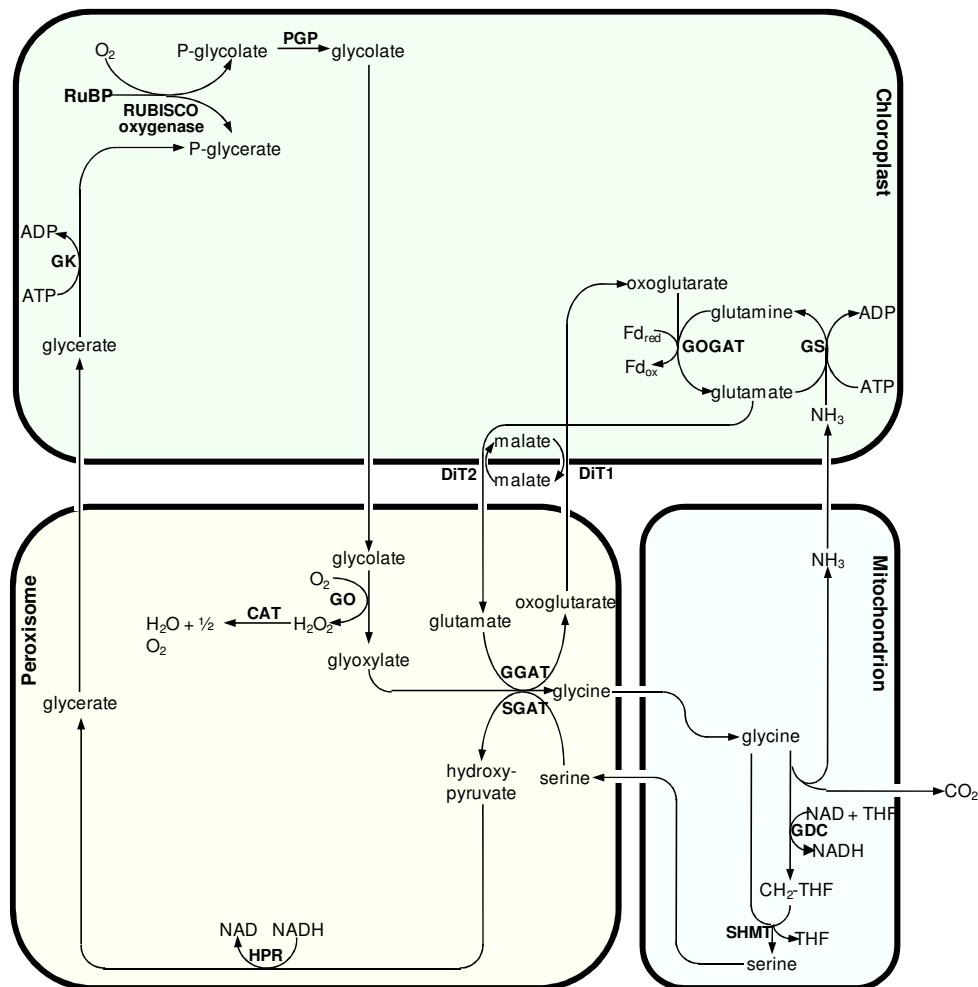


Figure 2: Overview of the major photorespiratory pathway in *Arabidopsis thaliana*. RuBP, ribulose-1,5-bisphosphate; RUBISCO, RuBP carboxylase/oxygenase; PGP, phosphoglycolate phosphatase; GO, glycolate oxidase; CAT, catalase; GGAT, glyoxylate:glutamate aminotransferase; GDC, glycine decarboxylase; SHMT, serine:hydroxymethyltransferase; SGAT, serine:glyoxylate aminotransferase; HPR, hydroxypyruvate reductase; GK, glycerate kinase; GS, glutamine synthetase; FdGOGAT, glutamate:oxoglutarate aminotransferase; THF, tetrahydrofolate; CH₃-THF, methyl-THF; CH₂-THF, methylene-THF; DIT1, dicarboxylate transporter 1; DIT2, dicarboxylate transporter 2. The stoichiometry of the reactions is not included. (Peterhansel et al., 2010, modified).

Two O₂ molecules have to be fixed by RubisCO (Figure 2, chloroplast), because two glycine molecules are needed to form one serine molecule (Figure 2, mitochondria) (Peterhansel et al., 2010). Half of the glycine is decarboxylated by glycine decarboxylase (GDC) forming NADH and methylene-THF (Oliver, 1981) and consuming NAD⁺ and tetrahydrofolate (THF). Methylene-THF reacts with a second glycine molecule to serine catalyzed by serine:hydroxymethyltransferase (SHMT) (Leegood et al., 1995). Serine is transported from the mitochondria back to peroxisomes. There, serine is first transformed into

hydroxypyruvate by SGAT following by a reduction to glycerate via hydroxypyruvate reductase reaction (HPR). The main photorespiratory hydroxypyruvate reductase is HPR1 (Timm et al., 2008) (see 1.5). The formed glycerate is transported to the chloroplast and phosphorylated to phosphoglycerate, which is channeled to the Calvin-Benson Cycle.

During the formation of glycine to serine CO_2 and NH_3 are released and NH_3 has to be refixed (Figure 2). This reaction is a link between carbon metabolism and nitrogen metabolism (Wingler et al., 2000). The re-assimilation of NH_3 during photorespiration is essential for the nitrogen status in plants (Wingler et al., 2000). The released and refixed nitrogen is an order of magnitude higher than nitrogen production during the nitrate reduction process (Keys et al., 1978). The refixation of NH_3 is catalyzed by glutamine synthetase (GS2) and ferredoxin-dependent glutamate:oxoglutarate aminotransferase (Fd-GOGAT) in the chloroplast.

Photorespiration is an energy consuming process that is activated by the oxygenase activity of RubisCO leading to the formation of one molecule 3PGA and one molecule 2PG, as previously described (Tolbert et al., 1968). During photorespiration, plants release carbon dioxide (CO_2) and ammonia (NH_3) that has to be refixed by a process that consumes ATP and reducing equivalents (Wingler et al., 2000). One CO_2 molecule and one NH_3 molecule are released by two oxygenation reactions (Sharkey, 1988). The end product of photorespiration is 3PGA, an intermediate that can be used to form sugars in the Calvin-Benson Cycle.

Beside the negative aspects, like energy consumption and reduction of photosynthetic capacity, photorespiration can prevent plants from damage (Kozaki & Takeba, 1996). An important aspect of damage protection is the photoprotective role of photorespiration (Heber et al., 1996). For example, overexpression of the photorespiratory enzyme glutamine synthetase improved the photorespiratory capacity and led to an increased tolerance to high light. Conversely, knock-out of the same gene led to a reduced photorespiratory capacity (Kozaki & Takeba, 1996). Photorespiration also provides metabolites for substances involved in abiotic or biotic stress responses like glycine for glutathione synthesis (Foyer et al., 1955). Glutathione is important for biotic and abiotic stress response in plants, e.g. because glutathione acts against oxidative damage as a reducing equivalent at high light conditions (Noctor and Foyer, 1998). Photorespiration itself can also act as energy sink preventing the overreduction of the photosynthetic electron transport chain by using the reducing equivalents for phosphoglycerate production at high temperatures as well as at high light (Wingler et al., 2000). Together, photorespiration has negative and positive aspects for plants and both have to be considered when the process is discussed.

The cycle of glycolate metabolism in plants is well characterized, but still open questions remain. In the last few years several alternative photorespiratory pathways were identified and investigated, these side pathways are described later (see 1.5).

1.4 Photorespiratory mutants in the major pathway

Understanding the whole photorespiratory pathway in the model plant *Arabidopsis thaliana* was possible by investigating the photorespiratory mutants. Somerville (2001) developed a screening system to select photorespiratory mutants. Therefore, chemically mutagenized *Arabidopsis* plants were grown at high CO₂ concentrations (1% CO₂). All plants showing chlorotic spots or even dying were excluded (Somerville, 2001). The remaining plants were shifted to normal air conditions (ambient air, 0.03% CO₂). Plants developing chlorotic spots at ambient air conditions were identified as putative photorespiratory mutants. Putative photorespiratory mutants were shifted back to high CO₂ concentrations. Real photorespiratory mutants recovered, because the photorespiratory rate was decreased by high CO₂ concentrations near to the active site of RubisCO (Somerville, 2001).

Due to this experimental set up many photorespiratory mutants were identified. Most of them were nonviable at ambient CO₂ conditions, but survived at high CO₂ concentrations for example knock-out mutants of phosphoglycolate phosphatase (Somerville & Ogren, 1979), knock-out mutants of serine:hydroxymethyltransferase (Somerville and Ogren, 1981) and glycerate kinase mutants (Boldt, 2005). Others showed a chlorotic phenotype or decreased biomass at ambient air conditions like catalase knock-out mutants (Queval et al., 2007), glutamate:glyoxylate aminotransferase mutants (Somerville and Ogren, 1980a; Igarashi et al., 2003) and serine:glyoxylate aminotransferase mutants (Somerville and Ogren, 1980b) in *Arabidopsis thaliana*. For the glutamine synthase a mutant was only found in barley (Keys, 2006) showing typical recovery at high CO₂ concentrations. Some photorespiratory mutants showed not as a single knock-out mutant a phenotype, but as double knock-out mutants. The single HPR1 and HPR2 mutants were viable under ambient air conditions and showed no photorespiratory phenotype. However, the double knock-out mutant was characterized by a reduced growth and chlorotic spots (Timm et al., 2008). The triple mutant HPR1/HPR2/HPR3 showed a clearer phenotype than the double mutant (Timm et al., 2011). Other photorespiratory knock-out mutants were unviable under ambient and high CO₂ concentration, for example the glycine decarboxylase P-protein double knock-out mutation was lethal at high CO₂ concentrations (Engel et al., 2007) suggesting an essential function beside photorespiration.

The two mutants studied in this thesis are explained here in detail, since they are relevant for the approach taken in this thesis.

1.4.1 Catalase 2 knock-out mutant

Catalase is an important enzyme for cellular defense against oxidative stress and is a member of the defense system for scavenging of hydrogen peroxide as well as superoxide radicals (Frugoli et al., 1996). No organism was found, that did not possess a catalase (McClung, 1997). The catalase in *Arabidopsis thaliana* is a member of a multigene family consisting of three different genes forming at least six isoforms (Frugoli et al., 1996). The three genes are *Cat1*, *Cat2* and *Cat3*. These genes share a high similarity of nucleotide sequences of the coding region (70-72%) as well as for amino acids sequences of the whole protein (75-84%) (Frugoli et al., 1996). *Cat2* is located on chromosome 4, while *Cat1* and *Cat3* were mapped to chromosome 1 (McClung, 1997). All *Cat* genes are expressed in leaves and inflorescences. *Cat1* mRNA appeared in bolts, leaves and roots, whereas *Cat3* mRNA was abundant in bolts, leaves and cauline leaves as well as *Cat2* mRNA. *Cat2* and *Cat3* mRNA were absent in roots, siliques and flowers (Frugoli et al., 1996). The expression level of all catalase genes are organ specific and depended on the developmental stages of the plant (Frugoli et al., 1996). The expression of *Cat2* and *Cat3* was characterized in the circadian rhythm, whereas expression pattern was different between both genes. *Cat3* mRNA was most abundant in the late evening in contrast to the mRNA peak of *Cat2* in the early morning (Zhong and McClung, 1996). Many genes encoding enzymes involved in photosynthesis are regulated by a circadian clock and are light induced including mRNA peak in the early morning (Giuliano et al., 1988). Due to this fact *Cat2* was identified as the catalase involved in detoxifying H₂O₂, which is produced during photorespiration (Zhong et al., 1994). This was supported by increased CAT2 activities from WT plants growing at normal air conditions compared to WT plants grown at high CO₂ concentrations (Queval et al., 2007).

In 1983 the first catalase mutant was found in barley (Kendall et al., 1983). Radioactive CO₂ measurements revealed that the CO₂ fixation was lower, but not completely blocked. The mutant was characterized by only 10% enzyme activity compared to WT and no activity was measured in isolated peroxisomes. Other photorespiratory enzymes activities were similar to WT activities (Kendall et al., 1983). The *Arabidopsis thaliana* *Cat2* mutant (Δ *Cat2*) showed several typically characteristics of a photorespiratory mutants. At high CO₂ concentrations no differences between mutant and WT were detected. In contrast, when growing the mutants at normal air conditions a decreased growth rate was observed (Queval et al., 2007). This difference was also found comparing fresh weight and dry weight of mutant plants with WT

plants. In addition another phenotype was observed, which was typical for Δ Cat2 mutants. Mutants were yellowish compared to WT plants at ambient air conditions, either because of a reduced chlorophyll content or chlorotic spots (Kendall et al., 1983; Vandenabeele et al., 2004). WT plants did not show any chlorotic spots at normal air conditions. These chlorotic spots were influenced by light intensities. Higher light intensities caused more chlorotic spots as well as cell death in the mutant line (Vandenabeele et al., 2004). The phenotype of Cat2 mutants (Δ Cat2) was not only different compared to WT, but also to gene expression levels. Genes involved in oxidative signaling pathways and oxidative stress response were more expressed in mutants than in WT (Vandenabeele et al., 2004; Queval et al., 2007).

The reduced chlorophyll content and the differently expressed genes have been used in this study to investigate the Cat2 knock-out mutant (Δ Cat2) and the influence of integrated alternative photorespiratory bypasses on the major photorespiratory pathway.

1.4.2 Glutamate:glyoxylate aminotransferase mutant

The peroxisomal aminotransferases play an important role during photorespiration. They are responsible for incorporation of nitrogen during the early photorespiratory pathway (Igarashi et al., 2006). Leaf peroxisomes have different aminotransferase activities including alanine:glyoxylate aminotransferase (AGAT), aspartate:oxoglutarate aminotransferase (AspAT), serine:glyoxylate aminotransferase (SGAT) and glutamate:glyoxylate aminotransferase (GGAT) (Liepman and Olsen, 2003). Two peroxisomal enzymes are involved in the transamination of glyoxylate to glycine during photorespiration: SGAT and GGAT. The former enzyme is identical to alanine:ketoglutarate aminotransferase and the latter enzyme can also act as glutamate:pyruvate and aspartate:glyoxylate aminotransferase (Nakamura and Tolbert, 1983; Havir, 1986).

Two genes for glutamate:glyoxylate aminotransferases are known: *Ggat1* and *Ggat2*. *Ggat1* and *Ggat2* show high similarities to each other, as well on their protein sequence level as on their amino acids levels (Liepman and Olsen, 2003). *Ggat1* and *Ggat2* transcripts were detected in grown seeds, mature leaves and green siliques in *Arabidopsis thaliana* (Liepman and Olsen, 2003). One difference appeared between *Ggat1* and *Ggat2* looking at transcript levels. *Ggat2* was also expressed in roots, whereas *Ggat1* transcripts were not observed (Liepman and Olsen, 2003). *Ggat1* levels were much higher than *Ggat2* levels in leaves (Igarashi et al., 2003; Igarashi et al., 2006). *Ggat1* showed a similar expression pattern like other genes from photosynthesis or photorespiration. A high mRNA level was observed in the morning and decreased during light exposure, although the enzyme activity was not affected (Igarashi et al., 2006). *Ggat1* knock-out lines (Δ Ggat) showed a typical

photorespiratory phenotype. On the one hand, the mutant was characterized by a reduced growth rate under photorespiratory growth conditions, like ambient air or high light (Igarashi et al., 2003). This phenotype was not observed growing the mutants at high CO₂, low irradianations or even on medium with sugars (Igarashi et al., 2003). On the other hand, the leaves were light green compared to WT plants. The differences in growth and chlorophyll content were higher at high light than at normal growth conditions (Igarashi et al., 2003). Due to the results from expression analysis and shifting experiments GGAT1 was identified as major glutamate:glyoxylate aminotransferase involved in photorespiration and leaf amino acid metabolism (Igarashi et al., 2003; Igarashi et al., 2006).

The reduced chlorophyll content and the role in amino acid metabolism could be used to investigate the knock-out mutant and to get hints for the importance of alternative pathways, which are described in the next chapter.

1.5 Alternative photorespiratory pathways

The aim of investigations in the last decades was to understand photosynthesis as well as photorespiration to find ways to increase the photosynthetic capacity and decrease the wasteful process of photorespiration. During several experimental set ups and using photorespiratory mutants different hints for alternative photorespiratory pathways were observed.

Zelitch investigated the glyoxylate conversion into glycine by glutamate:glyoxylate aminotransferases by using radiolabeled glyoxylate (Zelitch, 1972). He described that glyoxylate was converted in the peroxisomes to glycine and the resulting glycine is transported to the mitochondria, there in turn glycine was converted to serine and CO₂ was released. Beside the normal photorespiratory CO₂ release in the mitochondria, a CO₂ release in the chloroplast was observed (Figure 3, blue pathway). Radiolabeled glyoxylate was removed and no chloroplastidal CO₂ release was observed (Zelitch, 1972).

The plastidal glycolate oxidation is light dependent and increases at normal CO₂ concentrations (Kisaki and Tolbert, 1969). Although, the photorespiratory CO₂ release during the GDC/SHMT reaction is higher than the CO₂ release from the plastidal glycolate oxidation, intermediates could be measured (Zelitch, 1972; Oliver, 1981). It was postulated that glycolate is oxidized to formate by a non-enzymatic reaction, which is not inhibited by adding aminotransferase inhibitors or even KCN to the reaction mix, but negatively influenced by methylhydroxybutynoate a glycolate oxidase inhibitor (Oliver, 1981). In detail, glycolate was oxidized to formate using H₂O₂ and forming CO₂ and H₂O. The resulting formate was further

metabolized to CO₂ by formate dehydrogenase (Figure 3, blue pathway) (Kisaki and Tolbert, 1969; Oliver, 1981).

A similar alternative pathway was found in the peroxisomes. Here photorespiratory glyoxylate is decarboxylated to formate (Figure 3, light green pathway). This reaction is also a non-enzymatic reaction that requires H₂O₂ and produce CO₂, water and formate, like the previous described plastidal glycolate oxidation (Zelitch, 1972; Oliver et al., 1979). Unlike the plastidal reaction, the formate produced in the peroxisomal side pathway is not converted to CO₂, but rather used to synthesize methylene tetrahydrofolate (methylene-THF), which is channeled back to the major photorespiratory pathway and used for serine formation.

Prior investigations provided evidences for a mitochondrial side pathway producing glycine, which is further contributed to the major photorespiratory pathway (Figure 3, red pathway) (Bari et al., 2004; Niessen et al., 2007). In a two-step reaction glycolate is catalyzed via a glycolate dehydrogenase (GlcDH) and an alanine aminotransferase (AlaAT) (Bari et al., 2004; Niessen et al., 2007; Niessen et al., 2012). The resulting glycine is then used to synthesize serine.

Independent from the source, glycine is converted to serine via the combined GDC/SHMT reaction and further transported back to the peroxisomes, there serine is converted to hydroxypyruvate by HPR. Beside the peroxisomal HPR (HPR1), a cytosolic HPR (HPR2) as well as a chloroplastidal HPR (HPR3) was found (Timm et al., 2008; Timm et al., 2011). The peroxisomal and cytosolic HPR have overlapping functions. HPR2 takes over the function in the photorespiratory pathway, if HPR1 is knocked out (Figure 3, orange pathway) (Timm et al., 2008). HPR3 shows also slight indications for a role in the photorespiratory pathway. The photorespiratory phenotype of the triple mutant (HPR1/HPR2/HPR3) is even clearer than of the double mutant (HPR1/HPR2) (Timm et al., 2011).

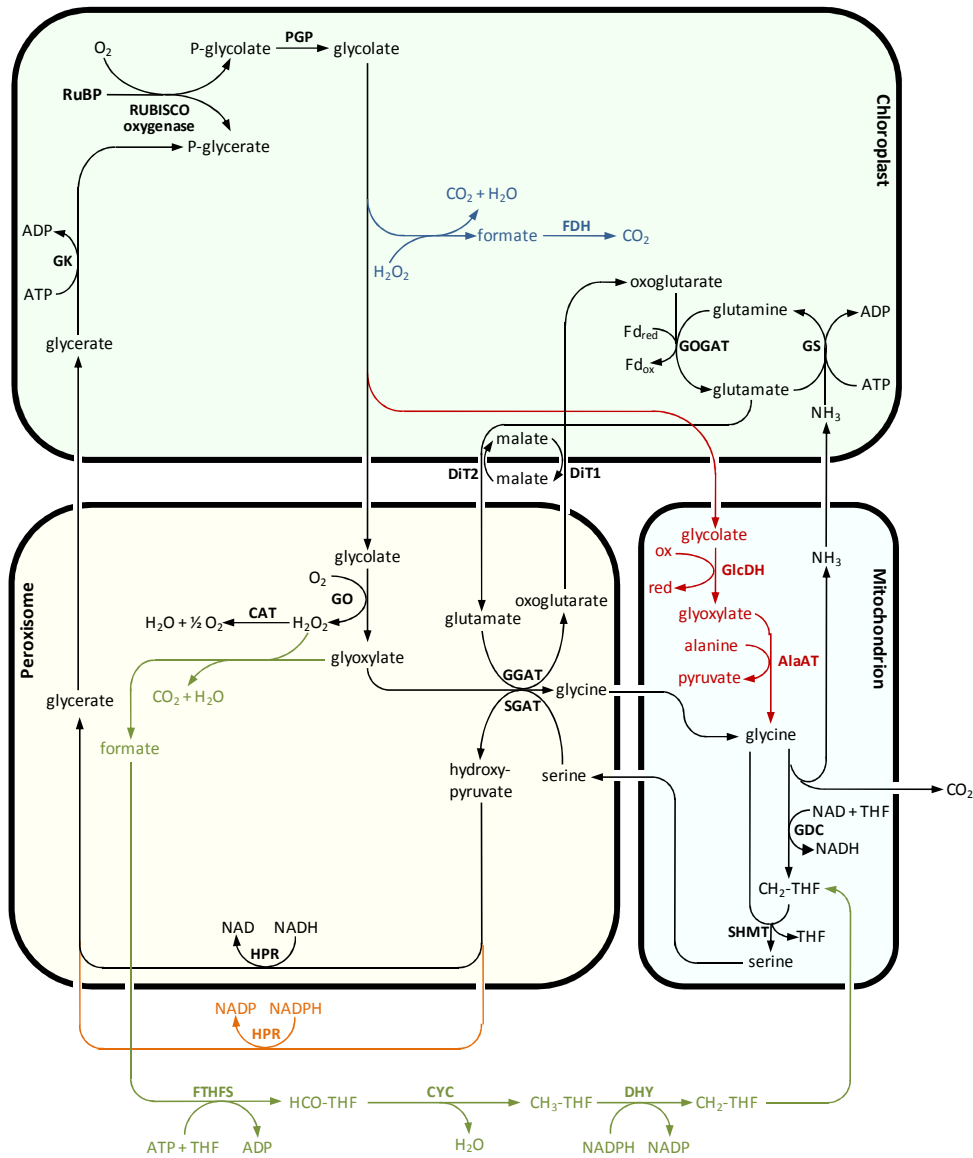


Figure 3: Overview of the major photorespiratory pathway including the known alternative photorespiratory pathways in *Arabidopsis thaliana*. RuBP, ribulose-1,5-bisphosphate; RUBISCO, RuBP carboxylase/oxygenase; PGP, phosphoglycolate phosphatase; GO, glycolate oxidase; CAT, catalase; GGAT, glyoxylate:glutamate aminotransferase; GDC, glycine decarboxylase; SHMT, serine:hydroxymethyltransferase; SGAT, serine:glyoxylate aminotransferase; HPR, hydroxypyruvate reductase; GK, glycerate kinase; GS, glutamine synthetase; FdGOGAT, glutamate:oxoglutarate aminotransferase; GldDH, glycolate dehydrogenase; AlaAT, alanine aminotransferase; FDH, formate dehydrogenase; FTHFS, 10-formyl-THF-synthetase; CYC, 5,10-methenyl-THF-cyclohydrolase; DHY, 5,10-methenyl-THF-dehydrogenase; THF, tetrahydrofolate; HCO-THF, formyl-THF; CH₃-THF, methenyl-THF; CH₂-THF, methylene-THF; DIT1, dicarboxylate transporter 1; DIT2, dicarboxylate transporter 2. The stoichiometry of the reactions is not included. (Peterhänsel et al., 2010, modified).

In order to understand the plastidal glycolate oxidation and the mitochondrial glycine formation, it is necessary to provide information about glycolate metabolism in prokaryotes. This is described in the next chapters.

1.5.1 Knock-out mutant of the alternative mitochondrial pathway

Earlier studies revealed the existence of a glycolate dehydrogenase (GlcDH) in mitochondria of higher plants that converts glycolate and has an indirect impact on photorespiratory CO₂ release (Bari et al., 2004; Niessen et al., 2012). Further studies showed that the glycolate converting process is a two-step reaction catalyzed by GlcDH and an aminotransferase (AlaAT) (Niessen et al., 2012). Labeling experiments with ¹⁴C-glycolate verified this hypothesis, because they indicated that glycolate oxidation in mitochondria is coupled with CO₂ release. The release of radioactive CO₂ could be influenced by knock-out of the GlcDH (Δ AtGlcDH) or by adding co-factors for aminotransferases. Δ AtGlcDH plants showed a drastic reduction in mitochondrial enzyme activity as well as a reduction of photorespiratory CO₂ release (Niessen et al., 2012). It is only one GlcDH known in *Arabidopsis thaliana*, but two aminotransferases (AlaAT1 and AlaAT2) are described that link glycolate oxidation to glycine formation in mitochondria of *A. thaliana* (Lee et al., 2008; Niessen et al., 2012). The produced glycine can be used in the glycine decarboxylase (GDC) reaction of the major photorespiratory pathway. The double knock-out of the two aminotransferases led to even more reduced photorespiratory CO₂ release. The importance of this contribution is unknown up to now.

1.6 Glycolate metabolism in *Escherichia coli*

Microorganisms can grow on glycolate and use this as a carbon source, because they possess a glycolate oxidizing pathway similar to the photorespiratory pathway found in plants. This pathway is well studied for *Escherichia coli*. Glycolate is oxidized to glyoxylate by glycolate oxidase (GO) reaction. The glycolate oxidase is also known as glycolate dehydrogenase (GlcDH), because the oxidation is an oxygen independent reaction in *E. coli* (Furuya and Hayashi, 1962; J. M. Lord, 1972). The GlcDH of *E. coli* (*EcGlcDH*) is a multiprotein complex consisting of three different subunits. These subunits are encoded by three different genes named *glcD*, *glcE* and *glcF* located in the *glc* operon of the *E. coli* genome (Pellicer et al., 1996). The produced glyoxylate can be seen as a branching point of glycolate metabolism, because it can be converted by two different mechanisms either to malate or phosphoglycerate (Chang et al., 1993; Pellicer et al., 1996). The first mechanism is characterized by the reaction of one glyoxylate with acetyl coenzyme A producing malate catalyzed by malate synthase G (Chang et al., 1993). The resulting malate is shuttled to the citric acid cycle (tricarboxylic acid cycle) and is used to produce energy and to provide precursors for amino acids metabolism (Hansen and Hayashi, 1962). The other mechanism is characterized by the condensation of two glyoxylate molecules forming tartronic semialdehyde catalyzed by glyoxylate carboligase (GCL) (Hansen and Hayashi, 1962). During the latter reaction, CO₂ is released. The produced tartronic semialdehyde is reduced

to glycerate by tartronic semialdehyde reductase (TSR) to be further phosphorylated to phosphoglycerate by glycerate kinase (GK) (Gotto and Kornberg, 1961). The enzymes glycolate dehydrogenase, glyoxylate carboligase and tartronic semialdehyde reductase as well as malate synthetase constitute the glycolate metabolism in *E. coli* (Pellicer et al., 1996).

1.7 Glycolate metabolism in cyanobacteria

A pathway that is similar to the bacterial glycolate pathway as well as a glycolate pathway similar to that of higher plants was discovered in cyanobacteria (Nelson and Tolbert, 1970; Cheng and Colman, 1974). In addition, some cyanobacteria were able to excrete glycolate, when the cultures were transferred from high CO₂ concentrations to low or ambient CO₂ concentrations (Goyal and Tolbert, 1996). Independently of the glycolate metabolism, in both pathways glycolate oxidation is firstly catalyzed by a GlcDH which remains for the bacterial glycolate metabolism as already pointed out. In *Synechocystis sp*, for example, the whole glycolate metabolism of bacteria and plants were found (Eisenhut et al., 2006).

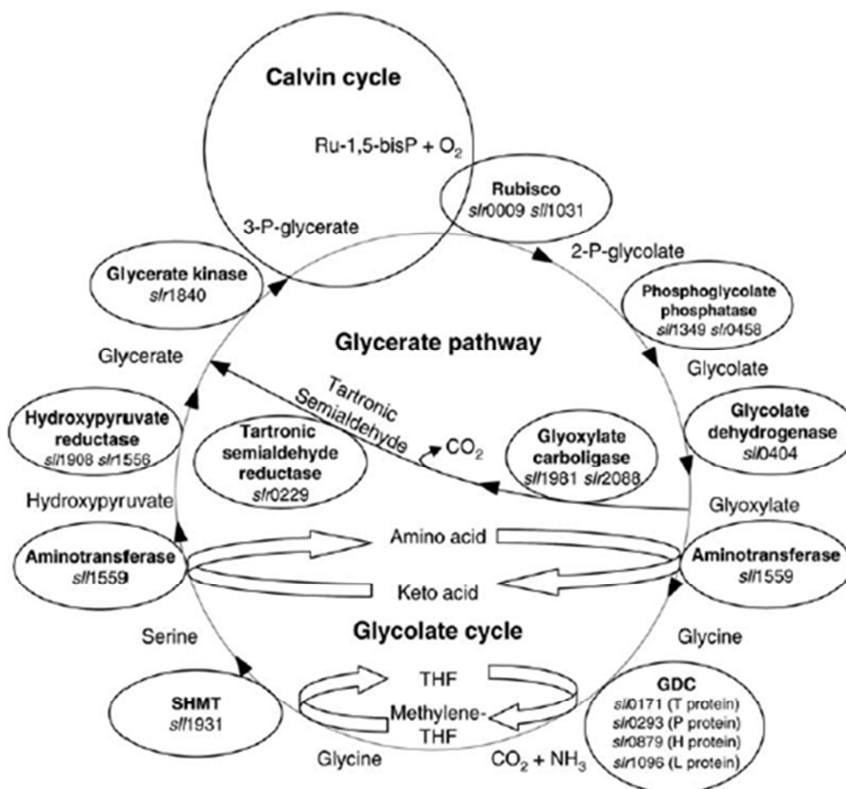


Figure 4: Glycolate metabolism of cyanobacteria including a plant-like glycolate metabolism (outer circle) and a bacterial-like glycolate metabolism (inner circle). The plant-like glycolate metabolism includes phosphoglycolate phosphatase, aminotransferases, glycine decarboxylase (GDC), serine:hydroxymethyltransferase (SHMT) and hydroxypyruvate reductase. The bacterial-like metabolism includes glycolate dehydrogenase, glyoxylate carboligase, tartronic semialdehyde reductase and glycerate kinase. (Eisenhut et al., 2006)

Figure 4 depicts a theoretical visualization of the glycolate metabolism of cyanobacteria. Phosphoglycolate is produced via oxygenase function of RubisCO and then dephosphorylated to form glycolate. The produced glycolate is then oxidized to glyoxylate via glycolate dehydrogenase (GlcDH). Here, the glycolate metabolism is divided, because the glyoxylate is converted to glycerate via the bacterial-like glycolate pathway or the plant-like glycolate pathway. Within the plant-like glycolate metabolism the glyoxylate is converted to glycine via an aminotransferase reaction. The produced glycine is then converted to serine by the GDC/SHMT reaction known from plants. Identical to what was observed in higher plants, CO₂ and NH₃ are released. Afterwards, serine is converted to hydroxypyruvate by a second aminotransferase reaction. Hydroxypyruvate is then reduced to glycerate by the HPR. Within the bacterial-like glycolate metabolism glyoxylate is converted to glycerate via two reactions: A glyoxylate carboligase and a tartronic semialdehyde reductase reaction (Stabenau and Winkler, 2005; Eisenhut et al., 2006). Independently of the source, the resulting glycerate is phosphorylated and channeled to the Calvin-Benson Cycle.

1.8 Glycolate metabolism in green algae

Although photorespiration is highly conserved in photosynthetic organisms, there exist some differences between plants and algae (Chauvin et al., 2008). One difference is the glycolate oxidation step. In higher plants glycolate is oxidized to glyoxylate via GO. In *Chlamydomonas reinhardtii*, a green algae, this step is catalyzed by a mitochondrial GlcDH (*CrGlcDH*) (Tural and Moroney, 2005; Chauvin et al., 2008). Most photorespiratory genes were found in *Chlamydomonas* genome and are up regulated after shift from high CO₂ to low CO₂ concentration (Tural and Moroney, 2005). So a GlcDH as well as a GO was identified in the *Chlamydomonas reinhardtii* genome. Further experiments revealed that only the GlcDH is well expressed and responsible for the oxidation of glycolate (Chauvin et al., 2008). The GO could not be detected, neither using Northern blot techniques nor qPCR measurements (Chauvin et al., 2008).

To conclude, the glycolate dehydrogenase of bacteria and algae differ from the enzymes found in plants and animals (Tolbert et al., 1949; Kun, 1952; Kun et al., 1954). The GO from plants and animals uses oxygen as electron acceptor and produce H₂O₂ during the glycolate oxidase reaction. Bacteria and algae use organic compounds instead of oxygen as an electron acceptor. Due to this, no H₂O₂ is produced during the glycolate pathway in these organisms. In addition, GO from plants and animals use L-lactate as an alternative substrate and are not cyanide sensitive (Tolbert et al., 1949). Bacterial and algal GlcDH use D-lactate

as an alternative substrate and the activity is negatively influenced by cyanide treatment (Kun, 1952; Kun et al., 1954).

1.9 Gene technology towards reduction of photorespiration

For a long time scientists used the modification of photorespiration as a tool to improve photosynthesis (Peterhänsel et al., 2012b) and to increase plant yields (Zelitch and Day, 1973). In recent years, different approaches have investigated how to bypass the major photorespiratory pathway and how to reduce the plant glycolate metabolism's energy loss. For this, three different approaches have been designed (Kebeish et al., 2007; Carvalho et al., 2011; Maier et al., 2012) and two of them have already been successfully tested in the model plant *Arabidopsis thaliana* (Kebeish et al., 2007; Maier et al., 2012). One pathway is integrated into the chloroplasts. This pathway is not a real bypass (Maier et al., 2012), but rather a complete pathway for glycolate conversion to CO₂ within plant chloroplast (Fahnenstich et al., 2008b; Maier et al., 2012). In the initial reaction, glycolate is oxidized to glyoxylate via glycolate oxidase (GO). The GO was relocated from the peroxisome to the chloroplast of *A. thaliana*. Hydrogen peroxide (H₂O₂) is produced during the oxidation reaction. This H₂O₂ has to be detoxified. For this reason, catalase was also relocated from the peroxisome into the chloroplast. The resulting glyoxylate is converted to malate by malate synthase using acetyl SCoA. The formed malate is then decarboxylated to pyruvate by NADP-malic enzyme. During this reaction the first CO₂ molecule is released (Maier et al., 2012). The second and final CO₂ is released during the oxidation step of pyruvate to CO₂ by pyruvate dehydrogenase (Figure 5, blue pathway) (Fahnenstich et al., 2008a; Maier et al., 2012). This pathway reminds of malate conversion in the glycolate metabolism in *E. coli*. The transgenic plants with integration of the complete pathway, but with only one copy of the catalase gene, showed an increase in growth, fresh weight and dry weight and an enhanced number of leaves (GMK3) (Maier et al., 2012). Some of the transgenic plants did not show the increased growth and biomass production (GMK9) (Maier et al., 2012). The GMK3 plants were characterized by a reduced flow through the photorespiratory pathway (Maier et al., 2012).

A second alternative photorespiratory bypass was introduced into peroxisomes. This bypass is reminiscent of the bacterial glycolate pathway of *E. coli*. The photorespiratory glyoxylate is converted to hydroxypyruvate by a two-step reaction (Figure 5, green pathway). In the first reaction, glyoxylate is converted to tartronic semialdehyde by glyoxylate carboligase. The formed tartronic semialdehyde is channeled back into the major photorespiratory cycle by conversion to hydroxypyruvate by a hydroxypyruvate isomerase reaction (HPI) (Carvalho et al., 2011). The integration of this bypass prevents ammonia release in mitochondria and

shifts CO₂ release to the peroxisome (Carvalho et al., 2011; Peterhänsel et al., 2012a). This alternative pathway was integrated into tobacco, but transgenic lines showed chlorotic spots on leaves, decreased content of sugars like glucose, fructose and sucrose and an increase of amino acids like glycine and serine (Carvalho et al., 2011). The decrease of soluble sugars and the increase of soluble amino acids like glycine and serine are typical characteristics for photorespiratory mutants. During further characterization, it became apparent the integrated HPI was not highly expressed. This might have led to an increased stress response increasing photorespiration instead of reducing it (Carvalho et al., 2011).

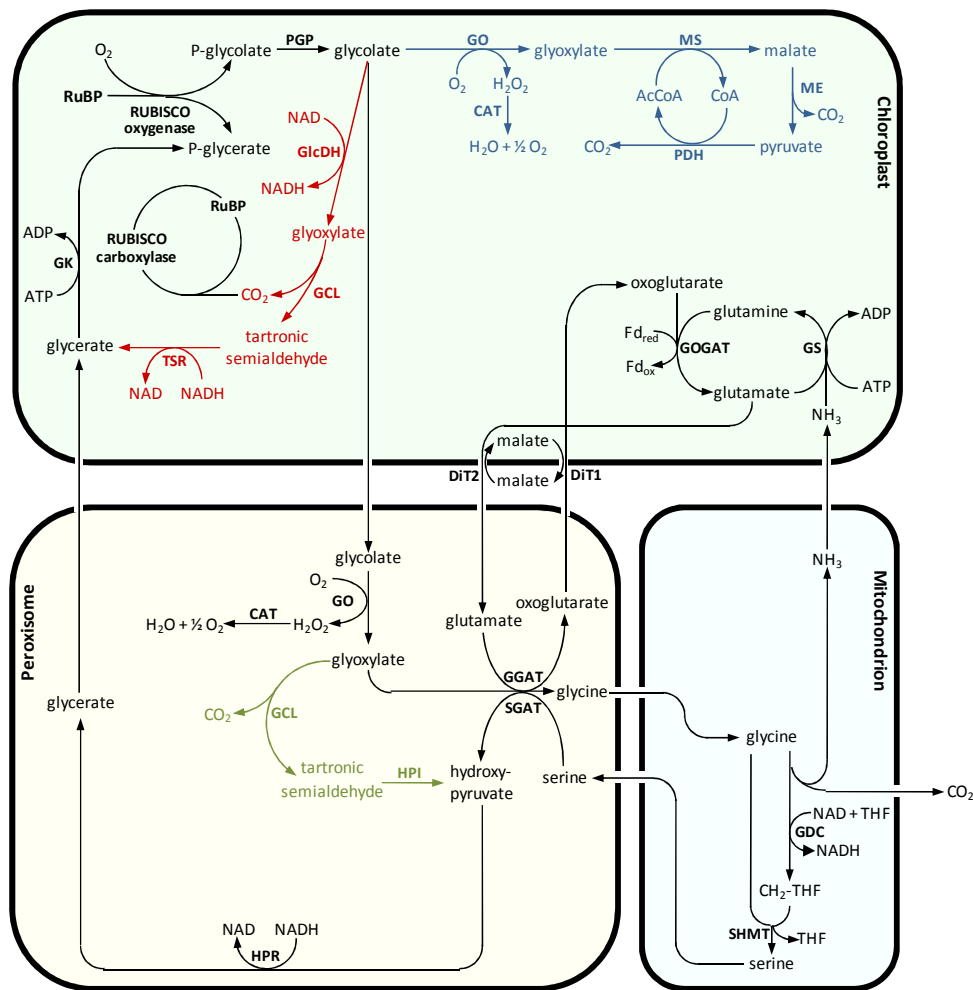


Figure 5: The photorespiratory major pathway including transgenic approaches to reduce photorespiration. RuBP, ribulose-1,5-bisphosphate; RUBISCO, RuBP carboxylase/oxygenase; PGP, phosphoglycolate phosphatase; GO, glycolate oxidase; CAT, catalase; GGAT, glyoxylate:glutamate aminotransferase; GDC, glycine decarboxylase; SHMT, serine:hydroxymethyltransferase; SGAT, serine:glyoxylate aminotransferase; CH₂-THF, methylene tetrahydrofolate; THF, tetrahydrofolate; HPR, hydroxypyruvate reductase; GK, glycerate kinase; GS, glutamine synthetase; Fd-GOGAT, glutamate:oxoglutarate aminotransferase; GlcDH, glycolate dehydrogenase; GCL, glycolate carboxylase; TSR, tartronic semialdehyde reductase; DIT1, dicarboxylate transporter 1; DIT2, dicarboxylate transporter 2. The stoichiometry of the reactions is not included. (Peterhänsel et al., 2010, modified).

For the third bypass, the bacterial-like glycolate metabolism was integrated supporting the chloroplast with CO₂ and glycerate (Figure 4, red pathway). This pathway was introduced to reduce the energy loss due to the major photorespiratory pathway and to reduce the loss of CO₂ as well as ammonia (Kebeish et al., 2007). The approach was also used to accumulate CO₂ near to RubisCO to increase the carboxylation reaction. Beside the complete glycolate metabolism of *E. coli*, the glycolate dehydrogenase (*EcGlcDH*) alone was also introduced to *Arabidopsis* chloroplasts. The introduction of the complete bacterial glycolate metabolism and the integration of *EcGlcDH* showed several positive effects on photosynthetic capacity, photosynthetic performance and biomass production (Kebeish et al., 2007). A similar dehydrogenase was found in *Chlamydomonas reinhardtii* (*CrGlcDH*) (Nakamura et al., 2005) and was used as a second glycolate oxidation system in the chloroplast. It is not completely understood what happened to glyoxylate in *EcGlcDH* or *CrGlcDH* plants, but maybe it is used to synthesize CO₂ and formate (Kisaki and Tolbert., 1969; Zelitch, 1972; Oliver, 1981). The formate might have further converted into CO₂ by formate dehydrogenase in the chloroplast, which reminds the alternative photorespiratory pathway described by Zelitch (Zelitch, 1972). Recent investigations revealed that the chloroplastidal pyruvate dehydrogenase (PDC) is part of the glycolate and glyoxylate pathway in *Arabidopsis thaliana* chloroplasts (Blume, 2013) and might be responsible for chloroplastidal CO₂ release. This was shown, because CO₂ production of isolated chloroplasts was inhibited by adding pyruvate, but not by related substances. Furthermore the PDC was enriched and it was observed that glyoxylate inhibited the NADH formation in the PDC fraction. An accumulation of the glyoxylate decarboxylation activity was also detected in the isolated PDC fraction (Blume, 2013).

1.10 Aim of this study

From former experiments we know that installation of a photorespiratory bypass has a positive influence of biomass production and other photorespiratory parameters of *Arabidopsis thaliana* (Kebeish et al., 2007). These mutants showed a higher oxidation of glycolate to CO₂ in the chloroplast, but the wild type also showed an oxidation of glycolate to CO₂. The responsible enzyme for this reaction could be inhibited with KCN, so it could be a GlcDH (Kebeish et al., 2007). Such a GlcDH is known in the mitochondria of *Arabidopsis thaliana* (Bari et al, 2004; Niessen et al., 2007). Hints were found that this enzyme could be dual-targeted to the mitochondria and chloroplast and contributes glycine to the major photorespiratory pathway in the mitochondria (Niessen et al., 2007; Niessen et al., 2012).

To understand the importance of the unclear chloroplastidal pathway and to determine the impact of the transgenic approaches the idea was to cross mutants with a photorespiratory

phenotype (Figure 6, black pathway) with overexpressors of chloroplastidal transgenic GlcDH (Figure 6, red pathway). Δ Cat2 and Δ Ggat, two knock-out mutants lines in the major photorespiratory pathway (Figure 6, black pathway) were crossed with 35S-*Ec*GlcDH as well as with 35S-*Cr*GlcDH, two GlcDH overexpressor lines (Figure 6, red pathway). This was done, because the photorespiratory pathway could be interrupted behind the chloroplastidal glycolate formation and the role of the glycolate-conversion in the chloroplast could be investigated.

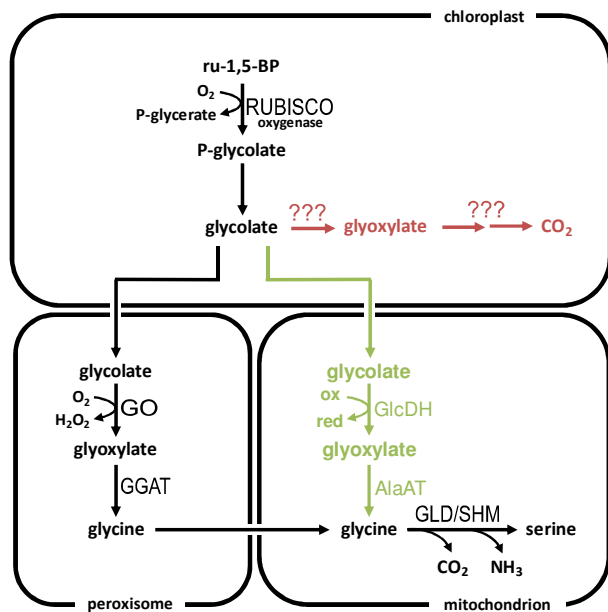


Figure 6: Overview of the glycolate pathway in higher plants up to serine formation in the mitochondria, which includes the unknown chloroplastidal bypass pathway and the known mitochondrial bypass pathway. RuBP, ribulose-1,5-bisphosphate; RUBISCO, RuBP carboxylase/oxygenase; P-glycerate, phosphoglycerate; P-glycolate, phosphoglycolate; GO, glycolate oxidase; GGAT, glyoxylate:glutamate aminotransferase; GLD, glycine decarboxylase; SHM, serine:hydroxymethyltransferase. black, major photorespiratory pathway; red, chloroplastidal bypass; green, mitochondrial bypass.

In addition, the impact of the mitochondrial side pathway (Figure 6, green pathway) on the major photorespiratory pathway was investigated. Therefore, Δ Cat2 and Δ Ggat were crossed with a second photorespiratory mutant of the mitochondrial pathway (Δ A*t*GlcDH) as well as with the overexpressors of the mitochondrial side pathway (35S-*Ai*GlcDH).

This investigation should help to understand the complex photorespiration in detail and to get hints about the importance about natural photorespiratory side pathways in higher plants.

2 Materials and Methods

2.1 Materials

2.1.1 Chemicals and consumables

The chemicals used throughout this work posed at least a degree of p.a. and were purchased from the following companies: Amersham Pharmacia Biotech (Freiburg), AppliChem (Darmstadt), BioRad Laboratories GmbH (München), Boehringer Roche (Mannheim), Calbiochem (Bad Soden), Carl Roth GmbH (Karlsruhe), Gibco BRL (Eggenstein), Hartmann Analytic (Braunschweig), Invitek (Berlin), Invitrogen (Leck, Netherlands), KMF Laborchemie Handels GmbH (St. Augustin), Kodak (Stuttgart), Life Technologies (Carlsbad, United states of America), Merck (Darmstadt), Metabion (Martinsried), Molbiol (Hamburg), New England Biolabs (Frankfurt), Peglab (Erlangen), Pharmacia (Freiburg), Promega (Madison, United States of America), Thermo Scientific Fermentas (St.- Leon-Rot), QIAGEN (Hilden), Roche Diagnostic GmbH (Mannheim), Serva (Heidelberg), Sigma-Aldrich (Taufkirchen), VWR (Darmstadt), Worthington (Lakewood, New Jersey, United States of America).

The consumables were obtained from: Applied Biosystems (Darmstadt), Beckman Coulter (Fullerton, United States of America), Biometra (Göttingen), BioRas Laboratories GmbH (München), Eppendorf (Hamburg), Fuji (Düsseldorf), Gibco BRL (Eggenstein), Greiner (Solingen), Hanna Instruments (Kehl), Heraeus (Osterode), Herolab (Wiesloch), Hettich Zentrifugen (Tuttlingen), Kodak (Stuttgart), Labomedic (Bonn), LI-COR[®] Biosciences (Lincoln, United States of America), Merck (Darmstadt), Millipore (Eschborn), MWG Biotech (München), Pharmacia (Freiburg), Raytest (Berlin), Serva (Heidelberg), Schott Glaswerke (Mainz), Sorvall (Bad Homburg), Wissenschaftliche Technische Werkstätten (Weilheim), Whatman (Maidstone, Kingdom of Great Britain), Zinsser Analytic (Frankfurt).

2.1.2 Instruments

Table 1: Instruments and equipment used throughout this study

Instruments and equipment	Company
Centrifuges and rotors	
5415R CI 023 (F45-24-11)	Eppendorf (Hamburg)
Optima L-100XP	Beckman-Coulter (Fullerton, USA)
Rotor SW 41 Ti	Beckman-Coulter (Fullerton, USA)
Sorvall RC 5 B Plus	Sorvall (Bad Homburg)

Material

Instruments and equipment	Company
SpeedVac Savant	Thermo Scientific (Waltham, USA)
Chlorophyll fluorescence	
IMAGING-PAM <i>M-Series</i>	Heinz Walz GmbH (Effeltrich)
Electroporation	
Gene Pulser TM	BioRad Laboratories GmbH (München)
ELISA-reader	
BioTek ELx808	BioTek (Vermont, USA)
Foto dokumentation	
Intas GDS	Intas (Göttingen)
GC/MS	
mass spectrometer	Leco Pegasus HAT (Mönchengladbach)
gas-phase chromatograph	Agilent 7890 A (Böblingen)
auto sampler	Gerstel MPS (Mülheim an der Ruhr)
Gel electrophoresis	
agarose gel equipment	Biozym Scientific GmbH (Hessisch Oldendorf)
Incubators and climate cabinets	
MobyLux Gro Banks	CLF Plant Climatics (Wertingen)
Minitron	Infors-HAT (Bottmingen)
Percival	
Percival	
pH meter	
F2 20/EL 20	Mettler Toledo (Gießen)
Photometer	
Genesys 10 UV scanning	Thermo Electron Corporation (Waltham, USA)
one time cuvette	Sarstedt (Nümbrecht)
UV cuvette	Sarstedt (Nümbrecht)
Real time PCR system	
ABI Prism 7300	Applied Biosystems (Darmstadt)
ABI Prism 7300 SDS software	Applied Biosystems (Darmstadt)
Retch	
MM400	Retch (Hamm)
stainless steel beads, 5mm	Qiagen (Hilden)
Scintillation counter	
Ls 5000TD	Beckmann (Fullerton, USA)
Thermocycler	
Vapo protect Mastercycler Pro	Eppendorf (Hamburg)

2.1.3 Software and internet-programs

Table 2: Software and internet-programs used throughout this study

Software/internet-program	Characteristics
ABI Prism® 7300 SDS Software 1.4	Software for enforcement and evaluation of ABI Prism® 7300 Sequence Detection System
Clone Manager Professional 9	Nucleic acid sequence analysis
Multiple Sequence Alignment by CLASTALW	internet program for sequence alignment, http://www.genome.jp/tools/clustalw/
National Centre for Biotechnologic Infomartions (NCBI)	internet database for sequencing, http://ncbi.nlm.nih.gov/
Oligonucleotide Properties Calculator (OligoCalc)	internet program for oligonucleotide analyses, http://www.basic.northwestern.edu/biotools/oligocalc.html
Pegasus	analyze chromatograms from GC-MS runs and quantification of peaks/metabolites
Tagfinder 4.1	Quantification of peaks/metabolites
The Arabidopsis Information Resource (TAIR)	internet database for <i>A. thaliana</i> , http://www.arabidopsis.org/
The European Arabidopsis Stock Centre (uNASc)	internet database for <i>A. thaliana</i> mutants, http://arabidopsis.info/
Salk Institute Genomic Analysis Laboratory (SIGNAL)	internet program to design primer system to identify t-DNA insertion mutants, http://signal.salk.edu/tdnaprimers.2.html
SegLab	internet program for sequencing, http://seqlab.de/
Software ImagingWin V2.40b	program to analyze data from the Imaging-Pam measurements, http://www.walz.com/products/chl_p700/imaging-pam_ms/downloads.html
Reverse Complement	internet program for converting DNA sequence to its reverse, http://www.bioinformatics.org/sms/rev_comp.html

2.1.4 Markers

Table 3: Markers used throughout this study

Marker	Company
GeneRuler 1kb DNA Ladder	Thermo Scientific Fermentas (St. Leon-Rot)
GeneRuler 50bb DNA Ladder	Thermo Scientific Fermentas (St. Leon-Rot)
λ-DNA/PstI-Marker, 24	Thermo Scientific Fermentas (St. Leon-Rot)

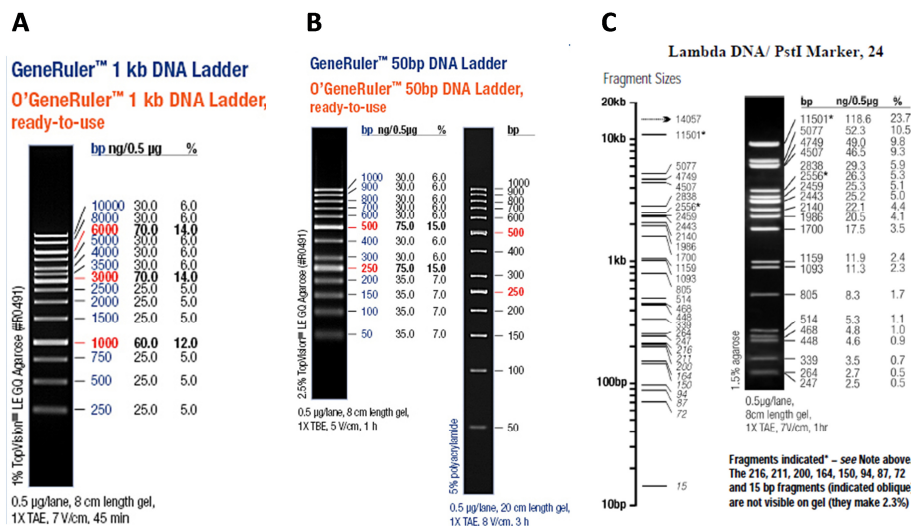


Figure 7: Markers used throughout this work for gel-electrophoresis. (a) GeneRuler™ 1 kb DNA Ladder (b) GeneRuler™ 50bp DNA Ladder, (c) Lambda DNA/PstI Marker, 24.

2.1.5 Reaction kits

Table 4: Reaction kits used throughout this study

Reaction kit	Company
Extraction of DNA from agarose gel slices	
Invisorb® Spin DNA Extraction Kit	Invitek (Berlin)
Purification of PCR products and restriction products	
MSB Spin PCRapace	Invitek (Berlin)
Plasmid preparation	
GeneJet Plasmid Miniprep Kit	Thermo Scientific Fermentas (St. Leon-Rot)

Reaction kit	Company
qPCR	
Platinum® SYBR® Green qPCR	Life Technologies (Carlsbad, USA)
SuperMix-UDG with Rox	

2.1.6 Enzymes

Table 5: Enzymes used throughout this study

Enzyme	Company
cDNA synthesis	
Moloney Murine Leukemia Virus Reverse Transkriptase (M-MLV-RT)	Thermo Scientific Fermentas (St. Leon-Rot)
DNA digestion	
DNase I	Thermo Scientific Fermentas (St. Leon-Rot)
Ligation	
T4-DNA-Ligase	Thermo Scientific Fermentas (St. Leon-Rot)
PCR amplification	
Dream Taq™ polymerase	Thermo Scientific Fermentas (St. Leon-Rot)
Phusion® hot Start II	Thermo Scientific Fermentas (St. Leon-Rot)
Restriction enzymes	
AscI	New England BioLabs (Frankfurt)
Bpu1102I/BpI	New England BioLabs (Frankfurt)
PmeI	New England BioLabs (Frankfurt)
SgrAI	New England BioLabs (Frankfurt)
XhoI	Thermo Scientific Fermentas (St. Leon-Rot)
XbaI	Thermo Scientific Fermentas (St. Leon-Rot)

2.1.7 Specific chemicals

Table 6: Specific chemicals used throughout this study

Specific chemicals	Company
Antibiotics	
Ampicillin	AppliChem (Darmstadt)
Carbenicillin	Duchefa (St. Louis, USA)
Kanamycin	Duchefa (St. Louis, USA)
Rifampicin	Duchefa (St. Louis, USA)
cDNA synthesis/PCR	
dNTPs	Thermo Scientific Fermentas (St. Leon-Rot)
Radioactive CO ₂ release	
[1,2- ¹⁴ C]-glycolate	Hartmann-Analytic (Braunschweig)
Liquid scintillation cocktail (Optiphase 'Highsafe' 2)	Perkin Elmer (Waltham, USA)

2.1.8 Material and chemicals for GC-MS analysis

Table 7: Material and chemicals for GC-MS analysis used throughout this study

Material / compound	Company
Column	
Agilent J&W GC Column VF-5ms	Agilent Technologies (Böblingen)
Extraction buffer	
¹³ C-Sorbitol	Fluka/Sigma-Aldrich (Taufkirchen)
Chloroform Rotisolv HPLC	Merck (Darmstadt)
Methanol	Merck (Darmstadt)
Wasser Rotisolv ultra	Roth (Karlsruhe)
Derivatization	
Methoxyamin-Hydrochlorid	Sigma-Aldrich (Taufkirchen)
Pyridine	Sigma-Aldrich (Taufkirchen)
Fatty acid methyl ester, FAMES	
Methyl arachidate	Sigma-Aldrich (Taufkirchen)
Methyl behenate (docosanoate)	Sigma-Aldrich (Taufkirchen)
Methyl hexacosanoate	Sigma-Aldrich (Taufkirchen)
Methyl myristate	Sigma-Aldrich (Taufkirchen)
Methyl laurate	Sigma-Aldrich (Taufkirchen)
Methyl octacosanoate	Fluka/Sigma-Aldrich (Taufkirchen)
Methyl octanoate	Sigma-Aldrich (Taufkirchen)

Material

Material / compound	Company
Methyl stearate	Sigma-Aldrich (Taufkrichen)
Palmitic acid methyl ester	Sigma-Aldrich (Taufkrichen)
Tetracosan acid methyl ester	VWR (Darmstadt)
Triacotanoic acid methyl ester	Ultra Scientific (N. Kingstown, USA)
Silylization	
N-Methyl-N-trimethylsilyltrifluoroacetamide (MSTFA)	Sigma-Aldrich (Taufkrichen)
Washing solutions for the column	
Ethylacetate	Sigma-Aldrich (Taufkrichen)
n-Hexan	Sigma-Aldrich (Taufkrichen)

2.1.9 Oligonucleotides

Table 8: Oligonucleotides used throughout this study

Primer (stock number)	Sequence (5'→ 3')	Intended use
cDNA synthesis		
Random nanomer (549)	NNN NNN NNN	[d(N)9] 1st strand synthesis
Cloning		
AtGlcDH_ampli_fw new (5051)	TTG GAC TAC TAT TGG GCG CG	to amplify <i>AtGlcDH</i> for overexpression vector 35S-AlaAT1/35S- <i>AtGlcDH</i>
AtGlcDH_ampli_rev new (5052)	CTC AAG TGT CAA CGT CCG C	to amplify <i>AtGlcDH</i> for overexpression vector 35S-AlaAT1/35S- <i>AtGlcDH</i>
Multiplex PCR		
Actin2 Fw (584)	GGT AAC ATT GTG CTC AGT GGT GG	Actin control for DNA isolation
Actin2 Rev (585)	GGT GCA ACG ACC TTA ATC TTC AT	Actin control for DNA isolation
p3'-3'g7-Rev (2994)	ATA TCA GCT GGT ACA TTG CCG TAG	check the presence of <i>CrGlcDH</i> (primer at the beginning of 3'g7 terminator)
Cr-GDH -RT-Fw2 (3301)	GCT TCT CTA CAA CAC CTG AAC CTT	check the presence of <i>CrGlcDH</i>
AtGDH_Fw (3041)	CGT GAG CAG ACG CAA ATT GTT C	check insert <i>AtGlcDH</i> in 35-AlaAT1/35S- <i>AtGlcDH</i> vector
AtGDH_Rv (3042)	ATC TCC GGC ATG AGC AAT AAC G	check insert <i>AtGlcDH</i> in 35-AlaAT1/35S- <i>AtGlcDH</i> vector
GlcF FW (3947)	CAG CGG GAA CAT ATG CGT TA	check the presence of the F subunit in <i>EcGlcDH</i> plants
GlcD FW (3949)	CAA CAT GCA CCC GTT AAT CCT TT	check the presence of the D and E subunit in <i>EcGlcDH</i> plants
GT-DEF Rev-2 (3953)	CAT GAG CGA AAC CCT ATA AGA ACC CT	universal revers primer of checking the presence of the <i>EcGlcDH</i> subunits (DE,F)
qPCR		
Actin2 Fw (584)	GGT AAC ATT GTG CTC AGT GGT GG	<i>A. thaliana</i> Actin reference gene
Actin2 Rev (585)	GGT GCA ACG ACC TTA ATC TTC AT	<i>A. thaliana</i> Actin reference gene
AGA-6-realtime_Fw (2810)	GGA GCT ATG TAT CTA TTC CCT TGC C	Gene expression of AlaAT1

Material

Primer (sotck number)	Sequence	Intended use
AGA-6-realttime_Fw (2811)	TTA AGA ATT CGT TTG CAG TAG AAA TTTG	Gene expression of AlaAT1
APX1 fw (6672)	CTC TGC TGG AAC TTT CGA TTG TC	H ₂ O ₂ stress response, gene expression (At1g07890)
APX1 rev (6673)	GGA ATT GCT CCC TGA TGG GG	H ₂ O ₂ stress response, gene expression (At1g07890)
At1g21250_Fw (4302)	GAT ACC ACC ACT ATG AGC TGC	Gene expression of Atwak1
At1g21250_Rv (4303)	GTG CTT CAT TCT CTG TTG TAT AC	Gene expression of Atwak1
At4g02380_Fw (4316)	AGC TGT TGC TTC GGC TGT GAT G	Gene expression of Atlea5
At4g02380_Rv (4317)	GAA CCG GTT TCG GGT CTG TAA TAA C	Gene expression of Atlea5
At2g38470_Fw (4318)	CTT GAC GAC GGT TAC AGA TGG AG	Gene expression of Atwrky33
At2g38470_Rv (4319)	CAA CCG ATG GTT GTG CAC TTG TAG	Gene expression of Atwrky33
AtGDH-taqman-FW1 (1412)	GGA TGG AAC ATG TAC TGG AGA ACA CG	Gene expression of AtGlcDH
AtGDH-taqman-REV1 (1413)	CCG GGT TCA TGA TAT CGT TTG GGT CC	Gene expression of AtGlcDH
cat1up (5215)	CTT CGA TCC GCT TGA TGT CAC	Catalase 1 gene expression
cat1down (5216)	GGA ACC ACA AGA GCA GGA CAG	Catalase 1 gene expression
cat2up (5217)	TGC TGG AAA CTA CCC TGA ATG G	Catalase 2 gene expression
cat2down (5218)	TCA ACA CCA TAC GTC CAA CAG G	Catalase 2 gene expression
cat3up (5219)	CCA CTT GAT GTG ACC AAG ATC TG	Catalase 3 gene expression
cat3down (5220)	GTA GAT TCC AGG AAC CAC AAG ACC	Catalase 3 gene expression
Cr-GDH -RT-Fw2 (3301)	GCT TCT CTA CAA CAC CTG AAC CTT	gene expression of CrGlcDH in transformed plants
Cr-GDH-RT-Rev2 (3302)	GTC CAC GGA AGT TGA TTC CA	gene expression of CrGlcDH in transformed plants
GAPDHnew_fw (5738)	GGA ATC TGA AGG CAA AAT GAA GG	Gene Expression of GAPDH
GAPDHnew_rev (5739)	TGT TGT CAC CAA CAA AGT CGG	Gene Expression of GAPDH
GGAT SALK_064982C fw (4244)	GAT GAC CAA CCT CCC TCC AAG	Gene expression (At1g23310) (T-DNA insertion line)
GGAT SALK_064982C rev (4245)	GTC TCC AGG CTT TGG AGG ATT A	Gene expression (At1g23310) (T-DNA insertion line)
GGAT 3'UTR border primer (4248)	GGG CAA AGA GAA AGA GTG TAC	3' UTR border primer At1g23310 (T-DNA insertion line)
GGAT1_mRNA_fw2 (4865)	GAAGTTCTGTTATAACGAGAAACTG	mRNA expression level of GGAT1
GGAT1_mRNA_rev2 (4866)	AACGGCGAACCCATTTCCATC	mRNA expression level of GGAT1
GLDP1_mRNA_fw1 (4746)	CATGCAATTGCTGATGCAGCTT	mRNA expression level of GLDP1
GLDP1/2_mRNA_rev1 (4748)	CATCATCCAAGGTGGTTGTTTC	mRNA expression level of GLDP1
GLYK_mRNA_fw1 (4754)	CAGATTGCTTTGCATAATTCCAAG	mRNA expression level of GLYK
GLYK_qPCR_rev (4685)	TTGATGAATCGGCTCTGTCA	hnRNA expression level of GLYK
GOX2_mRNA_fw1 (4735)	GTATTCTCATTGGCAGCTGAA	mRNA expression level of GOX2
GOX2_mRNA_rev1(4736)	CTTTAGGGACCGACCCCACTC	mRNA expression level of GOX2
gpx6up (5221)	GAT GTT AAC GGT GAC AAA GCT G	Gene expression gpx6 (H ₂ O ₂ stress gene)
gpx6down (5222)	TTG GTG CGA AAC GAT CG	Gene expression gpx6 (H ₂ O ₂ stress gene)
gsh2 fw (6664)	TAA CAT TCA CAA CCA TCT TGA TCA GTT	gene expression with similarity to glutathione synthetase

Material

Primer (stock number)	Sequence	Intended use
gsh2 rev (6665)	CAA TGT AGG CTT TGC GGT CCT G	gene expression with similarity to glutathione synthetase
gstF8up (5223)	CGA AGG TAA GCT CCA GAA AGT C	Gene expression gstF8 (H ₂ O ₂ stress gene)
gstF8down (5224)	AGA GTC AAA GAG CAC CTT GGA G	Gene expression gstF8 (H ₂ O ₂ stress gene)
HPR1_mRNA_fw1(4752)	CAGTTCTTGAAAGCAAATGGAG	mRNA expression level of HPR1
HPR1_qPCR_rev (4681)	AGCACCGGGTGAAGACTTAT	hnRNA expression level of HPR1
oxi1up (5227)	GTT GAG GAA ATC AAG GGT CAT G	Gene expression oxi1 (H ₂ O ₂ stress gene)
oxi1down (5228)	TGG ACG ATA TTC TCC ACA TCC	Gene expression oxi1 (H ₂ O ₂ stress gene)
OGlcF-taqman-Fw2 (3281)	CGC ACA AAA GTT GAA CGG AGA G	gene expression of the F gene in <i>EcGlcDH</i> plants (codon optimized)
OGlcF-taqman-Rev2 (3282)	AGT TGC CGA GCA AGA TCA GGA	gene expression of the F gene in <i>EcGlcDH</i> plants (codon optimized)
OGlcE-taqman-Fw2 (3285)	GAG CAG CAA CTT CCG TTC TTC	gene expression of the E gene in <i>EcGlcDH</i> plants (codon optimized)
OGlcE-taqman-Rev2 (3286)	ATC TCA ATG CTC CAC CCC AGT	gene expression of the E gene in <i>EcGlcDH</i> plants (codon optimized)
OGlcD-taqman-Fw2 (3289)	GTT CGA TGC TAA TGA GCC TGG T	gene expression of the D gene in <i>EcGlcDH</i> plants (codon optimized)
OGlcD-taqman-Rev2 (3290)	CGC ACA TCT GGT TGA TCT TCT CT	gene expression of the D gene in <i>EcGlcDH</i> plants (codon optimized)
PGLP1_mRNA_fw1 (4732)	CATACTTGCACTCTATTAATTTCCC	mRNA expression level of PGLP1
PGLP1_qPCR_rev (4658)	CGGACCTCCAAGGTATTGAA	hnRNA expression level of PGLP1
SHM1_mRNA_fw1 (4751)	CTGACATTATTGAGCATGAGAAAG	mRNA expression level of SHM1
SHM1_qPCR_rev (4679)	GTCATGACAGACCCAACAGC	hnRNA expression level of SHM1
SGAT_mRNA_fw1 (4737)	TCAAAGCCATTTGCATTGTCCA	mRNA expression level of SGAT
SGAT_qPCR_rev (4663)	AGCCGGATGCTTGTAGTGAT	hnRNA expression level of SGAT
SALK lines		
sensCAT2 new (5042)	CTC TCC CTT CTT CAC CAC CAA	primer for testing Δ Cat2 mutants (WT allele + T-DNA insertion)
revCAT2 new (5043)	GAC CAT GTC AGG GAA CTT CAT	primer for testing cat2 mutants (WT allele)
NewLB1 (4574)	TGG ACC GCT TGC TGC AAC TCT C	rev primer for T-DNA insertion
N50-new LP (4702)	GAG GAG GAA TTA ACT TTC CCG	primer for testing Δ AtGlcDH mutants (WT allele)
N50-new RP (4703)	CCA AGC AGT GAA GAG CAG AG	Primer for testing Δ AtGlcDH mutants (WT allele + T-DNA insertion)
SALK_064982C_LP (4161)	TTCCTCATCTTCTTTCTCTGGC	Primer for testing Δ Ggat mutants (WT allele)
SALK_064982C_RP (4162)	CTGCAAAACAAGCTGGAAAAG	Primer for testing Δ Ggat (mutants WT allele + T-DNA insertion)

Material

Primer (stock number)	Sequence	Intended use
Sequencing		
AtGlcDH+AlaAT wo SAR_seq fw 1 (5282)	GGC TGA GTG GCT CCT TCA AC	sequencing of AtGlcDH insert in A215-307; 7266-7285 (seq from Pnos - SAR - 35sPromotor)
AtGlcDH+AlaAT wo SAR_seq rev 1 (5283)	GGC CGG AGA AAA GAG AGA ATA G	sequencing of AtGlcDH insert in A215-307; 9322-9301 begin AtGlcDH gene (seq promotor/TL)
AtGlcDH+AlaAT wo SAR_seq fw (5284)	TCA TCG TTG TTG TGT ACC GTT AT	sequencing of AtGlcDH insert in A215-307; 10662-10684 (seq end of AtGlcDH gene+35S terminator)
AtGlcDH+AlaAT wo SAR_seq rev 2 (5285)	GTG GTT CAG TCT TTC TGC TTC	sequencing of AtGlcDH insert in A215-307; 10755-10774 (seq AtGlcDH gene from the end)
AlaAT+AtGlcDH (PmeI+SgrAI)_seq fw 1 (5286)	GGT GAC GTG ACC GTA CTT TCT	sequencing of AtGlcDH insert in A215-307; 926-946 begin AtGlcDH gene (seq gene)
AlaAT+AtGlcDH (PmeI+SgrAI)_seq rev 1 (5287)	GGA GCT GAC GAC AAG GCC	sequencing of AtGlcDH insert in A215-307; 888-905 begin of the AtGlcDH gene (seq promotor)
AlaAT+AtGlcDH (PmeI+SgrAI)_seq fw 2 (5288)	CTA TTC TCT CTT TTC TCC GGC C	sequencing of AtGlcDH insert in A215-307; 870-891 begin AtGlcDH gene (seq gene)
AlaAT+AtGlcDH (PmeI+SgrAI)_seq rev 2 (5289)	AGA AAG TAC GGT CAC GTC ACC	sequencing of AtGlcDH insert in A215-307; 926-946 begin of the AtGlcDH gene (seq promotor)
AlaAT+AtGlcDH (PmeI+SgrAI)_seq fw 3 (5290)	TAC GCG TTG CTC TGG CTC TT	sequencing of AtGlcDH insert in A215-307; 1582-1601 (seq AtGlcDH gene)
AlaAT+AtGlcDH (PmeI+SgrAI)_seq fw 4 (5291)	TGG AGA AGG AAC TGG GAA TAG	sequencing of AtGlcDH insert in A215-307; 2424-2444 (seq AtGlcDH gene-35S terminator)
AlaAT+AtGlcDH (PmeI+SgrAI)_seq rev 3 (5292)	ACG TCC GCC CCT CAT CTG	sequencing of AtGlcDH insert in A215-307; 4146-4129 (Rk1 ori to SAR region)

2.1.10 Plasmids

The following plasmids were used to create an overexpression vector with two genes (Figure 8), *AtGlcDH* (pTRAK-AtGDH, A215-142) and *AlaAT1* (pTRAK-AGA6, A215-182).

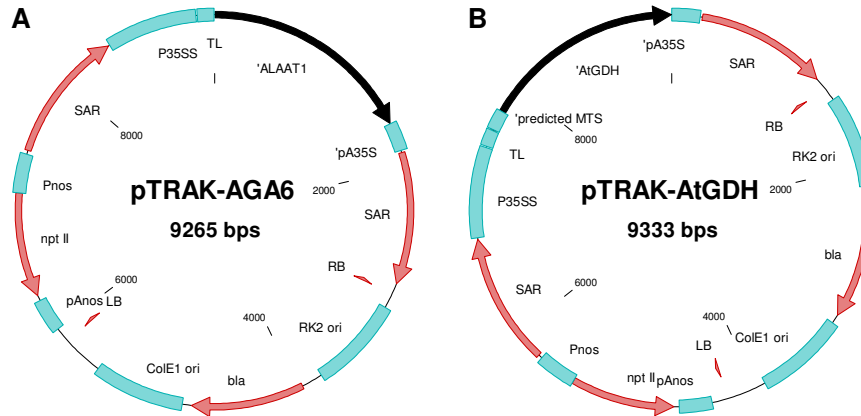


Figure 8: Structure of pTRAK-AGA6 (A215-142) and pTRAK-AtGDH (A215-182). Pictured are the vectors for overexpression of *AlaAT1* (A, pTRAK-AGA6) and *AtGlcDH* (B, pTRAK-AtGDH) in *E. coli* and *A. thaliana*. These vectors were used to create a new overexpression vector with both genes. The arrows symbolize the orientation of the genes. AGA6: alanine:glyoxylate aminotransferase; ALAAT1: alanine aminotransferase 1; *AtGDH*: glycolate dehydrogenase of *A. thaliana*; P35SS/pA35S: promoter and polyadenylation-/ termination sequence from CaMV; bla: β -lactamase gene for selection in bacteria (causes ampicillin and carbenicillin resistance in bacteria); npt II: neomycin-phosphotransferase typ II confers resistance to aminoglycoside antibiotics, like kanamycin, and was used for selection of transgenic plants; ColE1 ori: replication origin for vectors in *E. coli*; LB and RB: left and right border sequences of Nopaline-Ti-plasmids pTiT37; PAnos: polyadenylation of Nopaline synthase gene from *A. tumefaciens*; Pnos: promoter of Nopaline synthase gene from *A. tumefaciens*; RK2 ori: replication origin for vectors in *A. tumefaciens*; SAR: scaffold attachment region from the tobacco RB7 gene (ge U67919).

For this *AtGlcDH* was amplified by PCR using the vector A215-181 as template and specific primers for the gene including the 35S promoter and the SAR region (5051, 5052; Table 8). The fragment starts 35 bp before the 35S promoter, containing an extension for PmeI restriction side and ends 72 bp after SgrAI restriction side, which is already in the vector. The destination vector carrying *AlaAT1* (A215-142) was also restricted with SgrAI and PmeI. Both digestions were proofed by gel electrophoreses and were purified by using the Invisorb® Spin DNA Extraction kit (Figure 9). Afterwards the ligation was carried out with a ratio 1:3 of destination vector and insert. The ligation was performed over night at 16°C (2.2.1.7) and the new created vector was transformed to a competent *E. coli* strain (DH5 α , 2.2.2.1).

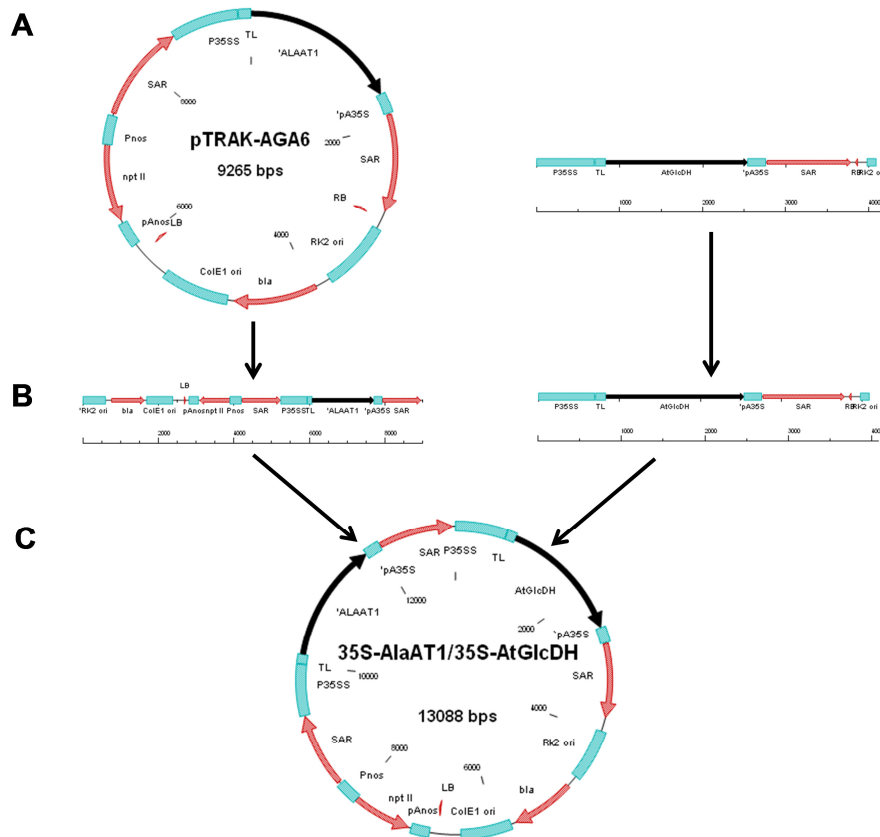


Figure 9: Cloning strategy to create an overexpression vector carrying ALAAT1 and AtGlcDH (35S-AlaAT1/35S-AtGlcDH). A: The destination vector (A215-141) and insert of interest (amplified *AtGlcDH*), B: destination vector and insert restricted with SgrAI and PmeI, C: the resulting vector carrying ALAAT1 and *AtGlcDH*. The arrows in the gene map symbolize the orientation of the genes. AGA6: alanine:glyoxylate aminotransferase; ALAAT1: alanine aminotransferase 1; AtGDH: glycolate dehydrogenase of *A. thaliana*; P35SS/pA35S: promoter and polyadenylation-/ termination sequence from CaMV; bla: β -lactamase gene for selection in bacteria (causes ampicillin and carbenicillin resistance in bacteria); npt II: neomycin-phosphotransferase type II confers resistance to aminoglycoside antibiotics, like kanamycin, and was used for selection of transgenic plants; ColE1 ori: replication origin for vectors in *E. coli*; LB and RB: left and right border sequences of Nopaline-Ti-plasmids pTiT37; PAnos: polyadenylation of Nopaline synthase gene from *A. tumefaciens*; Pnos: promoter of Nopaline synthase gene from *A. tumefaciens*; RK2 ori: replication origin for vectors in *A. tumefaciens*; SAR: scaffold attachment region from the tobacco RB7 gene (ge U67919).

2.1.11 *Escherichia coli* strains

In this study only one strain of *Escherichia coli* was used, the strain DH5 α [F^- , λ , $recA^-$, $endA^-$, $hsdR17$ (r_K^- , m_K^+), ($lacZYA-argF$), $supE44$, U169, $\Phi 80d/lacZ\Delta M15$, thi^-1 , $gyrA96$, $relA1$ (Hanahan, 1983)]. This strain was used for transformation, because the bacterial strain possesses a modified recombination system ($recA^-$), which results in reduced recombination probability, and lacks endonuclease ($endA^-$). *E. coli* was cultivated in LB medium or on LB plates (Table 9) over night at 37°C.

Table 9: Medium for *E. coli* cultivation

Indication	Compound	Final concentration
Luria Bertani (LB) medium	Yeast extract	0.5% (w/v)
	NaCl	1% (w/v)
	Trypton	1% (w/v)
	Agar (for plates)	1.5% (w/v)
For selection	Carbenicillin	100 mg/l

2.1.12 *Agrobacterium tumefaciens* strains

The bacterial strain GV3101 (pMP90RK): Gm^r, Km^r, Rif^r (Koncz and Schell, 1986) was used for transient and stable transformation of plants. This strain contains a non-oncogenic Ti plasmid pMP90RK, which represents a binary vector systems described by the above authors. The vector has two interesting parts for transformation of plants. The first one is the *vir*-region, which code for the enzymes responsible for mediating transduction of T-DNA to plant cells. The other one is the region that contains genes for two antibiotic resistances (gentamycin and kanamycin). The third resistance (rifampicin) is coded by the genome of the *Agrobacterium* itself. After introduction of derivatives of the plasmid, this bacterial strain was used for the transformation of *A. thaliana* plants on the basis carbenicillin (100 mg/l), kanamycin (50 mg/l) and rifampicin (100mg/l). The transformed bacterium was cultivated in YEB medium or on YEB plates (Table 10) for two days at 28°C.

Table 10: Medium for *Agrobacterium tumefaciens* cultivation

Indication	Compound	Final concentration
YEB medium	Beef extract	0.5% (w/v)
	Yeast extract	0.5% (w/v)
	Peptone	0.5% (w/v)
	Saccharose	0.5% (w/v)
	MgSO ₄	0.0492% (w/v)
	Agar (for plates)	8% (w/v)
For selection	Rifampicin	100 mg/l
	Carbenicillin	100 mg/l
	Kanamycin	50 mg/l

2.1.13 Plant material and growth conditions

2.1.13.1 *Arabidopsis thaliana*

In this study plants from the ecotype Col-O were used, independent of *Arabidopsis thaliana* wild type plants (WT) or mutants (Δ Cat2 and Δ Ggat). T-DNA insertion mutants were ordered from the Nottingham Arabidopsis Stock Centre (NASC). Homozygous plants were identified by PCR. Sterilized seeds were germinated on ½ MS plates (Table 11) and the plants were grown under defined conditions. This means 8 h illumination and 16 h darkness (short day conditions) at 22°C in the light period and 20°C during the night. The light intensity was 120 $\mu\text{mol photons/ m}^2 \text{ s}$ and the CO₂ concentration was around 400 ppm (ambient conditions).

The plants were grown for two and a half weeks at the normal conditions and then shifted. The shift depended on the experiment: Some plants were grown at the normal conditions and high CO₂ (2000 ppm) and shifted to low CO₂ (150 ppm) concentrations. After 1 h shift, 6 h and 27 h plant material were harvested for DNA/RNA isolation and gene expression analysis.

Table 11: Medium for plant growth

Indication	Compound	Final concentration
Murashige and Skoog Basal (MS) plate	MS-salt	0.22% (w/v)
	Plant agar	0.7% (w/v)
For selection	Antibiotics	50 $\mu\text{g/ml}$

2.1.13.2 *Nicotiana tabacum*

Nicotiana tabacum L. cv. Petit Havana SR1 was used for the transient transformation of the plasmids. Plants were grown in the green house at long day conditions (16 h illumination and 8h darkness). Six weeks old plants were transiently transformed with *A. tumefaciens*. The leaves were transformed with one plasmid, two plasmids (A215-141, A215-181) or the plasmid containing both genes (A215-307). This resulted in the overexpression of AlaAT1, AtGlcDH and both genes together in a tobacco leaf. After three days incubation, the infected leaves were harvested and mitochondria were isolated to perform further experiments, like measuring the radioactive CO₂ release.

2.2. Methods

2.2 Molecular Methods

2.2.1.1 Isolation of plasmid DNA

Plasmid DNA mini kits (GeneJet Plasmid Miniprep Kit, Fermentas) was used to isolate plasmid DNA from transformed DH5 α bacteria, a competent *E. coli* strain that were transformed with different plasmid-constructs (A215-142, A215-181, A215-307) according to the instructions provided with these kits. The principle of this kit is a SDS-alkaline-lysis of the bacteria cells, so that the plasmid-DNA can be isolated and purified.

2.2.1.2 Combined isolation of DNA and RNA from plant tissue

100 mg plant material was harvested for the isolation of DNA and RNA in a combined method, frozen into liquid nitrogen and homogenized with “ceramic beads”. 500 μ l DNA/RNA extraction buffer (Table 12) was added to the homogenized material and mixed. Afterwards, one volume of water saturated phenol was added and mixed gently for 10 to 15 min on a shaker at room temperature followed by centrifugation at 16000 x g for 10 min. The upper phase was transferred to a new tube and 0.1 volumes of 3 M NaAc (pH 5.2) and two volumes of ethanol (96%) was added and mixed thoroughly. The DNA and RNA were precipitated during the centrifugation at 16000 x g for 10 min at 4°C. The aqueous phase was removed and the resulting pellet was washed by adding 300 μ l 70% ethanol. Afterwards the mixture was centrifuged for 10 min (16000 x g, 4°C). The ethanol was completely removed and after complete drying of the pellet 100 μ l sterile H₂O was added to resuspend the DNA/RNA mixture.

Table 12: Buffers and solutions for DNA/RNA isolation

Indication	Compound	Final concentration
RNA/DNA extraction buffer	Tris-HCl (pH 7.6)	0.05 M
	SDS	0.5%
Precipitate RNA/DNA	NaAc (pH 5.2)	3 M
	EtOH	96%
Washing steps	EtOH	70%

2.2.1.3 Agarose gel electrophoresis

Agarose gel electrophoresis is a common used method in science. This method allows the separation of DNA fragments. The DNA is forced to migrate through an agarose matrix in response to an electric field. Agarose is a polysaccharide, which forms during polymerization a highly cross-linked matrix. Because of this nucleotides with different sizes migrate in different patterns. Large DNA fragments are easier to become enlarged and so they migrate slower through the matrix. Therefore small fragments run more quickly than the bigger fragments. This method was used to confirm the DNA/RNA isolation, the PCR fragments and the fragments of digested plasmids. Depending on the sample the concentration of the agarose gel was changed. On the one hand, a 2% (w/v) agarose gel was used for normal PCR fragments as well as for checking the DNA/RNA isolation. On the other hand, a 1% agarose gel was used to separate different fragments after a digestion. In order to see DNA or RNA on the gel, the gel has to be stained at first. For this 0.2% (v/v) ethidium bromide (1% solution) was added to the liquid agarose gel. Because of the ethidium bromide (Etbr) the DNA or RNA can be seen under ultra violet light. An appropriate amount of 6 x loading buffer (5 μ l) (Table 13) was added to all samples before the electrophoresis. The separation of the RNA molecules occurred generally with 120 V for 60 min in a 1% or 2% agarose gel using TAE buffer (Table 13). To identify the size of the fragments an adequate marker was added to the gel (Figure 7).

Table 13: Solutions and buffers needed for agarose gel electrophoresis

Indication	Compound	Final concentration
Orange G loading Dye (6x)	Glycerol (99,8%)	60%
	EDTA pH 8,0 (0,5 M)	60 mM
	Tris/HCl pH 7,6 (1M)	10 mM
	Orange G	0,03% (w/v)
	H ₂ O	ad to 500 ml
1x TAE-Puffer	Tris-Acetat	40 mM
	EDTA	1 mM

2.2.1.4 Restriction enzyme digestion

Restriction reactions were performed as described in the manufacturer's instruction.

2.2.1.5 Isolation of DNA fragments from agarose gels

To isolate DNA fragments (70 bp - 10 kb) from agarose gels, the Invisorb® Spin DNA Extraction Kit (Invitex, Berlin) was used according to the manufacturer's instruction.

2.2.1.6 Purification of PCR products

The MSB Spin PCRapace kit (Invitex, Berlin) was used to purify PCR products or digested plasmids. The kit was used according to the manufacturer's instruction.

2.2.1.7 Ligation

To ligate to different DNA fragments a defined mixture of vector, insert, buffer and enzyme was prepared (Table 14). The reaction was performed as described in the manufacturer's instruction, except the incubation, which was performed over night at 16°C.

Table 14: Ligation mixture

Compound	Final concentration
Vector/insert	1:3
T4 ligase	2 u
T4 ligase buffer	1 x
H ₂ O	ad 20 µl

2.2.1.8 Polymerase chain reaction

The Polymerase chain reaction (PCR) is a common used technique for enzymatic amplification and modification of a target DNA (Saiki et al., 1988). The target is flanked by two known sequences (a forward and a reverse primer), which are complementary to the (+) and (-) strand of the DNA. The new strand fragments are synthesized between the two primers by the catalysis of a *Taq* DNA polymerase. The amplification of the target sequence is performed by repeating different steps. In the first step the DNA is denatured, followed by the annealing of the complementary primers and, finally, the extension of the annealed primers (Saiki et al., 1988). Repeating the cycles of denaturation, primer annealing and extension results in an exponential accumulation of the target DNA fragment. The newly created DNA strands are themselves templates for the PCR primers. The reaction conditions (e.g. template concentration, annealing temperature and extension duration) were optimized for individual experiments on the basis of standard conditions (Table 15). Two important

conditions, which were mostly changed, were the template concentration and the annealing temperature of the primers (Table 16). The standard annealing temperature was 60°C, but to analyze the segregation of the T-DNA mutants the annealing temperature was changed to 58°C. The concentration of the samples was changed depending of the DNA concentration. Highly concentrated templates were diluted and more volume was used, if the concentration of DNA in the sample was low. The primer systems for the identification of the different genotypes are shown in Table 17.

Table 15: Standard PCR mixture

Compound	Final concentration
10 x DreamTaq Buffer	1 x
dNTP mix	200 µM
Forward primer	0.2 µM
Reverse primer	0.2 µM
Taq polymerase	0.02 µM
Template	0.2 pg – 2 ng/µl
H ₂ O	ad 25 µl

Table 16: Standard PCR conditions

Reaction step	Temperature	Duration	Cycle
Initial denaturation	95°C	5 min	1 x
Denaturation	95°C	30 sec	35 x
Annealing	50-60°C	90 sec	
Elongation	72°C	30 sec	
Deactivation	72°C	5 min	1 x
Rest	9°C	∞	

Table 17: Primer systems for identification of the different genotypes

Gene	Primer system	Fragment	Fragment size
Actin	584 + 585	Control isolation	100 bp
ΔCat2	5042 + 5043	genomic	746 bp
	5042 + 4574	T-DNA insert	993 bp
ΔGgat	4162 + 4162	genomic	949 bp
	4162 + 4754	T-DNA insert	733 bp
ΔAtGlcDH	4702 + 4703	genomic	1045 bp
	4703 + 4574	T-DNA insert	750 bp
35S-AlaAT1	3953 + 2810	check insertion	390 bp
35S-AtGlcDH	3953 + 3041	check insertion	760 bp
35S-CrGlcDH	2994 + 3301	check genotype	250 bp
35S-EcGlcDH	2994 + 3289	check genotype	450 bp

2.2.1.9 Multiplex PCR

In this type of PCR, it is possible to amplify more than one DNA fragment using more than one primer pair in the same PCR reaction mixture (Table 18). In this study this method was used to amplify the intern control *Actin2* together with the transgenic glycolate dehydrogenase from *Chlamydomonas reinhardtii* (*CrGlcDH*) and *Escherichia coli* (*EcGlcDH*). The standard multiplex PCR conditions were used for fragment amplification (Table 16).

Table 18: Multiplex PCR mixture

Compound	Final concentration
10 x DreamTaq Buffer	1 x
dNTP mix	200 μ M
Primer 1	0.2 μ M
Primer 2	0.2 μ M
Primer 3	0.2 μ M
Primer 4	0.2 μ M
<i>Taq</i> polymerase	0.02 μ M
Template	0.2 pg – 2 ng/ μ l
H ₂ O	ad 25 μ l

2.2.1.10 First strand cDNA synthesis from RNA

The complementary DNA (cDNA) is synthesized during a process catalyzed by the enzyme reverse transcriptase. Therefore a messenger RNA (mRNA) is used as a matrix, which is needed for the transcription to a complementary DNA strand.

The isolated DNA/RNAs samples from *Arabidopsis* wild type (WT), mutants or transformed plants were digested with DNase enzyme to remove the genomic DNA in the sample. The reaction mixture (Table 19) was incubated for 30 min at 37°C followed by an inactivation of the enzyme for 15 min at 70°C. After that 1 μ l of a “random nanomer” primer (primer number 549) was added. This primer attached to the messenger RNA during an incubation of 5 min at 75°C with following cooling on ice. Furthermore 7 μ l of the RT-reaction mix (Table 20) was added to each sample. The mixture was incubated for 1 h at 37°C. The reaction was inactivated at 70°C for 10 min. For negative samples, the enzyme was not added but all other conditions were equal. In the negative samples no cDNA should be synthesized and no signal should occur in the followed experiments. Some samples were diluted 1:4 and 1:16 with H₂O before cDNA synthesis. These samples represent the intern control of the reaction. After inactivation of the RT enzyme, the preparations were diluted 1:2. The resulting cDNA samples were used as a template for gene expression analysis (qPCR).

Table 19: Digestion of DNA

Compound	Final concentration
DNase I	1 u
DNase I buffer	1 x
RNA	1-5 µg
H ₂ O	ad 12 µl

Table 20: Reverse transcriptase reaction mix

Compound	Final concentration
dNTP mix	20 nmol
MMLV buffer	1 x
MMLV RT	200 u
H ₂ O	7 µl

2.2.1.11 Quantitative real-time polymerase chain reaction

The quantitative real-time polymerase reaction (qPCR) is also called real time polymerase chain reaction (RT-PCR). The method is based on a PCR, which is used to amplify and quantify a target DNA molecule at the same time. The quantification can be an absolute quantification or a relative amount, which is normalized to the DNA concentration or to the expression level of a house keeping gene. The detection of products is based on a non-specific fluorescence dye. This fluorescence dye interacts with double stranded DNA and is activated by light with a defined wave length. In this study, the fluorescence dye Platinum® SYBR® Green qPCR SuperMix-UDG with Rox (Life Technologies (Carlsbad, USA) was used. This dye was added to each sample, together with the master mix (Table 21). The accumulation of PCR products can be visualized by plotting the fluorescence of the interacting dye against the cycle number. The fluorescence is recorded by a camera during the exponentially phase of the developing product. This results in a visualization of this a sigmoidal curve. A dilution series was measured to control the linearity of the exponential phase. Another control was testing the product- and/or primer specificity during the qPCR. To test the product specificity, a dissociation curve was recorded at the end of the qPCR (Table 22). The dissociation curve was formed as a result of plotting the first deviation of the fluorescence against the melting temperature. The identification of the dissociation curve helps to identify specific primer products. The primer system was checked by visualizing the qPCR products on 2% (w/v) agarose gel containing ethidium bromide.

Table 21: Quantitative real-time polymerase chain reaction mix

Compound	Final concentration
Platinum® SYBR® Green SuperMix	1 nM
Primer A	0.2 µM
Primer B	0.2 µM
Template	0.2 pg – 2 ng/µl
H ₂ O	ad 20 µl

Table 22: Quantitative real-time polymerase chain reaction conditions

Reaction step	Temperature	Duration	Cycle
Initial denaturation	95°C	2 min	1 x
Denaturation	95°C	0.25 min	40 x
Elongation	60°C	2 min	
Dissociation curve	60°C - 95°C		1 x

2.2.1.12 Sequencing

The sequencing reactions were performed using the di-desoxy chain termination method with labeled nucleotides and a cycle sequencing protocol (Sanger *et al.*, 1977). The reaction was performed by the SeqLab company. For this 600-700 ng plasmid was mixed with 20 pmol of the used primers followed by adding water to a volume of 7 µl.

2.2.2 Microbiological Methods

2.2.2.1 Transformation of competent bacteria by heat-shock

The competent *E. coli* DH5α cells were stored at -80°C and defrosted on ice before using. Plasmid DNA (10-100 ng) or the ligated products (1-3 µl) were added to the competent cells, gently mixed and when incubated on ice for 30 min. After heat-shocking (45 sec at 42°C) the mixture was rested on ice. 1 ml of LB medium was added immediately to the tubes containing the heat-shocked bacteria. The transformed cells were incubated at 37°C for 60 min with continuous shaking (180 x g). A dilution series of the bacteria were performed. 50 µl and 100 µl of the diluted transformed bacteria were placed on LB-agar plates supplemented with antibiotics (Table 9) and incubated at 37°C overnight.

2.2.2.2 Transformation of *Agrobacterium tumefaciens* by electroporation

Competent *A. tumefaciens* cells were stored at -80°C and defrosted before using. In water resuspended plasmid DNA (0.2-1.0 µg) was added to the *Agrobacteria* and incubated on ice for some minutes. The DNA/cell mixture was transferred into an electroporation cuvette. After application of the pulse (25 µF/2.5 kV/200 Ω), the cells were diluted in 1 ml of YEB medium in a new tube and incubated at 28°C with shaking (200 x g) for 60 min. Finally, 50 µl and 100 µl of the transformed cells were placed on YEB-agar plates containing rifampicin (rif, 100 µg/ml), carbenicillin (carb, 100 µl/ml) and kanamycin (kan, 50 µg/ml) (Table 10). The plates were incubated at 28°C for three to four days.

2.2.2.3 “Floral-dip”-transformation of *Arabidopsis thaliana*

The transformation of *Arabidopsis* plants were performed as described by Clough and Bent (Steven J. Clough and Andrew F. Bent, 1998 Clough and Bent, 1998). At first, the bacteria have to be prepared. Therefore, different colonies of transformed *Agrobacteria* were picked and the vector was checked by a PCR. Positive colonies were inoculated into 5ml YEB-medium including the antibiotics (Table 10) to prepare the pre-culture. The cultures were incubated at 28°C over night with continuous shaking (180 x g). The pre-culture was transferred into 200 ml fresh YEB-medium, which contains antibiotics, and incubated again at 28°C for 2 days with shaking (180 x g). This culture was used to inoculate 800 ml YEB-medium containing antibiotics. The new culture was incubated at 28°C until an OD₆₀₀ of 1.0 was reached. Cells were spun down at 3000 x g at 4°C for 20 min. The pellet was resuspended with infiltration medium (Table 23).

Table 23: Composition of the 2x infiltration medium

Indication	Compound	Final concentration
2x Infiltration medium	MS	8.86 g/l
	Sucrose	100 g/l
	MES	20 mM

Arabidopsis wild type plants or mutants were allowed to grow for three weeks at short day conditions (8 h light at 22°C, 16 h dark at 20°C) on plates and when transferred into soil. After two weeks growing in soil, the plants were shifted to long day conditions (16 h light at 20°C and 8 h dark at 22°C) to enhance flower production. Open and fertilized blossoms were clipped. The above ground parts of the *Arabidopsis* plants were dipped in the *Agrobacterium* solution three times for 3 to 5 min each (Figure 10). The dipped plants were placed under a

cover for 24 h in order to maintain high humidity. The plants were then transferred to long day growth conditions (16 h light at 20°C and 8 h dark at 22°C) until the seeds were matured.



Figure 10: „Floral-dip“-transformation of *Arabidopsis thaliana* plants (Niessen, 2008).

2.2.2.4 Transient transformation of *Nicotiana tabacum* leaves

Positive colonies of transformed *Agrobacteria* were cultured as described (2.2.2.3). A single positive colony was picked and inoculated into 5 ml YEB-medium including antibiotics (rif 100 µg/ml, carb 100 µg/ml and kan 50 µg/ml). This pre-culture was incubated for 2 days at 28°C at continuous shaking (180 x g). The pre-culture was then transferred into 100 ml fresh YEB-medium, which contains antibiotics, and incubated at 28°C for overnight at shaking (180 x g). Cells were spun down at 3000 x g at 4°C for 10 min. The pellet was resuspended with 2x infiltration medium (Table 23) including 0.2 mM acetosyringone until the OD₆₀₀ of 0.4 was reached. The mixture was incubated for 30-60 min at room temperature without shaking. After this, the solution was infiltrated with a syringe into the leaf (Sparkes et al., 2006). Plants used for transformation were five to six weeks old. To handle the procedure easily the plants were watered 30 min before infiltration or the bottom of the leaf was carefully scratched with a yellow tip. The infiltrated plants were incubated for 3 days at normal growing conditions (long day conditions: 16 h light and 8 h dark).

2.2.3 Biochemical methods

2.2.3.1 Isolation of mitochondria from transient transformed *Nicotiana tabacum* leaves

To investigate the enzyme activities in a defined cell compartment, this compartment has to be isolated. For the isolation of mitochondria 5-10 g leaf material, which was transient transformed, (2.2.2.1) from five to six weeks tobacco plants were incubated into ice-cold grinding buffer (GB, Table 24). The cells were ground with a homogenizer by using an adequate volume of pre-cooled GB followed by filtration through three layers of miracloth. The chloroplasts were pelleted by centrifugation at 1100 x g for 20 min at 4°C. The supernatant was transferred into a new tube and then centrifuges again at 14000 x g for 30 min at 4°C (Sorvall centrifuge). The resulting pellet was resuspended in 1 ml 1 x Mannitol-wash-buffer (MB, Table 24) and transferred to a saccharose-percoll-gradient (Table 24) followed by another centrifugation at 40000 x g for 45 min at 4°C (ultra-centrifuge). Because of the last centrifugation the mitochondria were separate from the chloroplast and peroxisomes. The mitochondria were present in light white cloud at the bottom of the gradient. Chloroplast and Peroxisomes were at upper part of the gradient (Figure 11) in a green coat. The upper part of the gradient was thrown away and the mitochondria were slightly transferred to a new 1.5 ml tube. The mitochondria were washed with one volume MB and centrifuged at 16000 x g for 20 min at 4°C. The supernatant was carefully taken off and the mitochondria protein was extracted by resuspending the pellet in 50-150 µl of extraction buffer (Table 24). The mixture of mitochondria pellet and extraction buffer was incubated on ice for 10 min. After this time the mixture was centrifuged to separate the proteins from the cell brunches. The isolated protein was used for further experiments. The protein concentration was determined according to Bradford (2.2.3.3).

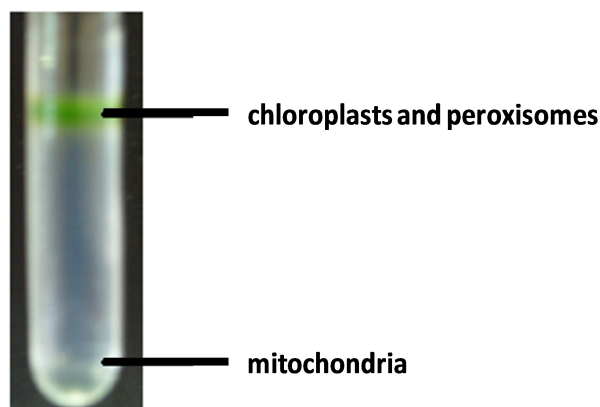


Figure 11: Gradient after ultra-centrifugation. Pictured is a 45% percoll gradient after ultra-centrifugation. The gradient was loaded with 500 µl of a mitochondria extract. Chloroplast and peroxisomes are mainly located in the green upper part of the gradient. Mitochondria were mainly located in the lower part of the gradient in a white cloud. (Niessen, 2008, modified).

Table 24: Buffers and solutions needed for mitochondria isolation

Indication	Compound	Final concentration
Grinding buffer (GB)	Hepes-KOH	50 mM
	MgCl ₂	1 mM
	EDTA	1 mM
	BSA	1 g/l
	Na-Ascorbat	0.2 g/l
	Mannitol	0.3 M
	Polyvinylpyrrolidone	5 g/l
Mannitol washing buffer (MB)	Mannitol	0.3 M
	Hepes-KOH	10 mM
	BSA	1 g/l
Sucrose washing buffer (2x) (SB)	Sucrose	0.3 M
	Hepes-KOH	10 mM
	BSA	1 g/l
Saccharose percoll gradient	Sucrose washing buffer (2x)	50%
	Percoll	45%
	H ₂ O	5%
Extraction buffer	Hepes-KOH pH 7.5	50 mM
	EDTA	2 mM
	MgCl ₂	5 mM
	Triton X-100	0.1%

2.2.3.2 Determination of protein concentrations in mitochondria extracts

Proteins were determined according to the method described by Bradford (Bradford, 1976). 1 µl of leaf protein extract was mixed with 199 µl of Bradford reagent (Table 25). After 5 min incubation at RT, the basic extinction at 595 nm was measured against a reagent blank prepared from 1 µl of the corresponding extraction buffer and 199 µl of Bradford reagent. The extinction was measured with the ELISA, which can use a small volume. To determine the protein concentration, a bovine serum albumin pH 7.0 (Serva) was used as a standard in a range between 1 and 10 µg.

Table 25: Bradford reagent

Compound	Final concentration
Coomassie Brilliant Blue G 250	100 mg/l
Ethanol 96% (v/v)	50 ml/l
Phosphoric acid 85% (v/v)	100 ml/l

2.2.3.3 Feeding of ^{14}C -glycolate to mitochondria extracts

0.1 mM [1,2- ^{14}C]glycolate (Hartmann Analytics, Braunschweig, Germany) was added to a mitochondrial extract corresponding to 50 μg protein. Specific radioactivity of ^{14}C -glycolate was 1850 MBq mmol^{-1} . Samples were incubated overnight at room temperature and released CO_2 was absorbed in 0.5 M NaOH under continuous mixing with a rotating magnet stir. The absorbed CO_2 was transferred to a scintillation tube and 1 ml liquid scintillation cocktail (Optiphase 'Highsafe' 2; Perkin Elmer, Waltham, USA) was added. The two liquids were gently mixed followed by measuring radioactive CO_2 release by a scintillation counter (Ls 5000TD, Beckmann, USA).

2.2.3.4 Isolation of metabolites

Plants were grown for 3 weeks at high CO_2 concentrations and then shifted to low CO_2 concentrations to isolate metabolites. Twenty plants were harvested for each genotype from the crossing of catalase 2 knock-out mutants ($\Delta\text{Cat}2$) with the glycolate dehydrogenase of *Chlamydomonas reinhardtii* (35S-*CrGlcDH*) and from the crossing of $\Delta\text{Cat}2$ with the glycolate dehydrogenase of *Escherichia coli* (35S-*EcGlcDH*). All genotypes from one crossing were grown side by side in a styrofoam box on soil. Thus, all four genotypes from the crossing of $\Delta\text{Cat}2$ with 35S-*CrGlcDH* were grown in the same styrofoam box including $\Delta\text{Cat}2$, $\Delta\text{Cat}2/35\text{S-}CrGlcDH$, azygous plants (az) and 35S-*CrGlcDH*. The same was done for the plants from the crossing of $\Delta\text{Cat}2$ with 35S-*EcGlcDH* ($\Delta\text{Cat}2$, $\Delta\text{Cat}2/35\text{S-}EcGlcDH$, az and 35S-*EcGlcDH*). Azygous plants (az) behave like wild type plants, because they do not possess the T-DNA insertion of $\Delta\text{Cat}2$ mutants and no overexpression vector.

Plants were harvested after 6 h light exposure under high CO_2 concentrations as well as under low CO_2 concentrations. After genotype identification, ten plants of the same genotype were pooled, grinded and stored at -80°C . Two spoons grinded material (ca. 40 mg) were used for metabolite isolation. Ice cold extraction buffer (1 ml, Table 26) was added to the frozen material including 5 μl of ^{13}C -sorbitol stock solution (Table 27) as an internal standard. The samples were mixed for 4-6 min at 4°C and afterwards centrifuged for 2 min at 4°C leading to a separation of two phases. 500 μl of the upper phase were transferred to a new tube and 250 μl of ultra-pure water was added. The compounds were mixed for 10 sec and again centrifuged for 2 min at 4°C . The metabolites are localized inside the upper phase. In the final step of the isolation, 250 μl of the upper phase were transferred to a micro-input. The rest of the upper phase was stored at -20°C as backup. The tube containing the micro-input was spaced into a vacuum pump. Overnight liquids were vaporized and metabolites were pelletized.

The derivatization of the samples was done by a program of Gerstel MPS and metabolites were separated by gas chromatography followed by the detection by mass spectrometer. Single compounds were identified using the programs Pegasus and Tagfinder 4.1.

Table 26: Extraction buffer for metabolites

Compound	Mixture
H ₂ O (ultra-pure)	1
Methanol (ultra-pure)	2.5
Chloroform (ultra-pure)	1

Table 27: Sorbitol stock solution

Compound	End concentration
¹³ C-sorbitol	2 mg/ml

2.2.4 Physiological Methods

2.2.4.1 Generation of double mutants

Arabidopsis mutants were allowed to grow for three weeks under short day conditions (8 h light at 22°C, 16 h dark at 20°C) on plates and then transferred into soil. After two weeks growing in soil, the plants were shifted to long day conditions (16 h light at 20°C and 8 h dark at 22°C). These conditions enhanced flower production. Open blossoms and fertilized ovary were clipped. Closed florescences were used for the crossing procedure (Figure 12). At first, the blossom was opened and one sepal was removed. After this, the other sepals and petals were carefully removed. So, only the stamen and the female part of the blossom remained. The stamen was removed very carefully. The anther should not be destroyed to prevent fertilization. After every except the female one was removed (mother plant), the stigma was fertilized by using the anther of the other mutant (father plant). After two or three days the style and the ovary should be thicker, this means that the flower was fertilized. The crossed plants were grown under long day conditions until the seed-capsules were brown and dry. The seeds were harvested and grown again. The identification of the genotypes was done by DNA/RNA isolation (2.2.1.2), followed by PCR (2.2.1.8). The plants were identified in the F₂ generation (Table 28) and defined genotypes (needed genotypes for the experiments) were grown until the third generation was reached. For the experiments four genotypes were used: homozygous plants for the *Cat2* knock-out mutation (Δ Cat2), homozygous plants with the Δ Cat2 mutation including overexpression (Δ Cat2/35S-*EcGlcDH* or Δ Cat2/35S-*CrGlcDH*),

azygous plants (az, wild type like plants) and the overexpression mutants without the Δ Cat2 mutation (35S-*Cr*GlcDH or 35S-*Ec*GlcDH).

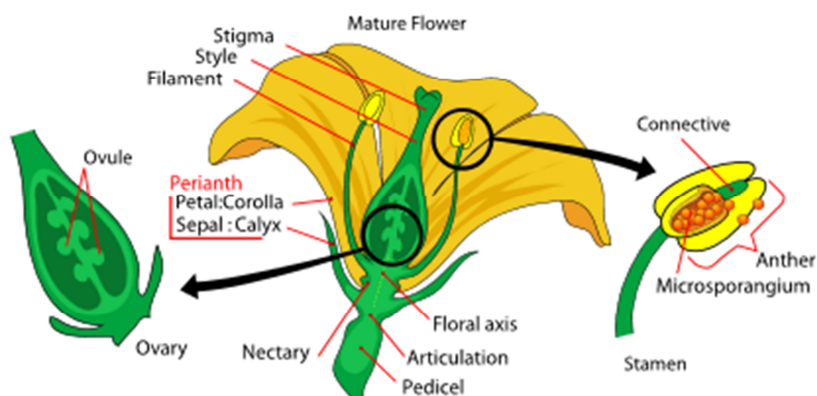


Figure 12: Diagram showing the main parts of an ambisexual blossom.

(http://upload.wikimedia.org/wikipedia/commons/7/7f/Mature_flower_diagram.svg; 17.03.2013)

Table 28: Segregation of the F₁ and F₂ generation of crossed *Arabidopsis* plants. (A): crossing of homozygous Δ Cat2 mutants with hemizygous overexpressors (35S-*Cr*GlcDH or 35S-*Ec*GlcDH). (B): crossing of Δ Cat2 mutants with homozygous Δ AtGlcDH mutants. Small letters represent the knock-out mutation of a gene and big letters the overexpression of a gene. A symbolizes the cat2 gene, B the overexpressed genes (35S-*Cr*GlcDH or 35S-*Ec*GlcDH) and C the AtGlcDH gene.

(a)	F1		F2			
	aabb	AABb	AB	Ab	aB	ab
		AaBb	AB	AAbb	AaBB	AaBb
			Ab	AAbb	AaBb	Aabb
			aB	AaBB	aaBB	aaBb
			ab	AaBb	aaBb	aabb

(b)	F1		F2			
	aaCC	AAcC	AC	Ac	aC	ac
		AaCc	AC	AACc	AaCC	AaCc
			Ac	AACc	AaCc	Aacc
			aC	AaCC	aaCC	aaCc
			ac	AaCc	aaCc	aacc

2.2.4.2 Chlorophyll fluorescence

In this study a pulse amplitude modulated fluorometer was used allowing measurements of fluorescence parameters and visualization of the resulting data. This is the so called Imaging-PAM system. Whole plants were dark adapted for 30 min to oxidize all reaction centers of the PSII. The dark adaption was followed by an initial light pulse of saturated light. This allows the detection of the maximal possible photosynthetic efficiency (F_v/F_m). The initiated light pulse was followed by a pulse series of saturated light with durations of 20 sec. After the initial light pulse measuring light, also called actinic light, was switched on. The series of saturated light pulses and the exposure to actinic light allows the detection of photosynthetic capacity in light situations ($Y(II)$). To get the best results the actinic light had the same intensity as the light conditions, in which the plants were grown. In this case, the actinic light intensity was 145 PAR (equates to $\sim 120 \mu\text{mol}/\text{m}^2 \text{ sec}$). The saturated light pulse overwhelms the electron acceptor pools and the difference between dark adapted plants and light adapted plants is the redundant energy loss by fluorescence. Energy can also be dissipated as heat and this is called non-photochemical quenching (NPQ). The fluorescence measurement was done for 30 min. After 30 min the F_v/F_m was determined and $Y(II)$ as well as NPQ was calculated using the steady state value of light adapted plants.

3 Results

3.1. Characterization of photorespiratory mutants

Defined mutants have to be chosen to investigate the influence of alternative pathways on the main photorespiratory pathway. Most photorespiratory mutants show lethal phenotypes at ambient air conditions, but few of them only show chlorotic spots and reduced growth when they are grown under this conditions. The catalase 2 (ΔCat2) mutant and the glutamate:glyoxylate aminotransferase (ΔGgat) were the mutants of choice. Both mutants are viable under ambient air and show the described phenotype when they are grown under this condition (Igarashi et al., 2003; Igarashi et al., 2006; Queval et al., 2007). These phenotypes were exacerbated when the plants were grown at low CO_2 concentrations. At high CO_2 conditions, a WT-like phenotype was observed.

At the start of my investigations I wanted to test the best parameters to characterize the mutants at normal growth conditions and under shifting conditions, thereby plants were grown at high CO_2 concentrations (1500-2000 ppm) and then shifted to ambient CO_2 (400 ppm) or even low CO_2 concentrations (150 ppm). The defined parameters should also be used for the investigation of the resulting genotypes from the crossing of main photorespiratory mutants and overexpressors or knock-outs of the alternative side pathways. T-DNA insertion mutants were ordered from the Nottingham Arabidopsis Stock Centre (NASC) and homozygous lines were identified by PCR (see 2.2.1.10).

Homozygous photorespiratory mutants (ΔCat2 , ΔGgat and $\Delta\text{AtGlcDH}$) and wild type plants were grown on plates at ambient air conditions for three weeks and chlorophyll fluorescence was measured (Figure 13). Three parameters were investigated to get a general overview about the photosynthetic performance of the used genotypes. The first parameter was the F_v/F_m value, which represents the maximal quantum yield of a plant (see 2.2.4.2). The second was the $Y(\text{II})$, the photosynthetic yield under the current light conditions and the third value was the non-photochemical quenching (NPQ) indicative of heat dissipation of excess energy. My hypothesis was that the photorespiratory mutants should perform different from the wild type depending on the parameter. I expected that the F_v/F_m and the $Y(\text{II})$ value of the knock-out mutants would be lower than the WT and the NPQ value bigger.

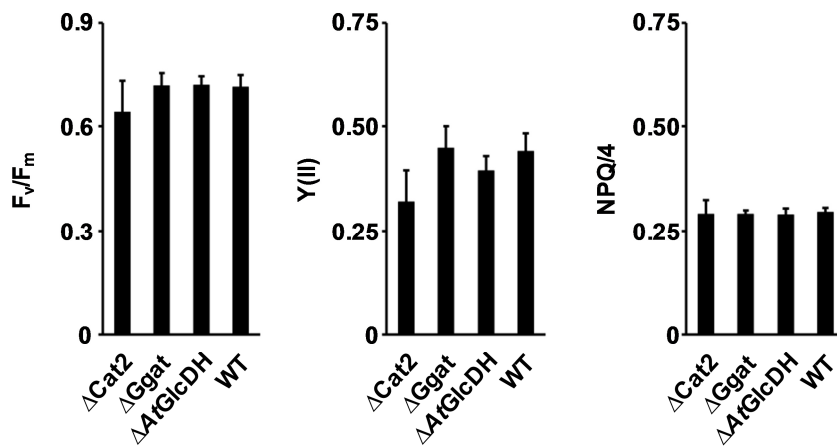


Figure 13: Chlorophyll-fluorescence of photorespiratory mutants and wild type (WT) plants at ambient air conditions (400 ppm CO₂). $\Delta Cat2$, $\Delta Ggat$, $\Delta AtGlcDH$ and WT plants were grown for three weeks on 1/2 MS plates and F_v/F_m (maximal quantum yield), $Y(II)$ (photosynthetic yield) and NPQ (non-photochemical quenching) were recorded using Imaging-PAM (2.2.4.2). The measurement was done for 30 min using a pulse of 20 sec between the saturated light pulses and an actinic light of 120 μE . Shown are the means $\pm SE$ from 3 independent experiments and at least 10 individuals per experiment for each genotype.

Figure 13 shows all three parameters. The $\Delta Cat2$ mutant showed the clearest differences compared to the wild type. The F_v/F_m value and the photosynthetic yield ($Y(II)$) were reduced, but interestingly the NPQ was not significantly affected. The other two photorespiratory mutants did not show differences compared to WT. Only the $\Delta AtGlcDH$ mutant was characterized by a slightly lower photosynthetic yield compared to WT. WT plants were characterized by a F_v/F_m value of about 0.78, which is lower than expected, because healthy plants have a theoretical F_v/F_m value of about 0.83 (Björkman and Demmig, 1987; Papageorgiou and Govindjee, 2005).

The outcome of this experiment was that $\Delta Cat2$ mutants were stressed at ambient air conditions, whereas the other two mutants, $\Delta Ggat$ and $\Delta AtGlcDH$, were not stressed under these conditions. In order to apply a stronger stress plants were grown for 3 weeks at ambient air conditions (400 ppm CO₂) and were then shifted for four days to low CO₂ concentrations (150 ppm CO₂). This shift should induce a more significant stress and the differences between WT and photorespiratory mutants were expected to be clearer.

Figure 14 demonstrates the results of measuring the chlorophyll fluorescence of stressed plants. The parameters were determined after the plants had been shifted for four days. Plants not treated were grown alongside as a positive control. All shifted genotypes showed a reaction to the new situation. A slight reduction in maximal photosynthetic capacity (F_v/F_m) compared to the value at ambient air conditions was observed in all described genotypes. The $\Delta Cat2$ mutant showed the most noticeable reaction to CO₂ stress. Maximal photosynthetic yield as well as non-photochemical quenching was reduced. The reduction of $Y(II)$ was over 50% compared to the value at ambient air conditions. Beside this, no differences compared to WT could be observed in the F_v/F_m value independent of whether

values were obtained at ambient CO₂ concentrations or low CO₂ concentrations. Again a lower F_v/F_m value of the WT plants was detected (0.75) than expected (0.83). This phenomenon was observed throughout the whole experiment giving rise to the assumption that the growing plants on ½ MS plates had an impact on the F_v/F_m value. The theoretical maximal quantum yield was determined by measuring plants in the natural environment growing on soil (Ritchie, 2006).

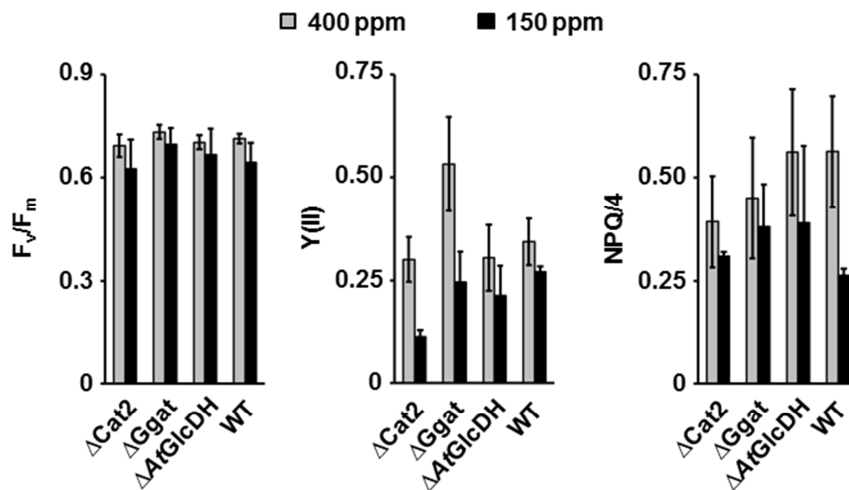


Figure 14: Chlorophyll fluorescence of photorespiratory mutants and WT plants under CO₂ stress. Three weeks old plants were shifted for four days from ambient CO₂ concentration (400 ppm) to low CO₂ concentrations (150 ppm). Half of the plants were still grown at ambient air conditions. Chlorophyll-fluorescence parameters, F_v/F_m (maximal quantum yield), Y(II) (photosynthetic yield) and NPQ (non-photochemical quenching) were recorded using Imaging-Pam (2.2.4.2). The measurement was done for 30 min using a pulse of 20 sec between the saturated light pulses and an actinic light of 120 μ E. Shown are the means \pm SE from 3 independent experiments and at least 10 individuals per experiment for each genotype.

On the one hand, the Δ Ggat mutant showed no differences in the F_v/F_m value compared to the WT at ambient CO₂ concentrations as well as at low CO₂ concentrations. Although a slight reduction was observed at low CO₂ concentrations compared to ambient CO₂ concentrations in the Δ Ggat background. On the other hand, slight differences between the Y(II) at ambient CO₂ concentrations could be observed compared to WT. This difference between Δ Ggat and WT was not detectable at low CO₂ concentrations. The Ggat mutant showed a reduction of 50% in the Y(II) value in comparison of the ambient CO₂ value and low CO₂ value, which is similar to the observation in the Δ Cat2 background.

Δ AtGlcDH showed a similar reaction to the CO₂ stress as WT plants. The F_v/F_m value changed only slightly as well as the Y(II) and the NPQ value. No differences between Δ AtGlcDH and WT could be found.

In summary only the Δ Cat2 mutant reacted noticeable to the changed CO₂ concentrations. The other two genotypes, Δ Ggat and Δ AtGlcDH, behaved like the WT, no striking differences were observed. This fact opposes the hypothesis that the three photorespiratory mutants

differ from the WT in F_v/F_m , $Y(II)$ and NPQ. Several reasons can influence the unexpected behavior of the mutants. For one, the gene might still be expressed like in the WT plants or only down regulated instead of completely knocked out. For another, the CO_2 stress may not be strong enough to see an effect in the $\Delta Ggat$ and $\Delta AtGlcDH$ mutants. To investigate the gene expression level of the knocked out gene in the mutant background compared to the WT, RNA was isolated from plants grown at ambient air conditions (2.2.1.2) and cDNA synthesized (2.2.1.10), followed by qPCR analysis (2.2.1.11). Figure 15 shows the relative expression levels of the knocked out genes in the mutant background and WT. Gene expression was standardized to *Actin2*. The $\Delta Cat2$ mutant showed the greatest reduction in RNA abundance compared to WT. The expression level of *Cat2* was only 5% of WT expression level. However, the expression level was only reduced to 30-40% in both $\Delta Ggat$ and $\Delta AtGlcDH$ mutants compared to WT. Following experiments revealed that $\Delta AtGlcDH$ mutant were knock-out mutants with a remaining gene expression of 10-20% compared to WT (data not shown).

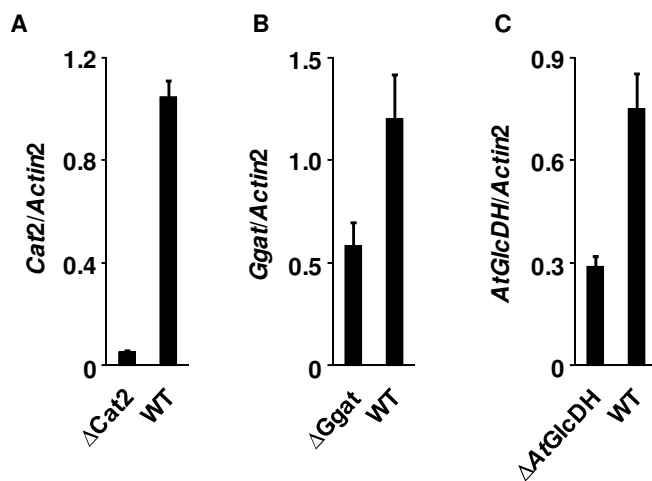


Figure 15: Relative gene expression of knocked out genes in the mutant background. A: relative *Cat2* expression in $\Delta Cat2$ mutants and wild type (WT) plants. B: relative *Ggat* expression in $\Delta Ggat$ mutants and WT and C: expression of *AtGlcDH* in the knock-out mutant background. Gene expression was standardized to the abundance of the *Actin2* transcript. Shown are the means \pm SE from 3 independent experiments and at least 6 individuals for each experiment and genotype.

Due to the inefficient knock-down and the high remaining photosynthetic activity, $\Delta Ggat$ and $\Delta AtGlcDH$ were excluded from the further Imaging-PAM analysis. However, $\Delta Ggat$ were still used to cross these plants with 35S-*EcGlcDH* or 35S-*CrGlcDH* plants as a second photorespiratory mutant in the major pathway. Also $\Delta AtGlcDH$ were still used for crossing with $\Delta Cat2$ and $\Delta Ggat$ for the combination of mutants of the major photorespiratory pathway with a mutant in a side pathway.

In the next experiment mutants were grown up at high CO₂ concentrations (1500 ppm). The shifting conditions were changed, because the investigations should start from a situation without a photorespiratory effect and plants were only afterwards pushed into photorespiratory conditions. Thus, Δ Cat2 and WT plants were growing now at high CO₂ concentrations (1500 ppm) for 3 weeks and then shifted to ambient CO₂ concentrations (400 ppm).

Figure 16 shows the results of measuring the chlorophyll fluorescence of shifted plants at different times after the shift. The individual experiments were shown separately, because the curves of the replicates were slightly different. WT plants and Δ Cat2 were grown side by side. The Δ Cat2 mutants showed significant differences in the F_v/F_m (ttest, $p \leq 0.008$), $Y(II)$ (ttest, $p \leq 0.003$) and NPQ (ttest, $p \leq 0.006$) values compared to WT in all three experiments from day five to day nine.

In the first experiment, Δ Cat2 mutants showed a reduced F_v/F_m compared to WT plants starting from day four after the shift. This was reproducible in the second and third experiment. For $Y(II)$, lower values in Δ Cat2 compared to WT were observed from day five on in all three experiments. Differences became significant in experiment two from day six on and in experiment three from day five on. No other differences were significant with $p < 0.05$. The NPQ value of the Δ Cat2 mutant did not differ at high CO₂ concentrations compared to WT. The difference between Δ Cat2 and WT plants appeared after one day at ambient CO₂ concentrations and grew with longer exposure to ambient CO₂ conditions. The resulting difference was observed during the whole shift and did not change, except in the first experiment. Here the Δ Cat2 showed only differences from four days after shifting up to eight days after shifting compared to WT. On day nine the differences disappeared and both genotypes reached the same NPQ value.

Together, Δ Cat2 mutants showed reduced F_v/F_m and $Y(II)$ values from five to nine days after treatment. Unexpectedly, NPQ was also reduced in Δ Cat2 mutants compared to WT plants.

The chlorophyll fluorescence measurement is a good method to investigate the differences in photosynthetic performance between the Δ Cat2 mutant and WT.

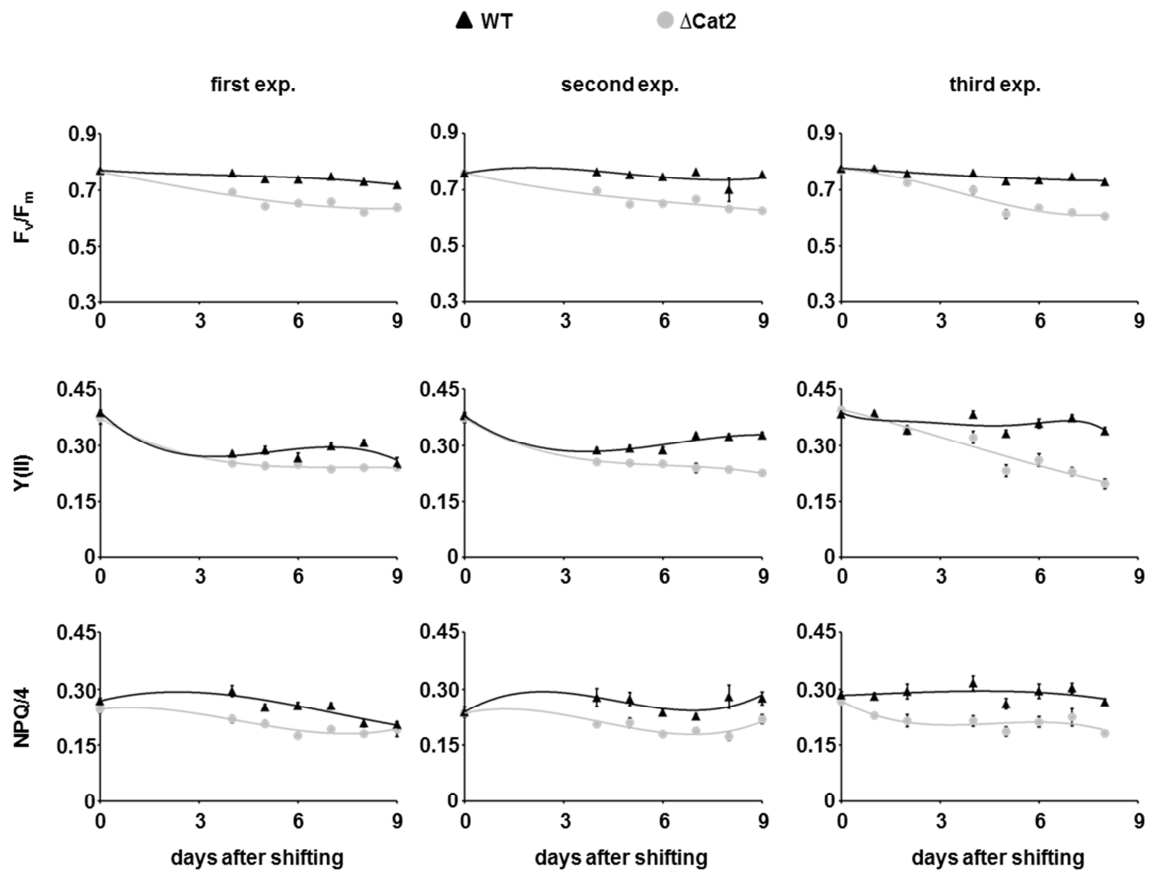


Figure 16: Chlorophyll-fluorescence of Δ Cat2 and WT plants during a shift from high CO_2 concentration to ambient CO_2 concentrations. Three weeks old plants were shifted for nine days from high CO_2 concentration (1500 ppm) to ambient CO_2 concentrations (400 ppm). Chlorophyll-fluorescence parameters, F_v/F_m (maximal quantum yield), $Y(II)$ (photosynthetic yield) and NPQ (non-photochemical quenching) were recorded every day using Imaging-Pam (2.2.4.2) starting at high CO_2 concentration (0 days after shifting) and ending at 9 days after shifting. The measurement was done for 30 min using a pulse of 20 sec between the saturated light pulses and an actinic light of 120 μE . Shown are means \pm SE from three independent experiments with at least 10 individuals for each genotype.

A second parameter was added to the characterization of the photorespiratory mutant. It is known that photorespiratory hydrogen peroxide (H_2O_2) accumulated in Δ Cat2 mutants, so that genes of the oxidative signaling pathway were already induced at ambient CO_2 conditions (Queval et al., 2007). Due to this, the expression of H_2O_2 -inducible genes was measured.

Figure 17 shows the results of the gene expression measurements of known H_2O_2 -inducible genes like the glutathione S-transferase phi 8 (*GstF8*), glutathione peroxidase 6 (*Gpx6*), ascorbate peroxidase 1 (*Apx1*) and oxidative signal inducible 1 (*Oxi1*). Beside, three additional genes (*Atwrky33*, *Atwak1* and *Atlea5*) were measured, which should be indirectly influenced by H_2O_2 due to their interactions with the ROS (reactive oxygen species) signaling pathways (Lippok et al., 2007), pathogen response (Meier et al., 2010) or the role in oxidative stress tolerance (Salleh et al., 2012).

The CO₂ stress was increased compared to the chlorophyll fluorescence measurements to achieve the best induction of H₂O₂-inducible genes. Therefore, plants were shifted from high CO₂ concentrations (2000 ppm) to low CO₂ concentrations (150 ppm). To be able to discriminate between light induced gene expression and H₂O₂ induced gene expression samples were harvested every 2 hours at high CO₂ as well as at low CO₂ conditions. The harvesting started in the darkness directly before the light was switched on (0 h) and ended shortly before the light was switched off (8 h).

It was hypothesized that the gene expression of H₂O₂-inducible genes would be higher in the Δ Cat2 mutants than in WT plants.

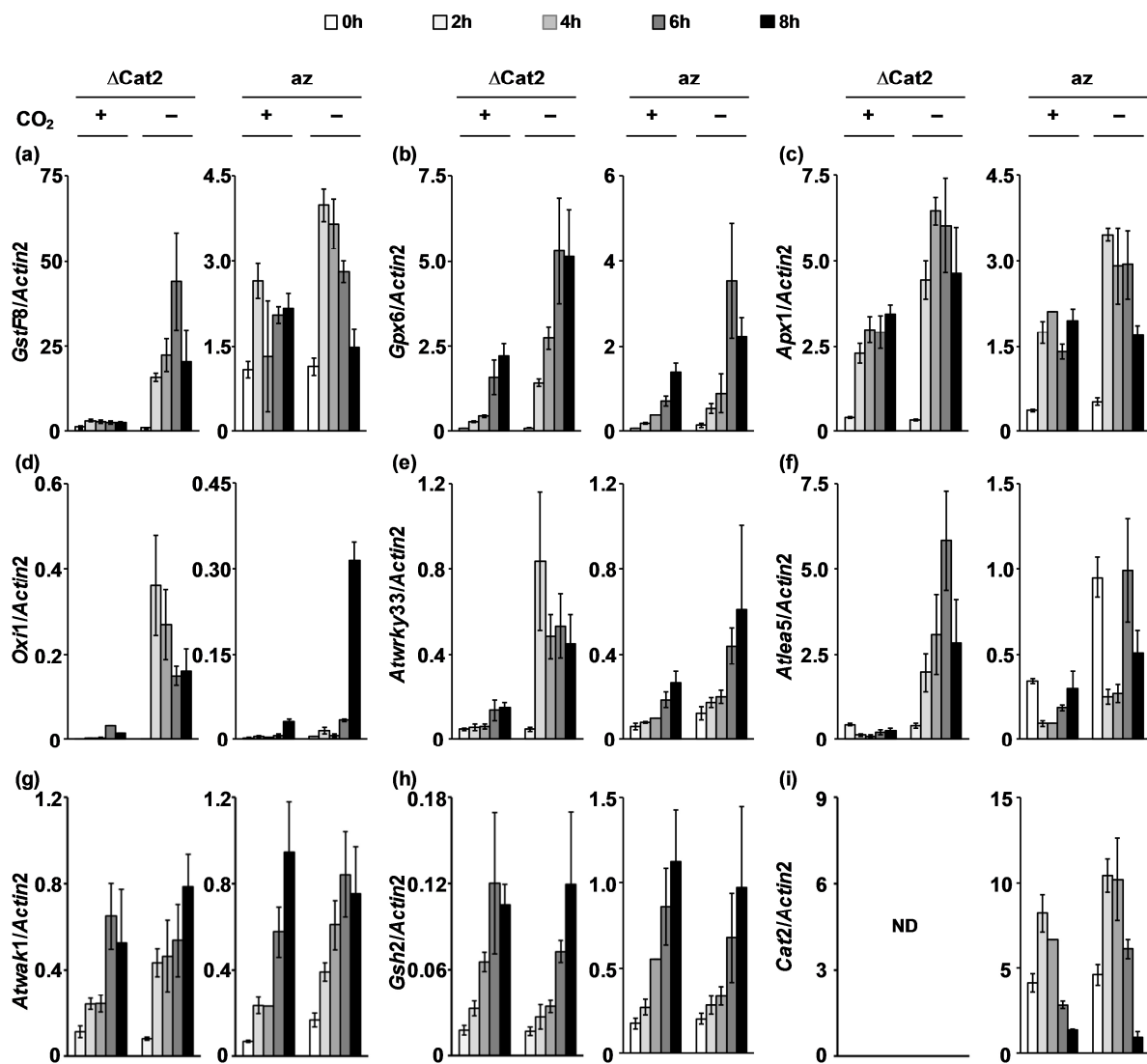


Figure 17: Gene expression of H₂O₂-inducible genes in *Cat2* knock-out mutants (Δ Cat2) and WT plants at high and low CO₂ concentrations during the day. Plants were grown three weeks under short day conditions (8 h light and 16 h darkness) and high CO₂ (2000 ppm) and some of the plants were shifted to low CO₂ concentration (150 ppm). Six plants were harvested in a two hours period and pooled. This was done for high CO₂ as well as for low CO₂ concentrations. The expression levels were standardized to expression level of *Actin2*. Shown are the means \pm SE from 4 independent experiments. ND: not determined.

The upper left graph shows the light regulation of *GstF8* in the mutant and control WT plants at two different CO₂ concentrations (Figure 17, a). The gene was obviously strongly induced by low CO₂ conditions in the Δ Cat2 background, but only slightly in the WT background (mind different scales). Under all conditions and in the different genetic backgrounds, *GstF8* was induced in the morning and declined in the afternoon.

When compared to the *GstF8* profile, the *Gpx6* expression showed a similar pattern in the Δ Cat2 background (Figure 17, b). An induction due to low CO₂ was observed, although the gene was not as strongly induced by low CO₂ concentrations as the *GstF8* gene. In the WT background the gene was only slightly induced. However, beside the influence of the CO₂ concentration on the expression level, a light induction of gene expression was also observed. The expression level at high CO₂ concentration was increased with longer light exposure independent of the genetic background.

The same was observed for the *Apx1* gene expression (Figure 17, c), although the induction due to CO₂ concentrations was not as evident as for the other two genes. The expression level at high CO₂ concentrations was higher in Δ Cat2 mutants than in WT as well as the induction due to low CO₂. The expression pattern of *Apx1* differed from the expression pattern of the other two genes (*GstF8* and *Gpx6*). The expression was induced after two hours light exposure, although the induction was stronger at low CO₂ conditions than at high CO₂. The expression level reached was received over the whole day and reduced shortly before the light was switched off. Due to this *Apx1* expression was CO₂ induced as well as light induced, but only slightly induced in the mutant.

The last measured H₂O₂-inducible gene was *Oxi1* (Figure 17, d). The RNA abundance was nearly not detectable under high CO₂ concentrations independently of the genotype, but could be already measured after 2 h exposure to low CO₂ conditions and normal light conditions. The gene expression of *Oxi1* started earlier during the day in the Δ Cat2 mutants than in WT plants. The expression was induced up to 300% after 2 h light and 2 h low CO₂ conditions. At low CO₂, *Oxi1* was already induced after 2 h in the Δ Cat2 background, but only after 8 h exposure to low CO₂ in the WT.

In conclusion, higher expression levels and higher induction of gene expression due to low CO₂ concentrations was detected in Δ Cat2 mutants than in WT plants; whereas the *GstF8* expression shows the strongest regulation in the Δ Cat2 background. Therefore, these genes could be used as indicators for the effect of alternative photorespiratory pathways (35S-*EcGlcDH* and 35S-*CrGlcDH*) in a mutant background (Δ Cat2 and Δ Ggat) as well as in the WT background.

The pathogen-inducible gene *Atwrky33* (*Arabidopsis thaliana wrky 33* transcription factor) also reacted to a reduction in CO₂ levels. In both WT plants and Δ Cat2 mutants, higher levels

were observed at low CO₂ (Figure 17, e). A light regulated gene expression was observed at high CO₂ concentrations indicating a light regulated expression.

Similar results were also obtained for *Atlea5* (late embryogenesis-associated protein 5) gene expression. The gene was strongly induced by low CO₂ concentrations in the Δ Cat2 background and only slightly induced in the WT background (Figure 17, f). Independent of the CO₂ concentration and the genetic background, the gene expression was increased in the morning and decreased in the evening.

A completely different expression pattern was observed for the *Atwak1* gene (*Arabidopsis thaliana* cell wall-associated receptor-like protein kinase 1) (Figure 17, g). The expression level was not influenced by changing the CO₂ concentration or even influenced by the genetic background. At high CO₂ as well as at low CO₂ concentration, the gene was induced during the day and reached the maximal expression in the early evening.

I also decided to measure transcript levels of *Gsh2*, because glutathione levels were induced in Δ Cat2 mutants (Queval et al., 2007). The glutathione pool in Δ Cat2 mutants was twice as high as in WT plants. My hypothesis was that the glutathione pool is regulated by changes in the expression level of *Gsh2*. However, gene expression did not differ neither between the genotypes nor between the different CO₂ concentrations. Only a light dependent induction of gene expression was evident (Figure 17, h).

The same result was observed with the expression of *catalase 2*. Δ Cat2 was not detectable in the Δ Cat2 mutant background as expected. In WT plants, expression increased in the morning and declined in the afternoon. This was independent of the CO₂ concentration (Figure 17, i).

In conclusion, gene expression studies are suitable for detecting H₂O₂ stress in both WT plants and Δ Cat2 mutants. The most regulated genes, with striking differences between Δ Cat2 and WT, were *GstF8* and *Gpx6*.

3.2 The importance of the chloroplastidal side-pathway

In order to test the impact of a chloroplastidal photorespiratory side pathway on the major pathway, I crossed Δ Cat2 mutants with overexpressors of a chloroplastidal glycolate dehydrogenase from *E. coli* (35S-*EcGlcDH*) and *C. reinhardtii* (35S-*CrGlcDH*). Overexpression of *EcGlcDH* in *Arabidopsis thaliana* plants led to a higher biomass and reduced photorespiration (Kebeish et al., 2007). So this pathway has an impact on the main photorespiratory pathway, whereas the importance of such side-pathway was not investigated until now. Also the natural pathway of glycolate conversion into CO₂ is unknown. Two different glycolate dehydrogenases were used, because, on the one hand, both enzymes should have the same effect on the major photorespiratory pathway and on the

other hand, the enzymes were the control for each other. The main hypothesis was that GlcDH has a positive impact on the major photorespiratory pathway.

3.2.1 Crossing of main photorespiratory mutants with overexpressors of a chloroplastidal glycolate dehydrogenase

I wanted to investigate the influence of *Ec*GlcDH and *Cr*GlcDH on the major photorespiratory pathway. For this, mutants in the major photorespiratory pathway (Δ Cat2 and Δ Ggat) were crossed with plants including 35S-*Ec*GlcDH or 35S-*Cr*GlcDH.

My hypothesis was that overexpression of chloroplastidal or mitochondrial GlcDH partially rescues the photorespiratory phenotype. Also, the level of H₂O₂-inducible genes should differ between photorespiratory mutants with 35S-GlcDH and without the overexpression of the GlcDH.

Homozygous Δ Cat2 and Δ Ggat T-DNA insertion mutants were crossed with 35S-*Ec*GlcDH or 35S-*Cr*GlcDH plants. The resulting F₁ generation was selfed. Genotypes in the F₂ generation were determined by PCR using defined primer systems for identification (see 2.2.1.10, Table 21). The most important genotypes from this crossing were the four genotypes of the photorespiratory mutant background including homozygous mutants as well as the combination with 35S-*Ec*GlcDH or 35S-*Cr*GlcDH (Table 29). The other important genotypes were the genotypes from the azygous background including the 35S-*Ec*GlcDH, 35S-*Cr*GlcDH and azygous plants, which means that these plants did not have the T-DNA insertion and did not express 35S-*Ec*GlcDH or 35S-*Cr*GlcDH (Table 29).

As previously described, only the combination of Δ Cat2 mutants with 35S-*Ec*GlcDH or 35S-*Cr*GlcDH were used for the physiological investigation and genotypes from this F₂ generation were again selfed and F₃ seeds were harvested.

These genotypes were used for chlorophyll fluorescence measurements, gene expression and metabolite profiling under shifting conditions from high CO₂ concentrations (2000 ppm CO₂) to low CO₂ (150 ppm CO₂).

Δ Cat2, Δ Cat2/35S-*Ec*GlcDH azygous and 35S-*Ec*GlcDH plants were grown side by side for three weeks at high CO₂ concentration (2000 ppm). Chlorophyll fluorescence parameters were measured from old leaves, which represent the third and fourth emerged leaf from one *A. thaliana* plant. The first measurement was done at high CO₂ concentrations representing the time point 0 and then each day after shift to lo CO₂. During the first experiment the shifting was only performed for nine days.

Table 29: Overview of the important received genotypes from the crossing of Δ Cat2 and Δ Ggat with 35S-*EcGlcDH* and 35S-*CrGlcDH* and their intended use.

Crossing	Background	Genotype	Intended use
Δ Cat2 x 35S- <i>EcGlcDH</i>	Δ Cat2	Δ Cat2 Δ Cat2/35S- <i>EcGlcDH</i>	chlorophyll fluorescence, gene expression and metabolite profiling
	az	az 35S- <i>EcGlcDH</i>	
Δ Cat2 x 35S- <i>CrGlcDH</i>	Δ Cat2	Δ Cat2 Δ Cat2/35S- <i>CrGlcDH</i>	chlorophyll fluorescence, gene expression and metabolite profiling
	az	az 35S- <i>CrGlcDH</i>	
Δ Ggat x 35S- <i>EcGlcDH</i>	Δ Ggat	Δ Ggat Δ Ggat/35S- <i>EcGlcDH</i>	back up
	az	az 35S- <i>EcGlcDH</i>	
Δ Ggat x 35S- <i>CrGlcDH</i>	Δ Ggat	Δ Ggat Δ Ggat/35S- <i>CrGlcDH</i>	back up
	az	az 35S- <i>CrGlcDH</i>	

Three independent experiments were done and Figure 18 shows the F_v/F_m , $Y(II)$ and NPQ values. The two genotypes did not show any differences in the F_v/F_m value at high CO_2 concentrations (Figure 18, first row). A slight difference in the F_v/F_m value was observed in the first experiment between both genotypes after the shifting to low CO_2 concentrations. Δ Cat2 mutants were characterized by a lower F_v/F_m value than the combination with 35S-*EcGlcDH*. Δ Cat2 mutants showed a quick reduction in the F_v/F_m value during the first three days. The difference between Δ Cat2 mutants and Δ Cat2/35S-*EcGlcDH* mutants were maximal for the F_v/F_m at the last day. No difference was observed between both genotypes in the second experiment for the F_v/F_m value, whereas the difference also appears during the third experiment. Here a maximum of the F_v/F_m value was also detected after nine days at low CO_2 concentrations and became smaller with longer exposure to low CO_2 conditions. During the first experiment $Y(II)$ differed between Δ Cat2 and Δ Cat2/35S-*EcGlcDH* plants (Figure 18, second row). The photosynthetic yield was lower in Δ Cat2 mutants (grey) compared to the combination with 35-*EcGlcDH* (black) at low CO_2 concentrations. The difference grew with longer exposure to low CO_2 and reached its maximum on day nine. This difference was not detected during the second experiment. Both genotypes reacted in the same way. The same was observed during the last experiment. In the first days, no difference was detected as well as in the last days of the measurement. Only in between, a slight difference between both genotypes was observed, which disappeared with longer exposure to low CO_2 .

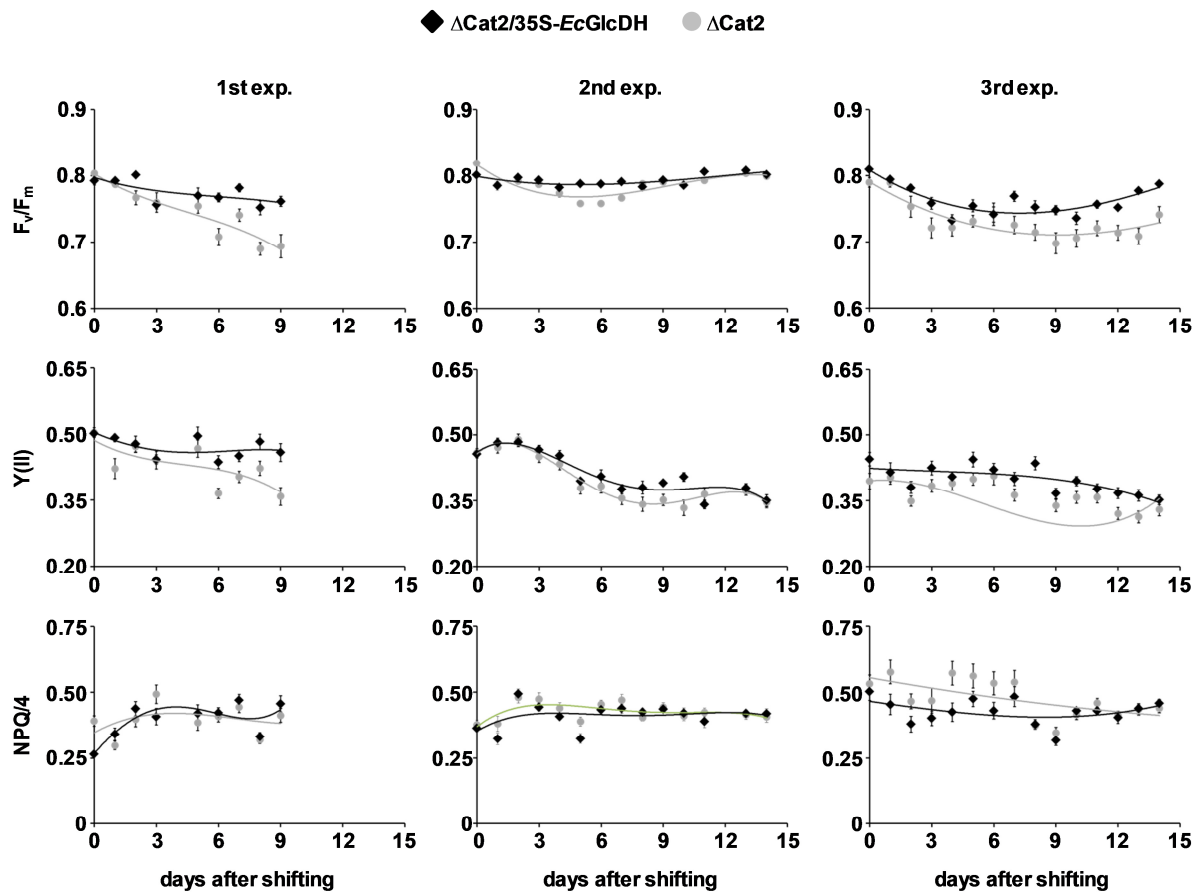


Figure 18: Chlorophyll fluorescence of old leaves of the Δ Cat2 mutant background from the crossing of Δ Cat2 with 35S-*EcGlcDH* during a shift from high CO₂ concentration to low CO₂ concentration. Three weeks old plants were shifted for 14 days from high CO₂ concentration (2000 ppm) to low CO₂ concentrations (150 ppm). Chlorophyll-fluorescence parameters, F_v/F_m (maximal quantum yield), $Y(II)$ (photosynthetic yield) and NPQ (non-photochemical quenching) were recorded every day using Imaging-Pam (2.2.4.2) starting at high CO₂ concentration (0 days after shifting) and ending at 14 days after shifting. The measurement was done for 30 min using a pulse of 20 sec between the saturated light pulses and an actinic light of 120 μ E. Shown are three independent experiments with at least 15 individuals for each genotype. Data points are means \pm SE.

No clear difference between Δ Cat2 and Δ Cat2/35S-*EcGlcDH* was observed concerning the NPQ value (lower row). It seemed that the Δ Cat2/35S-*EcGlcDH* mutants had a lower NPQ value than the combination without 35S-*EcGlcDH* in two out of three experiments at high CO₂ concentrations (first exp. and third exp.).

Figure 19 shows the result in the azygous background, i.e. 35S-*EcGlcDH* overexpressors were compared to az plants from the same cross. No differences were observed between azygous plants (az, grey) and 35S-*EcGlcDH* plants (black) independent of the chlorophyll fluorescence parameter or the period of exposure to low CO₂ concentrations.

Beside the measurements of old leaves, also younger leaves were used to investigate the influence of 35S-*EcGlcDH* on the major photorespiratory pathway. No differences between all four genotypes were observed in young leaves independent of the chlorophyll fluorescence parameter (Supplemental Figure 32+33).

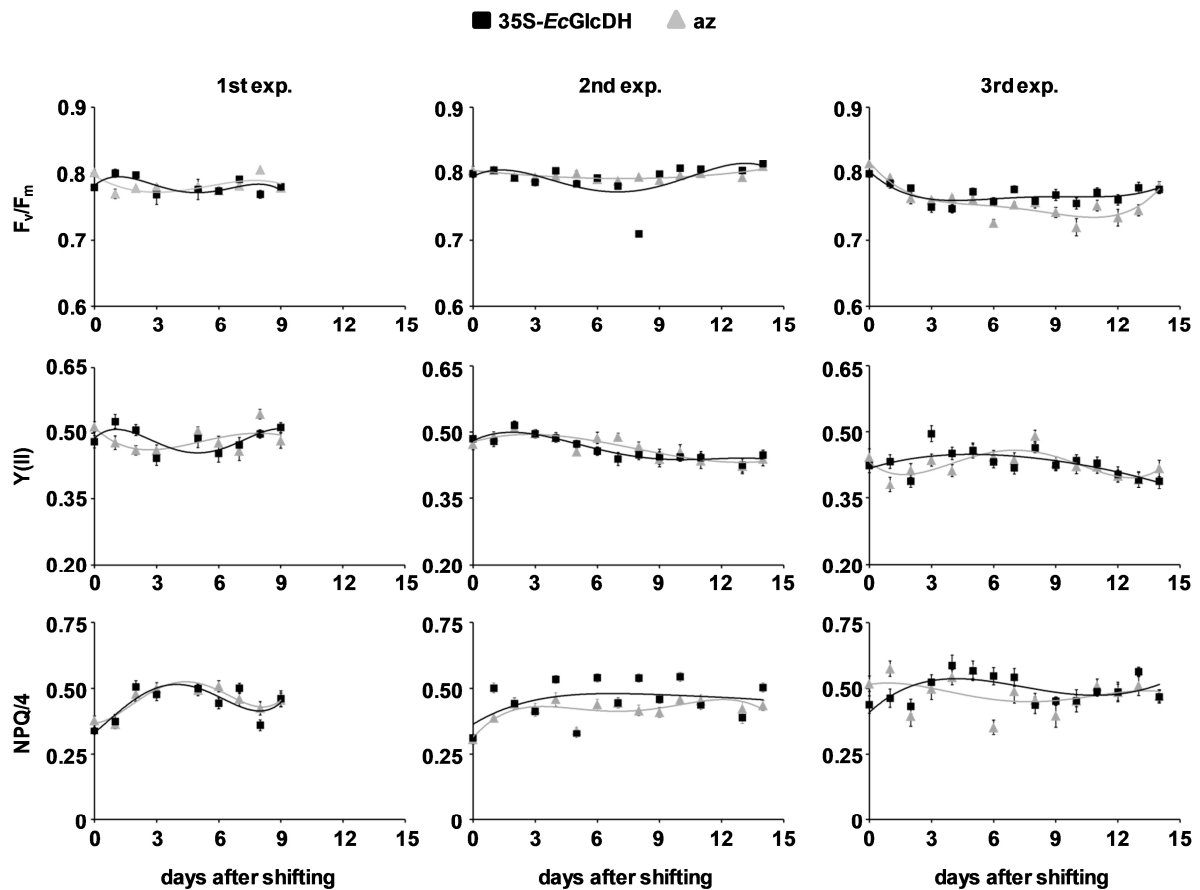


Figure 19: Chlorophyll fluorescence of old leaves of the azygous background from the crossing of Δ Cat2 with 35S-*EcGlcDH* during a shift from high CO₂ concentration to low CO₂ concentration. Three weeks old plants were shifted for 14 days from high CO₂ concentration (2000 ppm) to low CO₂ concentrations (150 ppm). Chlorophyll-fluorescence parameters, F_v/F_m (maximal quantum yield), $Y(II)$ (photosynthetic yield) and NPQ (non-photochemical quenching) were recorded every day using Imaging-Pam (2.2.4.2) starting at high CO₂ concentration (0 days after shifting) and ending at 14 days after shifting. The measurement was done for 30 min using a pulse of 20 sec between the saturated light pulses and an actinic light of 120 μ E. Shown are three independent experiments with at least 15 individuals for each genotype. Data points are the means \pm SE.

These results hint towards the influence of 35S-*EcGlcDH* on the major photorespiratory pathway. Seemingly, 35S-*EcGlcDH* had a slight impact on the photosynthetic performance in the Δ Cat2 mutant background looking at old leaves, but this influence was not stable and was not observed in the azygous background or young leaves independent of the genotype. To prove the impact of a chloroplastidial GlcDH, a second approach was used with a second GlcDH enzyme (*CrGlcDH*).

Figure 20 shows the results of the chlorophyll fluorescence measurements of the Δ Cat2 mutant background from the crossing of Δ Cat2 with 35S-*CrGlcDH*. Δ Cat2 mutants (grey) showed a lower F_v/F_m value than the Δ Cat2/35S-*CrGlcDH* plants (black) under shifting conditions during the first experiment (Figure 19, upper row). With longer exposure to low CO₂ concentrations the differences between both genotypes become bigger. However, this difference was not apparent in the second experiment. In the third experiment, a higher F_v/F_m

for the $\Delta\text{Cat}2/35\text{S-CrGlcDH}$ combination was only detectable during the first days of the shift. Thus results were inconsistent.

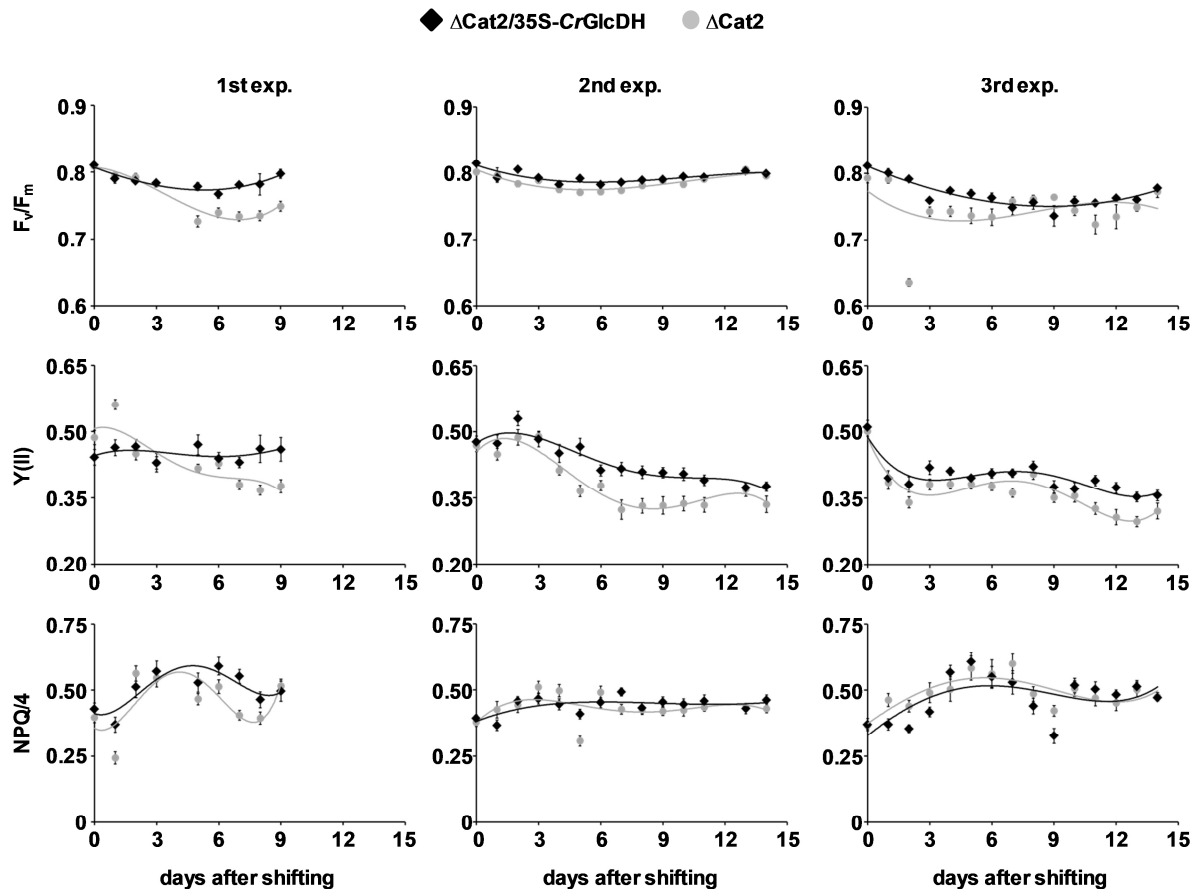


Figure 20: Chlorophyll fluorescence of old leaves of the $\Delta\text{Cat}2$ mutant background from the crossing of $\Delta\text{Cat}2$ with 35S-CrGlcDH during a shift from high CO_2 concentration to low CO_2 concentration. Three weeks old plants were shifted for 14 days from high CO_2 concentration (2000 ppm) to low CO_2 concentrations (150 ppm). Chlorophyll-fluorescence parameters, F_v/F_m (maximal quantum yield), $Y(\text{II})$ (photosynthetic yield) and NPQ (non-photochemical quenching) were recorded every day using Imaging-Pam (2.2.4.2) starting at high CO_2 concentration (0 days after shifting) and ending at 14 days after shifting. The measurement was done for 30 min using a pulse of 20 sec between the saturated light pulses and an actinic light of $120 \mu\text{E}$. Shown are three independent experiments with at least 15 individuals for each genotype. Data points are the means \pm SE.

A clear difference was observed for $Y(\text{II})$ from the first experiment (second row). $\Delta\text{Cat}2$ mutants had a lower $Y(\text{II})$ value than $\Delta\text{Cat}2/35\text{S-CrGlcDH}$. This distinction was maximal on day nine. During the second experiment a difference of the $Y(\text{II})$ value was also observed between both genotypes. The maximal difference was reached from day six to the eleventh day. At the end of the measurement the difference mainly disappeared. Also, a slight difference of the $Y(\text{II})$ value was observed during the third experiment between $\Delta\text{Cat}2$ and $\Delta\text{Cat}2/35\text{S-CrGlcDH}$. $\Delta\text{Cat}2$ and $\Delta\text{Cat}2/35\text{S-CrGlcDH}$ showed the same course of the $Y(\text{II})$ value at the beginning, whereas the $Y(\text{II})$ value of the $\Delta\text{Cat}2$ mutant plants decreased stronger after ten days shifting to low CO_2 than $\Delta\text{Cat}2/35\text{S-CrGlcDH}$ plants. NPQ (lower row) was not different between both genotypes independent of the experiment.

Figure 21 shows the result of measuring the chlorophyll fluorescence in azygous plants and corresponding 35S-CrGlcDH overexpressors. No differences were observed between the

genotypes neither for F_v/F_m or $Y(II)$ or NPQ independent of the period of exposure to low CO_2 concentrations except for $Y(II)$ of the last experiment. Here, the az plants (grey) were characterized by a lower $Y(II)$ value than the 35S-CrGlcDH plants (black). The difference between both genotypes was stable up to the tenth day of low CO_2 conditions. On day ten both genotypes reached a similar $Y(II)$ value.

Beside results of the old leaves of the four genotypes, also young leaves were measured. As expected, no differences were observed independent of the chlorophyll fluorescence parameter or the length of the shifting from high CO_2 to low CO_2 concentrations (Supplemental Figure 34+35).

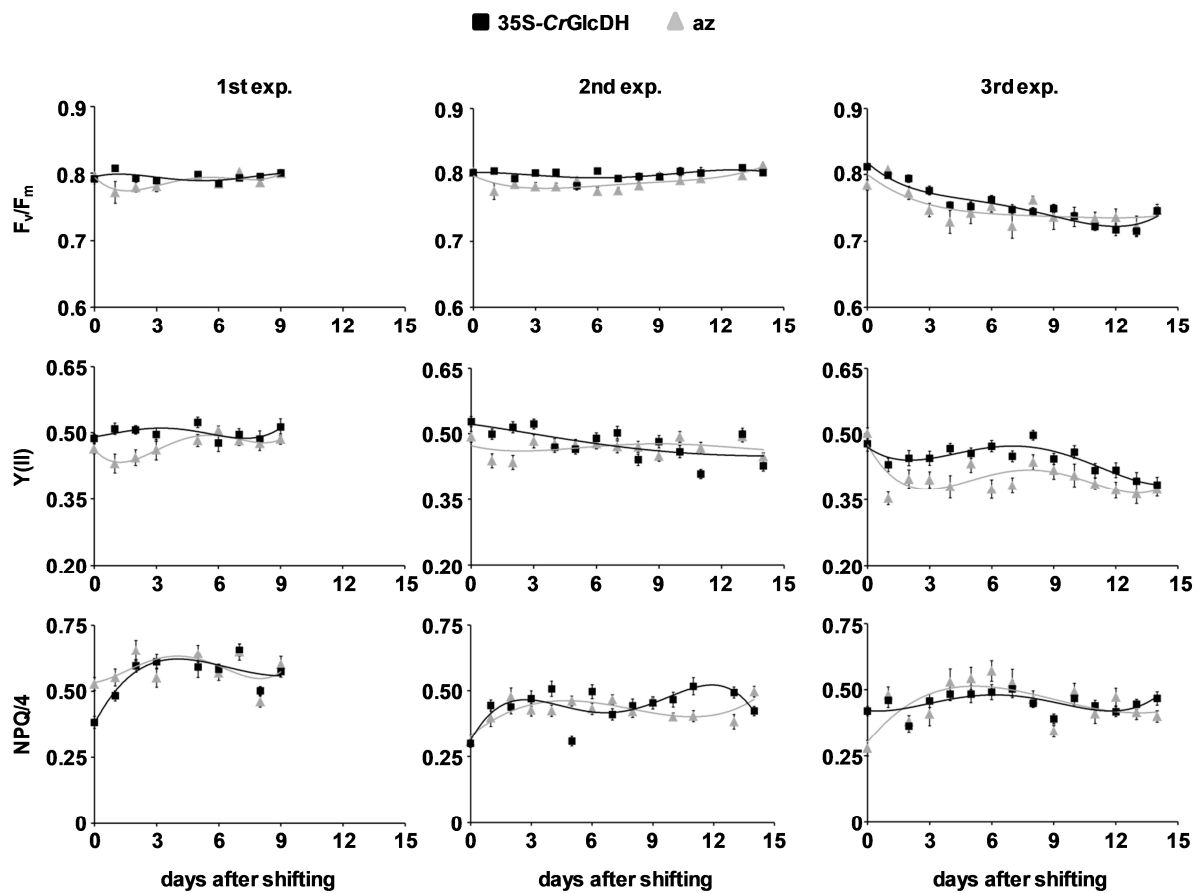


Figure 21: Chlorophyll fluorescence of old leaves of the azygous background from the crossing of Δ Cat2 with 35S-CrGlcDH during a shift from high CO_2 concentration to low CO_2 concentration. Three weeks old plants were shifted for 14 days from high CO_2 concentration (2000 ppm) to low CO_2 concentrations (150 ppm). Chlorophyll-fluorescence parameters, F_v/F_m (maximal quantum yield), $Y(II)$ (photosynthetic yield) and NPQ (non-photochemical quenching) were recorded every day using Imaging-Pam (2.2.4.2) starting at high CO_2 concentration (0 days after shifting) and ending at 14 days after shifting. The measurement was done for 30 min using a pulse of 20 sec between the saturated light pulses and an actinic light of 120 μE . Shown are three independent experiments with at least 15 individuals for each genotype. Data points are the means \pm SE.

In conclusion, the results of the chlorophyll fluorescence measurement were not clear and a second investigation was done to get better hints for the influence of a transgenic GlcDH to the major photorespiratory pathway and for the influence on a photorespiratory mutant.

Previous experiments showed that the gene expression level of H₂O₂-inducible genes differed between Δ Cat2 mutants and WT plants. The expression level was much higher in Δ Cat2 mutants than in WT plants. My hypothesis was that the gene expression of H₂O₂-inducible genes is lower in Δ Cat2 mutants containing an overexpressed GlcDH.

For this, Δ Cat2, Δ Cat2/35S-*EcGlcDH*, *az* and 35S-*EcGlcDH* plants were grown side by side for three weeks at high CO₂ concentrations and short day conditions (8 h light, 16 h darkness) and then were shifted to low CO₂ conditions as well as Δ Cat2, Δ Cat2/35S-*CrGlcDH*, *az* and 35S-*CrGlcDH* plants.

The expression level at high CO₂ (2000 ppm) was compared to the level at 1 hour shift to low CO₂ (150 ppm) as well as to 6 h, 27 and 30 h shifts to low CO₂ concentrations (Figure 22). The expression pattern of WT plants showed that the H₂O₂-inducible genes were also influenced by light (see also Figure 17). Due to this the high CO₂ samples were harvested after 4 h light at high CO₂ concentrations.

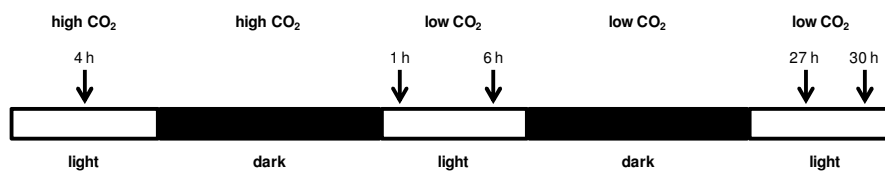


Figure 22: Harvesting time points during the shifting experiment from high CO₂ to low CO₂ concentrations. The arrows indicate the harvesting time points at high CO₂ as well as at low CO₂ conditions.

During the 27 h shifting and 30 h shifting the normal light dark rhythm was kept. Due to the dark period the photorespiration stops for 16 h and the plants rested. My hypothesis was that the expression level of H₂O₂-inducible genes would be lower after 27 h shifting to low CO₂ than after 6 h exposure to low CO₂ concentrations. Furthermore, I expected that the expression level of 30 h shift is equal to the 6 h shift.

Ten plants were harvested for each time point and were identified via PCR. Three plants were pooled and cDNA synthesis was performed from two independent pools. Three independent experiments were performed.

Figure 23 shows the results from three independent determinations of the expression level of H₂O₂-inducible genes from the genotypes. The first line shows the expression pattern of *GstF8* in the Δ Cat2 and *az* backgrounds, respectively. Despite small differences in the kinetics of induction, we did not observe clear differences between Δ Cat2 and Δ Cat2/35S-*EcGlcDH* or *az* and 35S-*EcGlcDH* plants. Only the difference between the Δ Cat2 background and the *az* background was detected in all three experiments looking at the expression level

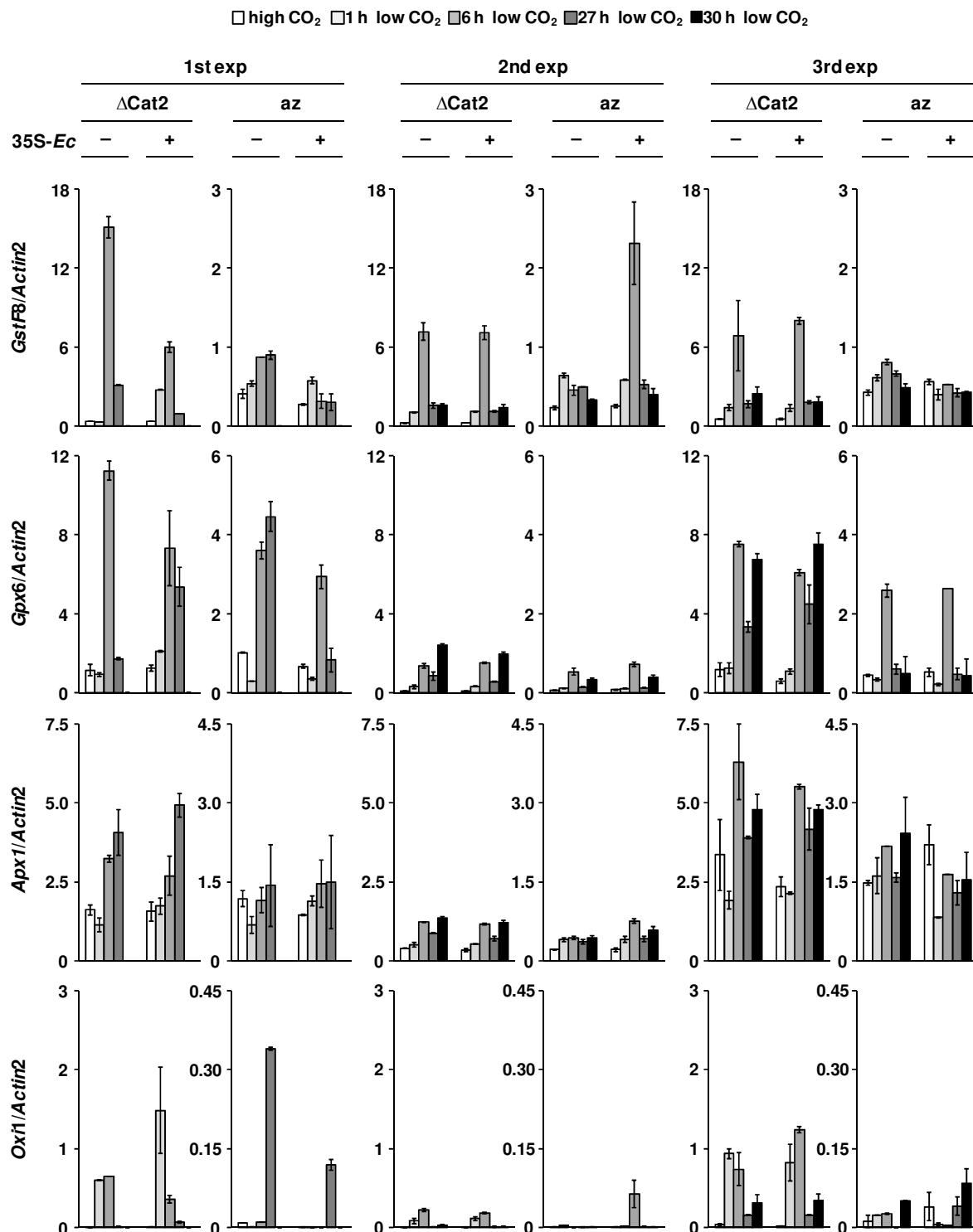


Figure 23: Gene expression of H₂O₂-inducible genes in the Δ Cat2 background and azygous background from the crossing of Δ Cat2 with 35S-*EcGlcDH* at high (0 h) CO₂ conditions and after shifting to low CO₂ concentrations for 1, 6, 27 and 30 h. Plants were grown three weeks under short day conditions (8 h light and 16 h darkness) and high CO₂ (2000 ppm) and were shifted to low CO₂ concentration (150 ppm). Ten plants were harvested for each time point and genotypes were identified via PCR following by pooling twice three plants and cDNA synthesis. This was done for high CO₂ as well as for low CO₂ concentrations. The expression levels were standardized to expression level of *Actin2*. Shown are the means \pm SE from two pools. Δ Cat2 represents the Δ Cat2 background and az the azygous background. 35S-*Ec* represents 35S-*EcGlcDH*, thereby – stands for the absence of 35S-*EcGlcDH* and + for the presence of 35S-*EcGlcDH*.

of *GstF8* (mind different scales). This difference was also observed in the pre-experiments. The expression level of 27 h exposure to low CO₂ was smaller than the expression level after 6 h shifting to low CO₂ indicating that the gene expression is induced by light as well as by low CO₂.

The second line of Figure 23 shows the expression level of *Gpx6*. The expression level was higher in the Δ Cat2 background than in the az background (mind different scales). After 6 h shifting to low CO₂ an induction of the expression level was detected in the Δ Cat2 background as well as in the az background. In two out of three replicates the gene expression of *GstF8* was higher in Δ Cat2 plants than in Δ Cat2/35S-*EcGlcDH* plants. Beside the described expression pattern no stable differences were observed between az and 35S-*EcGlcDH*.

The third line shows the expression level of *Apx1* under the described shifting conditions. No clear differences were observed between Δ Cat2 and Δ Cat2/35S-*EcGlcDH* plants. The expression level was induced after 6 h shifting to low CO₂ conditions. In the azygous background also no differences were detected between az and 35S-*EcGlcDH*. Interestingly, expression levels were not clearly induced after shifting the plants from high CO₂ to low CO₂ concentrations. This result was not expected, because the previous experiments showed an induction of the expression level due to low CO₂ and light. A slightly higher expression was observed in the Δ Cat2 background compared to the az background.

The last lane of Figure 23 shows the expression pattern of *Oxi1*. The expression level of *Oxi1* was near the detection limit at high CO₂ concentration. Also the expression level was higher in the Δ Cat2 background than in the az background. An induction of expression was detected after 1 h shifting to low CO₂. This was even higher after 6 h shifting to low CO₂ conditions. No clear differences were detected between Δ Cat2 and Δ Cat2/35S-*EcGlcDH* as well as between az and 35S-*EcGlcDH* plants. The first experiment was an exception for the az background. The expression level of *Oxi1* was higher in az plants than in 35S-*EcGlcDH*, but this was only observed in this experiment.

In conclusion, the expression levels of H₂O₂-inducible genes did not differ looking at the individual backgrounds. The hypothesis that the expression level of H₂O₂-inducible genes is higher in Δ Cat2 mutants than in Δ Cat2/35S-*EcGlcDH* mutants was not verified.

A different result was observed looking at the same experiment with 35S-*CrGlcDH* as the GlcDH enzyme.

Figure 24 shows the results from three independent determinations of the expression levels in the four genotypes. The first lane illustrates the expression pattern of *GstF8* in Δ Cat2 mutant background as well as in the az background. Expression level of *GstF8* was higher in the Δ Cat2 background than in the az background in all independent experiments, although the expression intensity was higher in the first experiment than in the following ones.

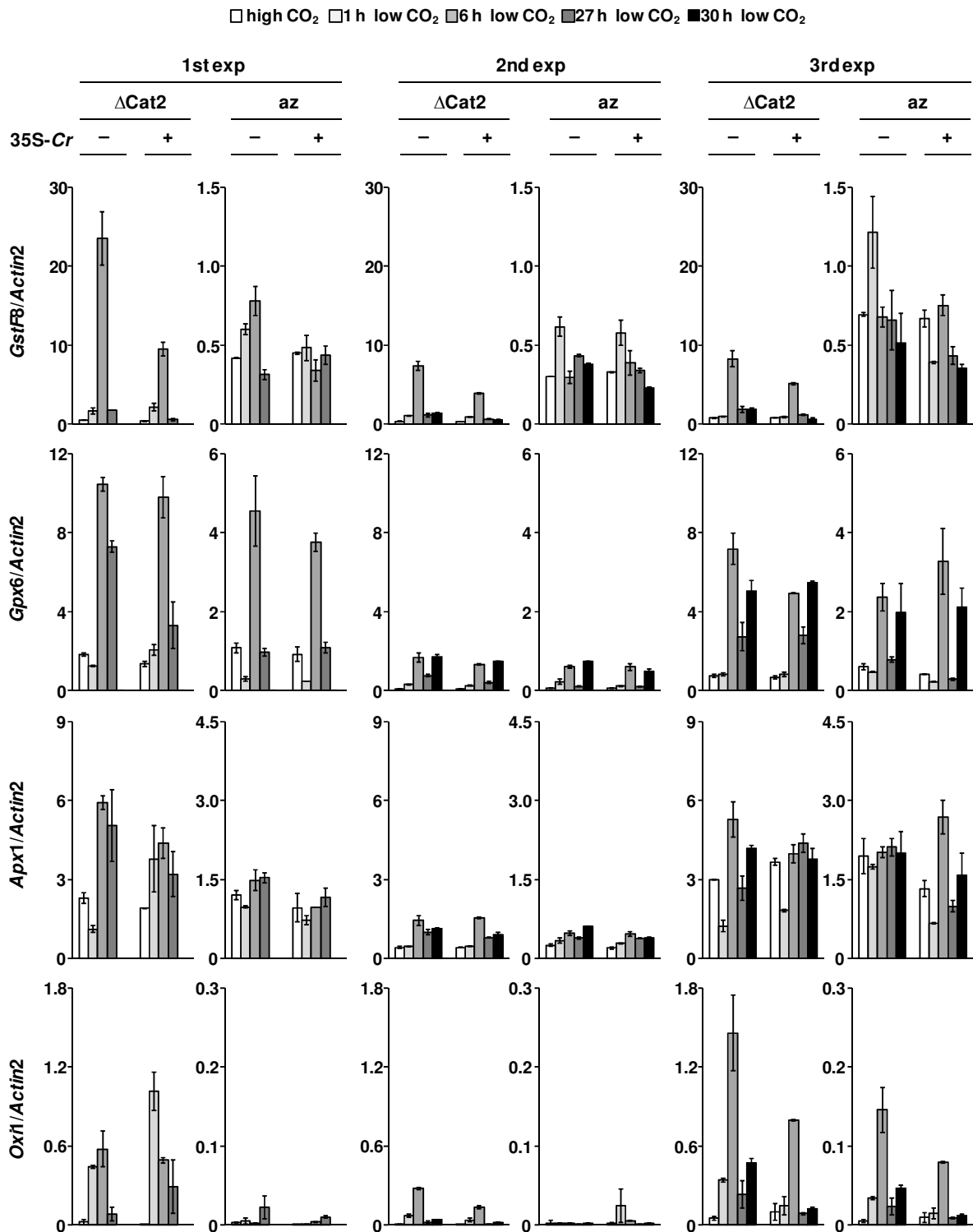


Figure 24: Gene expression of H₂O₂-inducible genes in the ΔCat2 background and azygous background from the crossing of ΔCat2 with 35S-CrGlcDH at high (0 h) CO₂ conditions and after shifting to low CO₂ concentrations for 1, 6, 27 and 30 h. Plants were grown three weeks under short day conditions (8 h light and 16 h darkness) and high CO₂ (2000 ppm) and were shifted to low CO₂ concentration (150 ppm). Ten plants were harvested for each time point and genotypes were identified via PCR following by pooling twice three plants and cDNA synthesis. This was done for high CO₂ as well as for low CO₂ concentrations. The expression levels were standardized to expression level of *Actin2*. Shown are the means ±SE from two pools for each experiment. ΔCat2 represents the ΔCat2 background and az the azygous background. 35S-Cr represents 35S-CrGlcDH, thereby – stands for the absence of 35S-CrGlcDH and + for the presence of CrGlcDH.

Further, the induction of gene expression due to low CO₂ was higher in the Δ Cat2 background than in the az background. The expression level in az and 35S-*CrGlcDH* plants was induced after 1 h exposure to low CO₂ and in the Δ Cat2 mutant background the maximal expression was reached after 6 h at low CO₂ concentrations. Here *GstF8* expression was 100% higher induced in az than in 35S-*CrGlcDH* plants (after 1 h exposure to low CO₂) and 150% to 250% times higher induced in Δ Cat2 than in Δ Cat2/35S-*CrGlcDH* plants (after 6 h exposure to low CO₂). The difference between Δ Cat2 and Δ Cat2/35S-*CrGlcDH* after 6 h shifting was highly significant in the first two experiments ($p < 0.05$ for the first experiment, $p < 0.02$ for the second) and lightly significant in the last replicate ($p < 0.1$). The hypothesis that the expression level of *GstF8* is high in Δ Cat2 mutants than in Δ Cat2/35S-*CrGlcDH* was verified.

The second line of Figure 24 illustrates the results of the expression level of *Gpx6* in Δ Cat2 background and in the az background. The expression of *Gpx6* was higher in the Δ Cat2 background than in the az background like *GstF8*. The gene expression was highly induced after 6 h exposure to low CO₂ conditions independent of the genotype. A difference was observed in plants containing 35S-*CrGlcDH* and plants without *GlcDH* transgene. In Δ Cat2 plants the gene expression was 100% to 150% higher than in Δ Cat2/35S-*CrGlcDH* plants ($p < 0.1$) and 80% to 130% higher in az plants than in 35S-*CrGlcDH* plants ($p < 0.5$). Due to this over expressing *CrGlcDH* has an impact on the expression level of *Gpx6*, the expression is reduced in plants containing 35S-*CrGlcDH* compared to plants without. The outcome was that the hypothesis was verified that Δ Cat2 plants had a higher induction of *Gpx6* than Δ Cat2/35S-*CrGlcDH*.

The third lane of Figure 24 shows the expression pattern of *Apx1* in all four genotypes from the crossing of Δ Cat2 with 35S-*CrGlcDH*. The maximal gene expression was reached after 6 h exposure to low CO₂ conditions. Gene expression was generally twice as high in Δ Cat2 background as in the az background. On top of that, a different gene expression was observed looking at Δ Cat2 and Δ Cat2/35S-*CrGlcDH* plants. *Apx1* gene expression was light higher in Δ Cat2 than in Δ Cat2/35S-*CrGlcDH* plants after 6 h shifting to low CO₂ concentrations ($p < 0.5$). A difference between az and 35S-*CrGlcDH* was not observed.

The last lane illustrates the expression pattern of *Oxi1* in the described genotypes. The expression level was near to the detection limit at high CO₂ concentrations as well as in the az background independent of the length of the low CO₂ treatment. In general, an induction of *Oxi1* was observed after one hour exposure to low CO₂ concentrations in the Δ Cat2 background. I did not observed notable differences between the genotypes for *Oxi1* expression due to high differences between the several replicates.

Due to the results of the gene expression analyses, the hypothesis that over expressing 35S-*CrGlcDH* leads to a reduced expression of H₂O₂ induced genes was verified. The gene

expression was more influenced in the Δ Cat2 background than in the az background. A reduced expression of *GstF8* and *Gpx6* was observed in Δ Cat2 as well as in the az background, but no clear influence on *Apx1* and *Oxi1* expression was detected independent of the background.

Interestingly, the gene expression of H₂O₂-inducible genes is influenced by 35S-*Cr*GlcDH, but not by 35S-*Ec*GlcDH although both enzymes catalyze the same reaction and were both targeted to the chloroplast. To get better insights about the different influence of 35S-*Ec*GlcDH and 35S-*Cr*GlcDH, metabolites were isolated and identified via GC-MS. I used segregating populations for the screen that were homozygous for Δ Cat2, but hemizygous for 35S-*Ec*GlcDH or 35S-*Cr*GlcDH. Samples were harvested after 6 h light induction at high CO₂ concentrations as well as at low CO₂ concentrations. Plants were shifted for 6 h to low CO₂ and then harvested. 20 plants of each cross were individually harvested, the genotypes were identified via PCR (2.2.1.2, 2.2.1.8), ten plants of the same genotype were pooled and metabolites were isolated. This was done three times in independent experiments.

The method was first checked by analyzing the metabolites of Δ Cat2 mutants compared to az plants. My hypothesis was that differences should occur in low CO₂ samples exclusively. Figure 25 shows the relative amount of nine selected metabolites from Δ Cat2 and az plants growing at high CO₂ concentrations (grey bar) and after shifting to low CO₂ conditions for 6 h (black bar). The first graph shows the metabolite level of glycine in Δ Cat2 and az plants. Interestingly, the amount of glycine was lower in Δ Cat2 than in az plants at high CO₂ and low CO₂ conditions. Δ Cat2 plants were characterized by a slight smaller amount of serine at high CO₂ concentrations and a higher amount at low CO₂ conditions compared to az plants. A higher alanine amount was detected at high CO₂ concentrations compared to low CO₂ independent of the genotype.

The second line of Figure 25 shows the amount of three different sugars in Δ Cat2 and az plants. No major changes in sucrose and ribose levels were detected in the genotypes independent of the CO₂ concentration. The glucose amount was lower in Δ Cat2 plants at high CO₂ concentrations as compared to az plants. The amount of glucose did not change in Δ Cat2 plants due to shifting the plants to low CO₂ concentrations. In contrast, the amount of glucose declined at low CO₂ concentrations compared to high CO₂ in az plants.

The last lane shows other amounts of metabolites, which differ depending on the genotype or CO₂ concentration. No clear differences were observed in the fumarate content, an intermediate in the citric acid cycle, independent of the genotype and CO₂ concentration. The amount of aspartate was higher at high CO₂ than at low CO₂. The decrease of aspartate was stronger in Δ Cat2 plants than in az plants. The last graph shows the amount of threonic acid, which is a metabolite in the ascorbic acid metabolism. The level of threonic acid is increased due to low CO₂ concentrations in both genotypes. Δ Cat2 mutants were characterized by a

sevenfold stronger accumulation of threonic acid due to low CO₂ concentrations than az plants. Ascorbic acid metabolism is important in stress response and detection to oxidative stress.

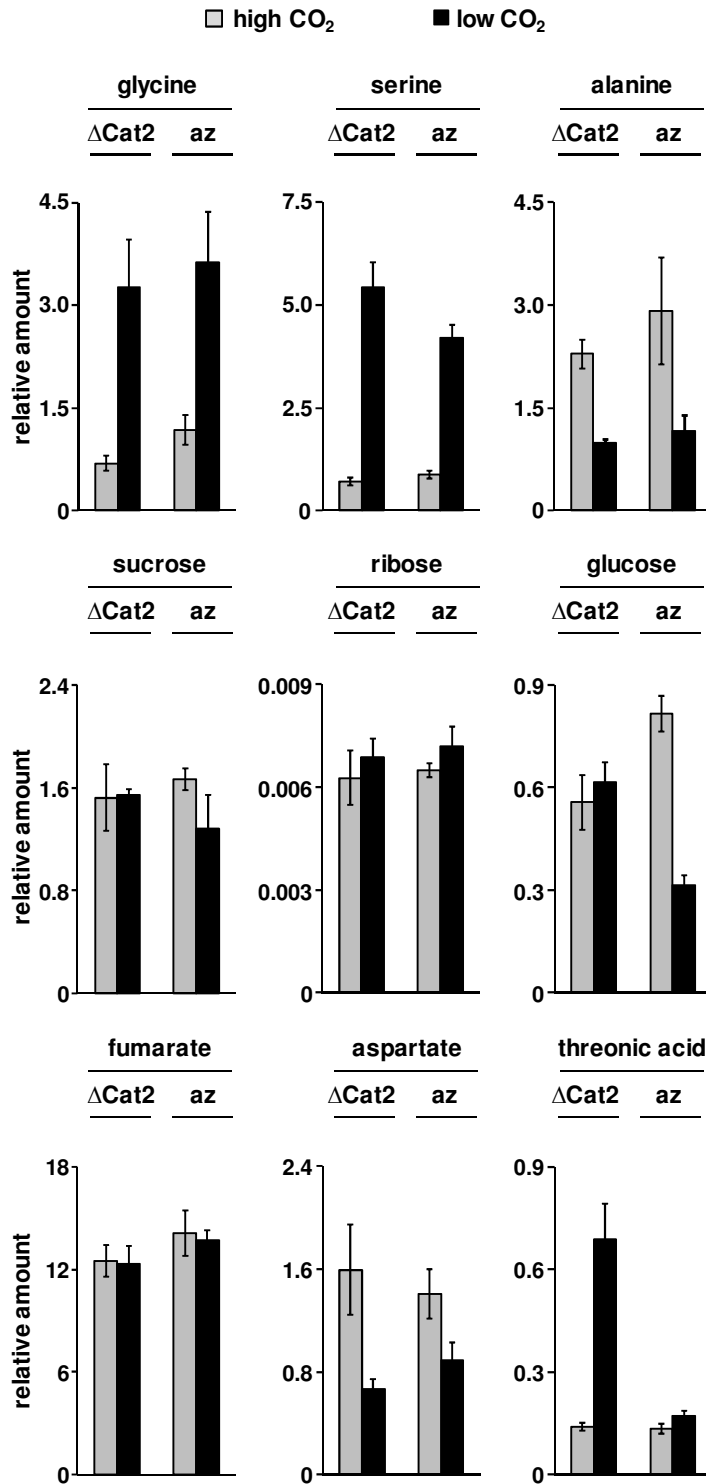


Figure 25: Metabolite profiles of Δ Cat2 and az plants were grown for three weeks at high CO₂ concentrations (2000 ppm) and were then shifted to low CO₂ (150 ppm) conditions. The amount of the isolated metabolite was standardized to ¹³C-sorbitol, which was used as internal standard. Shown are the means \pm SE from pools of 10 plants from 3 independent experiments.

My hypothesis was that photorespiratory amino acids such as glycine and serine accumulate more in the Δ Cat2 than in az plants due to low CO₂ concentrations. However, differences between the genotypes were insignificant. I also expected sugar amounts to be lower at low CO₂ concentrations than at high CO₂ concentrations, because carbon fixation is reduced under these conditions. This expectation was verified in az plants, but not in Δ Cat2 plants.

Due to these results the analysis was continued with all genotypes from the crossing of Δ Cat2 with 35S-*Ec*GlcDH and 35S-*Cr*GlcDH.

Figure 26 shows the result of the metabolite analysis of the Δ Cat2 background from both crossings. Shown are nine profiles out of 31 identified metabolites. These nine metabolites were selected, because they were directly or indirectly influenced by photorespiration. The first line shows the results of three different amino acids. The first graph represents the amount of glycine at high CO₂ (grey bar) as well as at low CO₂ concentrations (black bar) of Δ Cat2, Δ Cat2/35S-*Ec*GlcDH, Δ Cat2 and Δ Cat2/35S-*Cr*GlcDH. An accumulation of glycine was observed due to low CO₂ independent of the genotype. The accumulation of glycine was different in the both Δ Cat2 plants. Δ Cat2 mutant from the crossing with 35S-*Cr*GlcDH were characterized by a stronger glycine accumulation due to low CO₂ than Δ Cat2 from the crossing with 35S-*Ec*GlcDH. No differences were detected between Δ Cat2 and Δ Cat2/35S-*Ec*GlcDH, whereas a clear difference was observed between Δ Cat2 and Δ Cat2/35S-*Cr*GlcDH. Δ Cat2 mutants showed a higher glycine accumulation than the corresponding GlcDH transgene. The second graph shows the serine amounts. In all genotypes, an accumulation due to low CO₂ was observed. No clear difference was observed between Δ Cat2 and Δ Cat2/35S-*Ec*GlcDH, whereas a striking difference was detected between Δ Cat2 and Δ Cat2/35S-*Cr*GlcDH. The third graph shows the amount of alanine. A decrease in the alanine amount due to low CO₂ was observed in all four genotypes. Here, a difference between Δ Cat2 and Δ Cat2/35S-*Ec*GlcDH was detected. The decrease was stronger in Δ Cat2 than in Δ Cat2 plants containing 35S-*Ec*GlcDH. A difference between Δ Cat2 and Δ Cat2/35S-*Cr*GlcDH was not detected independent of the CO₂ concentration.

The second line shows the metabolite amounts of different sugars. No differences were observed for sucrose independent of the CO₂ concentration and genotype. For ribose, a slight induction due to low CO₂ was detected in Δ Cat2, Δ Cat2/35S-*Ec*GlcDH and Δ Cat2/35S-*Cr*GlcDH, but not for Δ Cat2 from the crossing with 35S-*Cr*GlcDH. The third graph represents the glucose level at high CO₂ and low CO₂ concentrations. There was a tendency for a reduction in glucose levels after CO₂ shift in three out of five tested genotypes. I did not observe a clear difference when comparing 35S-*Ec*GlcDH and 35S-*Cr*GlcDH with their respective controls. A slight difference was observed for fumarate looking at the origins of Δ Cat2, Δ Cat2/35S-*Ec*GlcDH and Δ Cat2/35S-*Cr*GlcDH. The level of fumarate was lower in

Δ Cat2 and Δ Cat2/35S-*Cr*GlcDH than in Δ Cat2 and Δ Cat2/35-*Ec*GlcDH. No clear differences were detected in Δ Cat2 and Δ Cat2/35S-*Ec*GlcDH independent of the CO₂ concentration.

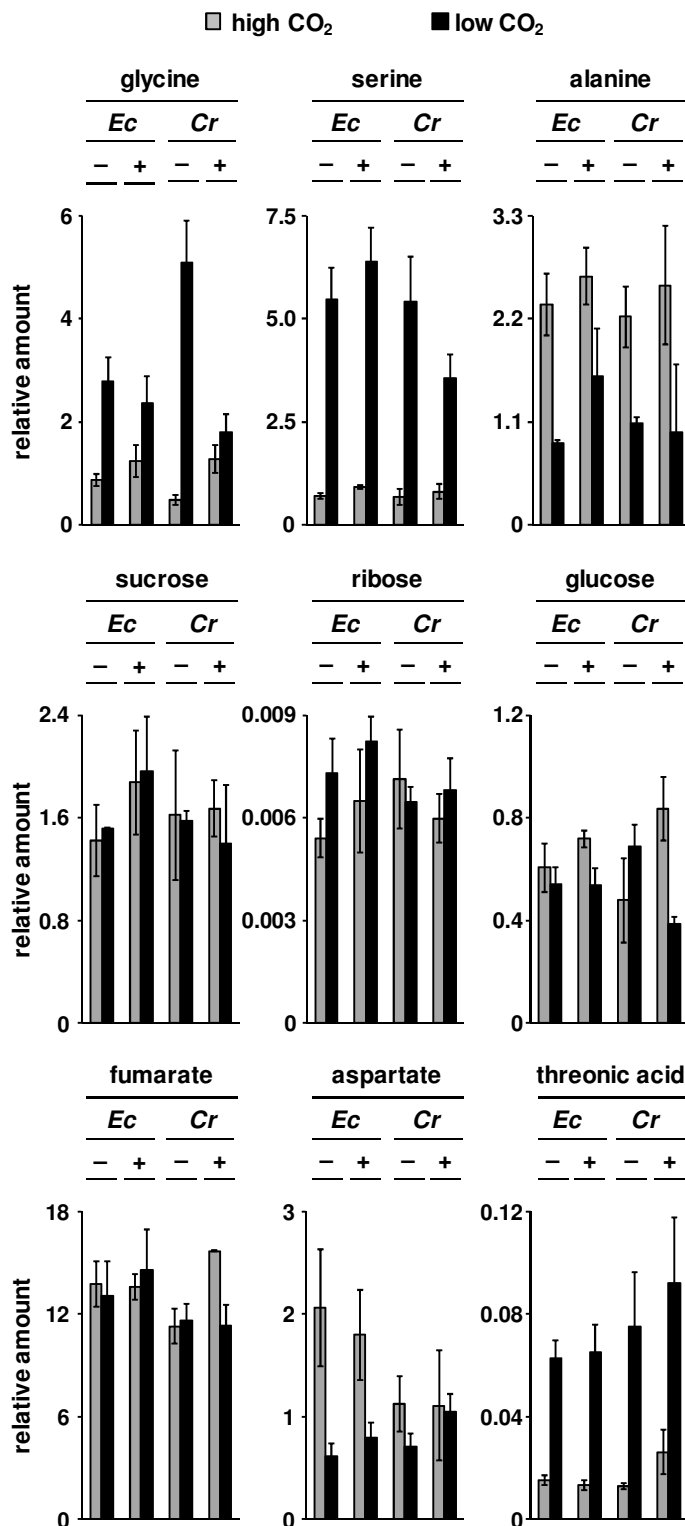


Figure 26: Metabolite profiles of the Δ Cat2 background from the crossing of Δ Cat2 with 35S-*Ec*GlcDH and 35S-*Cr*GlcDH. Plants were grown for three weeks at high CO₂ concentrations (2000 ppm) and were then shifted to low CO₂ (150 ppm) conditions. The amount of the isolated metabolite was standardized to ¹³C-sorbitol, which was used as internal standard. Shown are the means \pm SE from pools of 10 plants from 3 independent experiments. *Ec* and *Cr* represent 35S-*Ec*GlcDH or 35S-*Cr*GlcDH, thereby – stands for the absence of 35S-*Ec*GlcDH or 35S-*Cr*GlcDH and + for the presence of 35S-*Ec*GlcDH or 35S-*Cr*GlcDH.

In contrast, a clear difference in the Δ Cat2/35S-*Cr*GlcDH was detected, the amount of fumarate decreased due to low CO₂ treatment. A striking difference was observed for aspartate concerning the origin of the four genotypes. The amount of aspartate was higher in Δ Cat2 and Δ Cat2/35S-*Ec*GlcDH plants than in Δ Cat2 and Δ Cat2/35S-*Cr*GlcDH plants. The decrease of the level of aspartate was lower in Δ Cat2/35S-*Ec*GlcDH than in Δ Cat2 plants. The amount of aspartate decreased in Δ Cat2 and Δ Cat2/35S-*Cr*GlcDH plants due to low CO₂ treatment, whereas the decrease was stronger in Δ Cat2 than in Δ Cat2/35S-*Cr*GlcDH. In all four genotypes, a strong accumulation of threonic acid was detected due to low CO₂ conditions. The accumulation was similar for all genotypes.

In conclusion, the serine, glycine, glucose, aspartate and threonic acid contents increased due to the shift to low CO₂. Alanine was negatively influenced by low CO₂ and decreased by the treatment. The content of sucrose and ribose did not show any changes due to the treatment.

Figure 27 shows the metabolite profile in the az background of the crossing from Δ Cat2 with 35S-*Ec*GlcDH and 35S-*Cr*GlcDH. Glycine amounts in az, 35S-*Ec*GlcDH and 35S-*Cr*GlcDH plants increased due to low CO₂ concentrations in three out of four genotypes. No increased glycine level was detected in 35S-*Ec*GlcDH plants. In general, the accumulation was stronger in az plants than in the corresponding 35S-*Ec*GlcDH or 35S-*Cr*GlcDH overexpressors. Induction of glycine due to low CO₂ concentrations was maximal in az plants from the crossing of Δ Cat2 with 35S-*Cr*GlcDH. Also, the difference between az and GlcDH overexpression was higher in az and 35S-*Cr*GlcDH compared to az and 35S-*Ec*GlcDH plants. The level of serine at high CO₂ concentration was similarly independent of the genotype. An accumulation of serine due to low CO₂ concentration was observed in all four genotypes, whereas the increase of the serine amount was higher in az plants as compared to the corresponding GlcDH. The level of alanine is similar in all genotypes at high CO₂ conditions and a decrease of the amount was detected due to the shift to low CO₂. The decrease of alanine content was stronger in 35S-*Ec*GlcDH than in the corresponding az plants and also higher in 35S-*Cr*GlcDH plants as compared to the corresponding az.

The level of sucrose was higher at high CO₂ concentrations than at low CO₂. The error bars of the az plants and the corresponding 35S-*Cr*GlcDH plants were relative high so an interpretation was not possible. The decrease of the sucrose amount due to low CO₂ conditions was higher in az plants compared to the corresponding 35S-*Ec*GlcDH plants. No differences were detected for ribose independent of the genotype and CO₂ concentration. Az plants were characterized by a higher glucose level at high CO₂ concentrations as compared to the corresponding overexpressed GlcDH. A reduction was observed in all genotypes due to low CO₂ concentrations, whereas the decrease of the glucose was higher in 35S-*Ec*GlcDH than in az plants and higher in az plants than in 35S-*Cr*GlcDH plants.

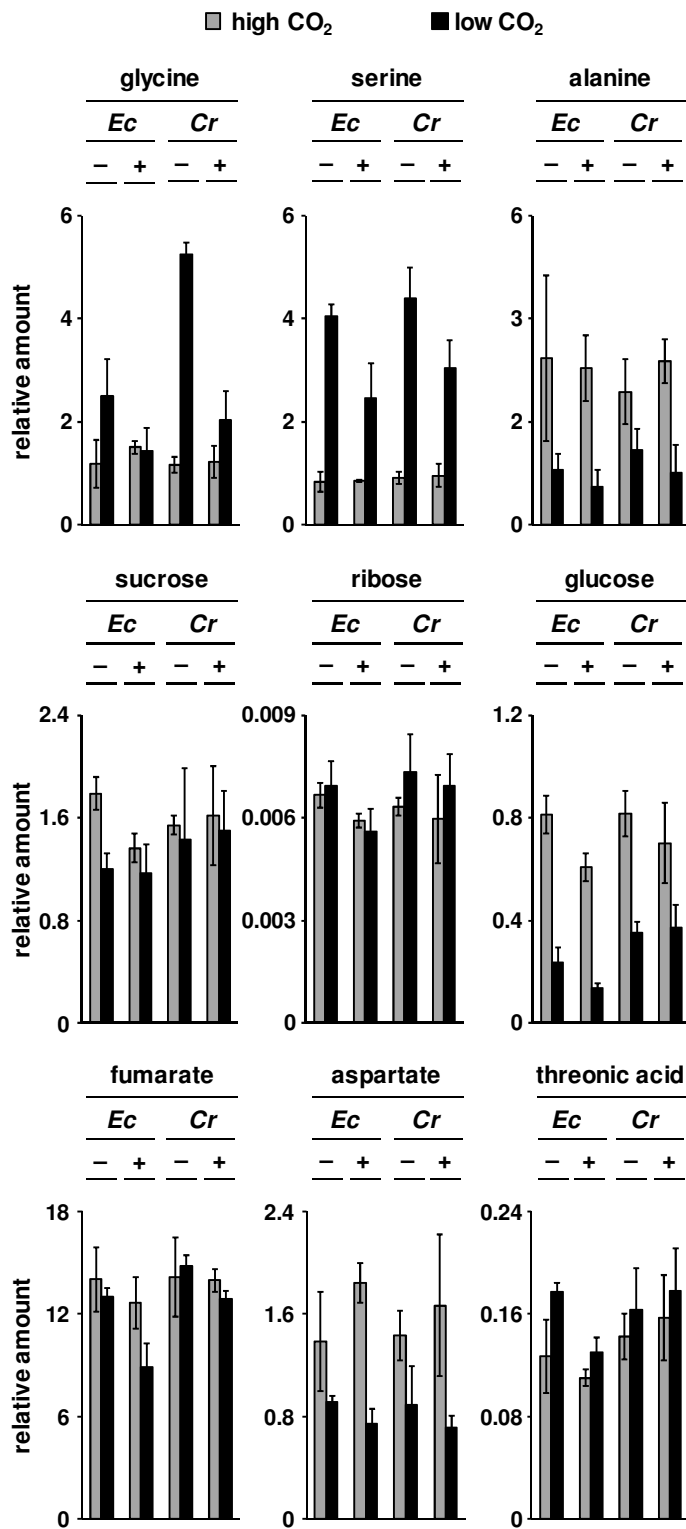


Figure 27: Metabolite profiles of the az background from the crossing of Δ Cat2 with 35S-*EcGlcDH* and 35S-*CrGlcDH*. Plants were grown for three weeks at high CO₂ concentrations (2000 ppm) and were then shifted to low CO₂ (150 ppm). The amount of the isolated metabolite was standardized to ¹³C-sorbitol, which was used as internal standard. Shown are the means \pm SE from pools of 10 plants from 3 independent experiments. *Ec* and *Cr* represent 35S-*EcGlcDH* or 35S-*CrGlcDH*, thereby - stands for the absence of 35S-*EcGlcDH* or 35S-*CrGlcDH* and + for the presence of 35S-*EcGlcDH* or 35S-*CrGlcDH*.

A decrease in the amount of fumarate was observed in all genotypes due to low CO₂, except in az plants from the crossing Δ Cat2 with 35S-*Cr*GlcDH. The decrease due to low CO₂ conditions was higher in 35S-*Ec*GlcDH compared to az plants. The same was observed for 35S-*Cr*GlcDH. A reduction of aspartate was detected in all genotypes due to the shift to low CO₂. The reduction was higher in 35S-*Ec*GlcDH and 35S-*Cr*GlcDH plants compared to the corresponding az plants. An increase of the threonic acid was observed in all genotypes due to low CO₂ concentrations, but no differences were observed between az and their corresponding GlcDH.

In conclusion, the integration of a GlcDH transgene has an impact on the chlorophyll fluorescence, gene expression and metabolite level in the Δ Cat2 background as well as in the az background under shifting conditions from high to low CO₂. This was observed in the genotypes from the crossing of Δ Cat2 with 35S-*Ec*GlcDH as well as Δ Cat2 with 35S-*Cr*GlcDH. The influence of 35S-*Cr*GlcDH was stronger than the influence of 35S-*Ec*GlcDH, because the influence was observed in all experiments, whereas the impact of 35S-*Ec*GlcDH was only detected looking at the metabolite levels.

3.3 The importance of the mitochondrial side-pathway

In order to test whether the mitochondrial side pathway contributes to the major photorespiratory pathway (see 1.5.1) and whether this pathway plays an important role for the whole metabolism of plants, I crossed Δ Cat2 mutants with Δ AtGlcDH knock-out mutants and combined the Δ Cat2 mutant with overexpressors of the mitochondrial side pathway (35S-*Ala*AT/35S-*At*GlcDH).

3.2.1 Crossing of two photorespiratory knock-out mutants

I wanted to test the function of mitochondrial glycolate oxidation in the background of a mutation in the major pathway. For this, photorespiratory knock-out mutants were crossed with the mitochondrial *At*GlcDH knock-out mutant (Δ AtGlcDH). The catalase 2 (Δ Cat2) and the glutamate:glyoxylate aminotransferase 1 (Δ Ggat) knock-out mutants were chosen, because the major photorespiratory pathway is knocked out in these mutants upstream of the GDC reaction. Moreover, both mutations are not lethal at ambient air conditions, although they show a photorespiratory phenotype (Igarashi et al., 2003; Queval et al., 2007). In contrast, the single Δ AtGlcDH did not show a photorespiratory phenotype at ambient air conditions (Niessen et al., 2007). The hypothesis was that a combination of both knock-out mutants can lead to a stronger phenotype or to an unviable plant at ambient air conditions.

Homozygous *Cat2* (Δ *Cat2*) or *Ggat1* (Δ *Ggat1*) and *AtGlcDH* (Δ *AtGlcDH*) mutants were crossed. F_1 plants resulting from this cross were selfed and genotypes in the F_2 were determined by PCR with primers specific for the insertion site (see 2.2.1.10, Table 21). An exemplary result is shown in Figure 28 for the crossing of Δ *Cat2* and Δ *AtGlcDH*. The most important genotypes from this crossing were the Δ *Cat2* homozygous, Δ *AtGlcDH* homozygous, the azygous (WT like) plants and the double mutant Δ *Cat2*/ Δ *AtGlcDH* homozygous plants.

Table 30: Summary of the PCR amplification results of the F_2 generation from the crossing of Δ *Cat2* and Δ *AtGlcDH* mutants. + represents the presence of gene and – represents the absence of gene. -/+ represents hemizygous plants, which show a T-DNA insertion as well as a genomic PCR fragment.

Sample	Δ <i>Cat2</i>	Δ <i>AtGlcDH</i>	Genotype
I	-/-	+/+	Δ <i>Cat2</i> homozygous
II	+/+	-/-	Δ <i>AtGlcDH</i> homozygous
III	-/-	-/-	Δ <i>Cat2</i> / Δ <i>AtGlcDH</i> homozygous
IV	+/+	+/+	azygous (az)
V	-/-	-/+	Δ <i>Cat2</i> / Δ <i>AtGlcDH</i> hemizygous
VI	-/+	-/-	<i>Cat2</i> hemizygous/ Δ <i>AtGlcDH</i>
VII	-/+	+/+	<i>Cat2</i> hemizygous
VIII	+/+	-/+	<i>AtGlcDH</i> hemizygous
IX	-/+	-/+	<i>Cat2</i> hemizygous/ <i>AtGlcDH</i> hemizygous

Nine different genotypes could be found via PCR (see Table 30). Columns 1-4 represent the four different primer systems for genotype identification. Thereby, column 1 and 2 belong to the *Cat2* mutation and 3-4 to the *AtGlcDH* mutation. In detail, the primer system for the *Cat2* T-DNA insertion was used in line 1, the *Cat2* genomic system in line 2, the *AtGlcDH* T-DNA system in line 3 and the *AtGlcDH* genomic system in line 4. For sample I (Figure 28) two fragments were amplified in the PCR: one fragment with the *Cat2* T-DNA insertion system and one with the *AtGlcDH* genomic system. So this sample represents a *Cat2* homozygous knock-out mutant (Δ *Cat2*). The sample II was identified as an *AtGlcDH* homozygous knock-out mutant (Δ *AtGlcDH*). Here the Δ *Cat2* genomic primer system and the Δ *AtGlcDH* T-DNA primer system showed an amplified fragment. A fragment from Δ *Cat2* and Δ *AtGlcDH* T-DNA insertion appeared in sample III (Figure 28), so this sample is a Δ *Cat2* homozygous and Δ *AtGlcDH* homozygous knock-out mutant (Δ *Cat2*/ Δ *AtGlcDH*). Sample IV shows bands in line 2 and 4, this means fragments with both genomic primer systems. This pattern is an azygous plant for both mutations.

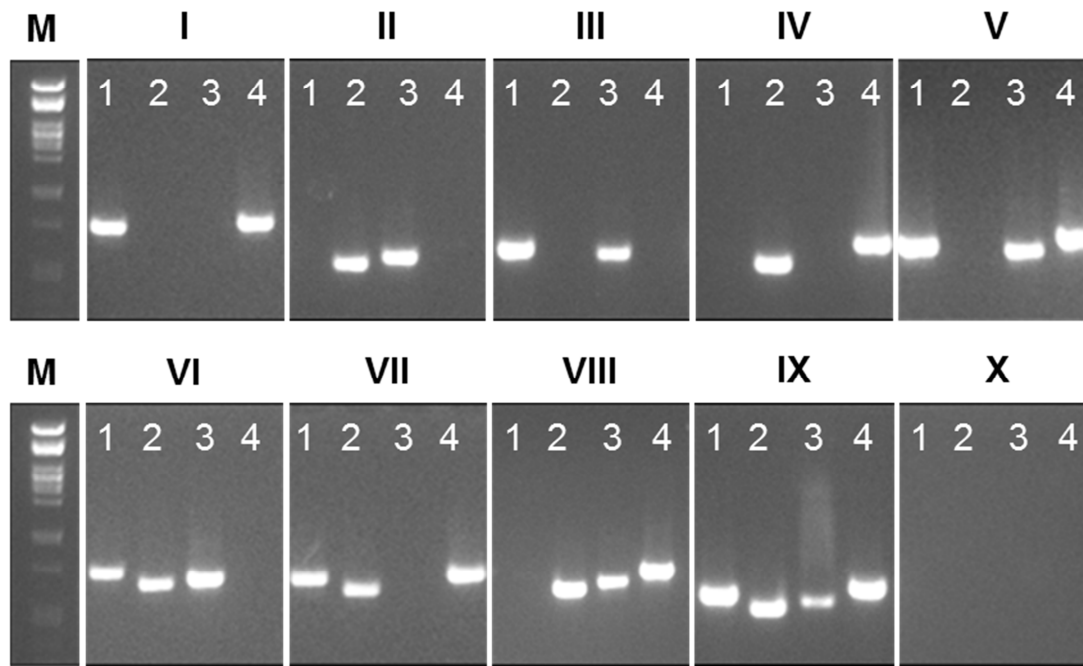


Figure 28: Identification of the T-DNA insertion and the genomic sequence from the F₂ generation resulting of the crossing from Δ Cat2 with Δ AtGlcDH. DNA/RNA was isolated from leaves of four weeks old plants and 2 μ l of the samples were used for the PCR. M represents the Lambda DNA/PstI Marker, 24 (Fermentas). The result of the PCR amplification of one sample is plotted to line 1-4. All fragments belong to one sample. The primer system for *Cat2* T-DNA insertion was applied to line 1 (993 bp), in line 2 the system for *Cat2* genomic sequence was used (746 bp). The same counts for the line 3 and 4, but here the primer system for the *AtGlcDH* T-DNA insert (line 3, 750 bp) and the *AtGlcDH* genomic sequence (line 5, 1045) was used. The Roman numerals represent the different samples, whereas IX stands for the positive control (hemizygous for both T-DNA insertions) and X for the negative control (water). (a) Δ Cat2, (b) Δ AtGlcDH, (c) Δ Cat2/ Δ AtGlcDH, (d) az, (e) Δ Cat2/AtGlcDH hemi, (f) Cat2 hemi/ Δ AtGlcDH, (g) Cat2 hemi and (h) AtGlcDH hemi. The gel was running for 45 min at 120 V.

Beside the described genotypes, other combinations were found. For example the *Cat2* hemizygous plant, which showed a fragment in line 1 and 2, with and without the *AtGlcDH* mutation (Figure 28, VI and VII). Mutants with a reciprocal combination were also detected. Thus, hemizygous *AtGlcDH* plants with and without *Cat2* mutation were identified (Figure 28, V and VIII). A *Cat2* hemizygous/*AtGlcDH* hemizygous plant (sample IX) was used as a positive control for the PCR and water (sample X) as a negative control.

Around 100-140 seeds were germinated on plates for each experimental set up and only 75% to 80% of these seeds were grown to plantlets. In total 405 F₂ plants from the cross of Δ Cat2 and Δ AtGlcDH were used for genotyping and only five plants were homozygous for both T-DNA insertions (see Table 31). Three of these five plants died after six weeks of growth at ambient CO₂ concentration. Plants were additionally grown for four weeks at high CO₂ concentrations (1500 ppm) and then shifted to 700-800 ppm CO₂ after transferring the plants from plate to soil. Two plants, homozygous for both T-DNA insertions, survived in this screen and seeds from the F₃ generation could be harvested. Furthermore, three other

Results

genotypes, including Δ Cat2, Δ AtGlcDH and az, were grown side by side with the double mutants and the seeds of the F₃ generation were harvested.

Table 31: Observed and theoretical segregation rate of the F₂ generation from the crossing of Δ Cat2 and Δ AtGlcDH. Numbers indicate the observed and expected number of individuals for each genotype. Hemi represents plants with one mutated allele.

Genotype	Observed	Expected	χ^2
Δ Cat2	43	25	13.72
Δ AtGlcDH	29	25	0.66
Δ Cat2/ Δ AtGlcDH	5	25	17.16
az	29	25	0.66
Δ Cat2/AtGlcDH hemi	35	51	5.74
Cat2 hemi/ Δ AtGlcDH	31	51	8.97
Cat2 hemi	54	51	0.2
AtGlcDH hemi	34	51	6.48
Cat2 hemi/AtGlcDH hemi	145	101	25.27
total number	405	405	

Most obvious, the Δ Cat2/ Δ AtGlcDH double mutant was only represented by five instead of the 25 plants. In addition, Δ Cat2 and Cat2 hemi/AtGlcDH hemi also showed a distorted segregation ratios with significant p values ($p < 0.05$).

The observed segregation was re-tested in the F₃ generation with segregants of two survivors that were rescued at high CO₂ concentrations. Beside the double mutant (Δ Cat2/ Δ AtGlcDH), segregants of the single mutant (Δ Cat2 and Δ AtGlcDH) and az (WT like) plants were investigated. 80 seeds per genotype from all four genotypes were grown side by side on 1/2 MS plates for three weeks at ambient CO₂ conditions. After three weeks the segregation was observed (Table 32) and the phenotypes were photographed using a binocular microscope (Figure 29). Stage-based phenotyping as described by Boyes (Boyes et al., 2001) was used. He described different growth stages of germinated plantlets depending on number of leaves, rosette diameter and development of flowers. In this work, only the leaf number dependent phenotyping at an early growth stage was used. After three weeks germinated plants with emerged cotyledons were defined as the 1.02 stage, plants with four leaves as 1.04 and plants with more than six leaves >1.06 (Boyes et al., 2001).

Δ AtGlcDH and az showed a similar distribution of the different plant sizes. More than 80% of the germinated plants had at least six leaves. The single Δ Cat2 mutant was characterized by an intermediate phenotype. 53 plants of germinated Δ Cat2 mutants had six or more leaves, whereas 13 plants only had developed cotyledons and 13 plants had two leaves beside the

cotyledons. For the $\Delta\text{Cat2}/\Delta\text{AtGlcDH}$ double knock-out mutant only two plants had more than six leaves after three weeks growing at ambient CO_2 conditions. These two plants were yellowish and smaller than the single mutants or az plants. 17 plants had four leaves also showing a yellowish phenotype and abnormal developed leaves. More than 75% of the double mutant did not show a normal development. 37 plants had only emerged cotyledons or even died at ambient CO_2 conditions after the cotyledons emerged and 32 seeds did not germinate.

Table 32: The growth phenotypes of three weeks old plantlets are shown below, using the stage-based phenotypic analysis of Boyes (Boyes et al., 2001). The numbers represent the number of plants depending to the defined phenotypic growth stage.

Genotype	Not germinated	Stage 1.02	Stage 1.04	Stage > 1.06
ΔCat2	6	13	16	53
$\Delta\text{AtGlcDH}$	0	0	10	76
$\Delta\text{Cat2}/\Delta\text{AtGlcDH}$	32	37	17	2
az	2	4	9	72

The ΔCat2 mutant plants showed the typical phenotype of a photorespiratory mutant. The cotyledons and older leaves were yellowish, whereas young leaves were green (Figure 29, first line). All investigated ΔCat2 plants showed the described phenotype. ΔCat2 mutants were also smaller compared to az plants (Figure 29, last line). The other single mutant, $\Delta\text{AtGlcDH}$, did not show significant differences as compared to az plants. The plants had the same size and leaves were also as green as az leaves (Figure 29, second line). However, cotyledons as well as the third and fourth emerged leaf of $\Delta\text{AtGlcDH}$ plants were often curled from the double mutant that reached stage 1.04. Interestingly, two different phenotypes were observed (Figure 29, third line). One phenotypes is characterized by a green to yellowish plant, which is smaller than the single mutants and az plants. Leaves of this phenotype are curled independent of the leaf number or leaf type. The other phenotype is characterized by small and yellow leaves. The leaves were also abnormal, bigger and not as round as the leaves of az plants. Independent of the phenotype, $\Delta\text{Cat2}/\Delta\text{AtGlcDH}$ plants died after four weeks grown at ambient CO_2 conditions.



Figure 29: Phenotype of the $\Delta\text{Cat}2$, $\Delta\text{AtGlcDH}$, $\Delta\text{Cat}2/\Delta\text{AtGlcDH}$ and *az* of the F_3 generation from the crossing of $\Delta\text{Cat}2$ with $\Delta\text{AtGlcDH}$ mutants. Plants were grown at ambient air conditions for three weeks and pictures were taken using a binocular microscope. Four individuals were pictured for each genotype starting with the single mutants $\Delta\text{Cat}2$ and $\Delta\text{AtGlcDH}$, following by the double mutant and *az* (WT like plants).

Due to the fact that the segregation of double mutants is distorted at ambient CO_2 concentrations and the fact that the F_2 generation of $\Delta\text{Cat}2/\Delta\text{AtGlcDH}$ survived at high CO_2 concentration (1500 ppm), but not at ambient CO_2 conditions (400 ppm) the assumption emerged that the genotype is not viable at ambient CO_2 concentrations. The results from the F_3 generation affirmed the hypothesis. Double mutants showed distorted germination, distorted growth rates and phenotypes. More investigations are necessary to proof and confirm the hypothesis.

3.2.2 Overexpression of the mitochondrial side pathway

As an alternative to testing phenotype of mutants, I also tested the importance of the mitochondrial side pathway by overexpression and physiological assays. To this end, both *AtGlcDH* and *AlaAT1* were simultaneously overexpressed in a transient transformation of tobacco leaves (see 2.2.4.4).

Overexpression vectors of *ALAAT1* (35S-*AlaAT1*) and *AtGlcDH* (35S-*AtGlcDH*) were designed (Niessen et al., 2012) and transiently transformed to intact tobacco leaves. As a control, also single overexpressors were generated. Overexpression of the transgenes was verified by RT-qPCR (data not shown). Both vectors were transformed alone and in a

combination. As a positive control, leaves were infiltrated with *Agrobacterium* carrying a vector that encodes an unrelated protein. Mitochondria were isolated of this infiltrated leaves and fed with ^{14}C -glycolate. Figure 30 shows the $^{14}\text{CO}_2$ release in transiently transformed tobacco plants.

The overexpression of ALAAT1 and *AtGlcDH* alone resulted in a similar increase in the CO_2 release of about 65% compared to the unrelated protein control. The simultaneous overexpression of both enzymes caused an enhancement of CO_2 release from ^{14}C -glycolate by 250% as compared to the control. Thus, overexpression of the components of the mitochondrial side pathway boosted glycolate conversion to CO_2 in this organelle. The overexpression of both enzymes was required to boost the CO_2 release from mitochondria. Because of this result, another approach was initiated with the goal to create an overexpression vector carrying ALAAT1 as well as *AtGlcDH* on one vector backbone.

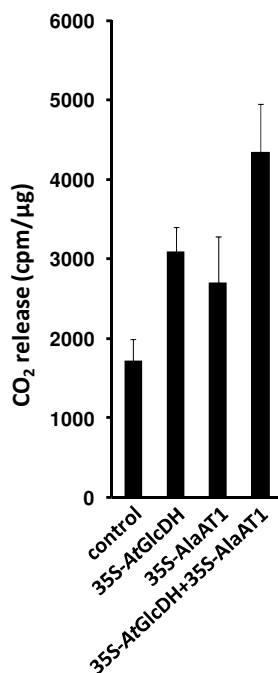


Figure 30: $^{14}\text{CO}_2$ release in transiently transformed tobacco plants over expressing RFP (control), AlaAT1 (35S-AlaAT1), *AtGlcDH* (35S-*AtGlcDH*) and both in a combination (35S-AlaAT1+35S-*AtGlcDH*). Isolated mitochondria corresponding to 50 μg protein were incubated with ^{14}C -glycolate. $^{14}\text{CO}_2$ release were captured in NaOH and determined by scintillation counting. Shown are the means \pm SE from at least 3 independent experiments. Cpm, counts per minute.

For this *AtGlcDH* was amplified by PCR using the vector A215-181. The amplified gene was used as template and ligated to the destination vector carrying ALAAT1 (A215-142) (see 2.1.20). To identify positive clones a PCR was performed.

Two positive clones (I and III) were used for transient transformation of intact tobacco leaves (Figure 32). Expression of the two genes from two different vectors was used as a positive control. As an additional control, leaves were infiltrated with *Agrobacterium* carrying the RFP gene, like in the previous experiments. Mitochondria were again isolated and labeled with

¹⁴C-glycolate. The simultaneous overexpression of *AtGlcDH* (35S-*AtGlcDH*) and *AlaAT1* (35S-*AlaAT1*) from two vectors resulted in an increase in the CO₂ release of about 120% compared to the control (Figure 32, 35S-*AtGlcDH*+35S-*AlaAT1*). The overexpression of both enzymes in one vector caused an enhancement compared to the control of 177% using clone I and an increase of 334% using clone III. Clone III was used for stable transformation of *Arabidopsis thaliana* plants by floral-dip-transformation (2.2.2.3).

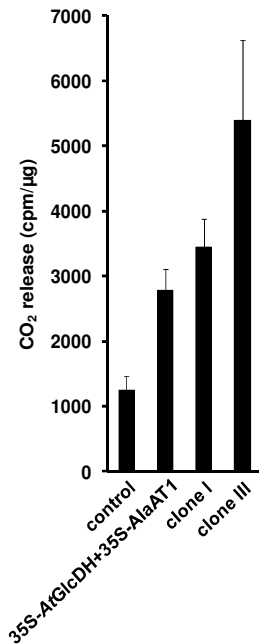


Figure 31: ¹⁴CO₂ release transiently transformed tobacco plant leaves overexpressing a red fluorescent protein (control), *AlaAT1* in a combination with *AtGlcDH* (35S-*AlaAT1*+35S-*AtGlcDH*) and both overexpressed in one vector (clone I and III). Isolated mitochondria corresponding to 50 µg protein were incubated with ¹⁴C-glycolate. ¹⁴CO₂ release were captured in NaOH and determined by scintillation counting. Shown are the means ±SE from at least 3 independent experiments. Cpm, counts per minute.

Wild type plants (WT), homozygous *Cat2* mutants (Δ *Cat2*) and homozygous *Ggat1* mutants (Δ *Ggat*) were transformed. The generated T₁ generation was identified via PCR.

Table 33: Results of the identification of the T₁ generation: WT, Δ *Cat2* and Δ *Ggat* plants were dipped with double vector 35S-*AlaAT1*/35S-*AtGlcDH* and T₁ plants were identified via PCR. + represents the presence of gene and – represents the absence of gene (knock-out).

Δ <i>Cat2</i>	Δ <i>Ggat</i>	Δ <i>AtGlcDH</i>	Genotyp
+ / +	+ / +	+	35S- <i>AlaAT1</i> /35S- <i>AtGlcDH</i>
- / -	+ / +	+	Δ <i>Cat2</i> /35S- <i>AlaAT1</i> /35S- <i>AtGlcDH</i>
+ / +	- / -	+	Δ <i>Ggat</i> /35S- <i>AlaAT1</i> /35S- <i>AtGlcDH</i>

The positive 35S-*AlaAT1*/35S-*AtGlcDH*, Δ *Cat2*/35S-*AlaAT1*/35S-*AtGlcDH* and Δ *Ggat*/35S-*AlaAT1*/35S-*AtGlcDH* T₁ were grown and propagated. T₂ seeds were harvested and are available for further investigations.

4. Discussion

4.1 Using *catalase 2* mutants for the investigation

Mutants in the major photorespiratory pathway were crossed with overexpressors of transgenic GlcDH in chloroplast (35S-*Ec*GlcDH and 35S-*Cr*GlcDH) and mitochondria (35S-*AlaAT*/35S-*At*GlcDH) or with a knock-out mutant of the mitochondrial side pathway (Δ *At*GlcDH) to investigate the importance of alternative side pathway on the major photorespiratory pathway. Two different photorespiratory mutants were used during this work. One of these mutants was the homozygous catalase 2 mutant (Δ Cat2). This mutant was characterized by a higher H₂O₂ content, because the photorespiratory H₂O₂ is not detoxified any longer. Higher H₂O₂ contents led to bleached leaves, reduced growth rate and reduced chlorophyll content at ambient CO₂ concentrations compared to WT plants (Frugoli, 1996; Queval et al., 2007) as well as to the activation of the oxidative stress response (Queval et al., 2007). Gene expression was influenced due to accumulation of H₂O₂. Genes involved in oxidative stress response like *GstF8*, *Gpx6*, *Apx1* and *Oxi1* were higher expressed in Δ Cat2 plants than in WT at ambient CO₂ concentration as well as during shifting experiments from high CO₂ (2000 ppm) to ambient (400 ppm) or low CO₂ (150 ppm) concentrations (Figure 17). Additionally, it was observed that different parameters of chlorophyll fluorescence measurements were reduced in Δ Cat2 compared to WT at ambient CO₂ conditions like F_v/F_m , Y(II) and NPQ as well as during shifting conditions from high CO₂ to ambient or low CO₂ conditions. The other photorespiratory mutant was the homozygous glutamate:glyoxylate aminotransferase knock-out mutant (Δ Ggat). This mutant showed an intermediate photorespiratory phenotype, which was characterized by a reduced growth rate and chlorotic lesions (Igarashi et al., 2003; Igarashi et al., 2006). This phenotype was not observed during this study. The Δ Ggat mutants looked like WT plants, no reduced growth or chlorotic lesions were observed. Chlorotic spots, reduced growth and reduced chlorophyll fluorescence were only observed under high irradiances like high light intensities and high temperature. Previous studies described that the Δ Ggat phenotype was influenced by increasing light intensities and temperature leading to a stronger phenotype (Igarashi et al., 2003). Due to the high light and high temperature, the WT was also characterized by reduced F_v/F_m and Y(II) value under these conditions (data not shown) and some chlorotic spots on leaves were observed, so these conditions were not suitable for the investigation. Δ Cat2 mutants showed a stronger phenotype under increased light intensities and even died after two weeks growing under these conditions. Former investigations revealed that Δ Cat2

plant developed cell death after shifting the plants for 8 h to high light intensities (Vanderauwera et al, 2005). Two more facts argue against the usage of the Δ Ggat mutants as a tool to investigate the influence of *Ec*GlcDH and *Cr*GlcDH on the major photorespiratory pathway. First, Δ Ggat mutants did not show strong differences in the F_v/F_m , Y(II) and NPQ values at ambient CO₂ concentrations. Furthermore, it was pointed out that the mutant was rather a knock-down than a knock-out mutant. The remaining *ggat* expression led to a reduced effect on the phenotype. A similar effect was observed in Δ Cat2 mutants. Δ Cat2 mutants with 7% residual expression of the WT level were significantly retarded in growth and underwent spontaneous lesion formations, whereas mutants with a residual expression of 20% showed no apparent phenotypical differences compared to WT (Vanderauwera et al., 2005). Also enzyme activities can influence the phenotype of photorespiratory mutants. Aminotransferases are well known for their function and how they can use several substrates. Four different aminotransferase were located to the peroxisomes including a glutamate:glyoxylate aminotransferase (GGAT), serine:glyoxylate aminotransferase (SGAT), alanine:glyoxylate aminotransferase (AGT) and aspartate:2-oxoglutarate aminotransferase (AspAT) (Rehfeld and Tolbert, 1972). Two of these enzymes are responsible for the transamination reaction during photorespiration and both can use several substrates for the reaction (Liepman and Olsen, 2001). In vitro assays showed that recombinant enzymes can use different amino donors and acceptor combinations. The recombinant GGAT for example used glutamate:glyoxylate as well as alanine:glyoxylate, glutamate:pyruvate and alanine:2-oxoglutarate as donor:acceptor combination (Liepman and Olsen, 2003). The recombinant SGAT used also beside glutamate:glyoxylate, alanine:glyoxylate as well as serine:pyruvate as a combination, whereas serine was the favored amino donor and glyoxylate the favored acceptor (Liepman and Olsen, 2001). Yu et al. described a competition between the different substrates of aminotransferases in the peroxisomes of plants inhibiting each other (Yu et al., 1984). A competition between alanine and glutamate was observed, but not between serine, glutamate or alanine (Betsche et al., 1983; Yu et al., 1984). The GGAT activity is according to this negatively influenced by adding serine or alanine to the mix. Because SGAT can also catalyze the transamination reaction of glyoxylate to glycine the flow through photorespiration is not completely stopped (Nakamura and Tolbert, 1983), but rather down regulated in Δ Ggat mutants, which might explain the intermediate photorespiratory phenotype of Δ Ggat mutants at ambient CO₂ concentration and low irradiation (Igarashi et al, 2003; Igarashi et al., 2006; Peterhänsel, 2010).

At the moment the effect of 35S-*Ec*GlcDH and 35S-*Cr*GlcDH in photorespiratory knock-out mutant background is unknown. It can happen that the integration of 35S-*Ec*GlcDH and 35S-*Cr*GlcDH has no effect to a complete photorespiratory knock-out mutant, but to a knock-down mutant. Furthermore, the necessity of the mitochondrial side pathway is also unknown.

The combination of the knock-out mutant in the mitochondrial side pathway ($\Delta AtGlcDH$) with a strong photorespiratory mutant ($\Delta Cat2$) can lead to even stronger photorespiratory phenotype or to an unviable mutant at ambient CO_2 conditions. So maybe it is better to use both, a complete knock-out mutant ($\Delta Cat2$) and a knock down mutant ($\Delta Ggat$) to investigate the impact of alternative photorespiratory mutants to the major pathway. So $\Delta Cat2$ and $\Delta Ggat$ were still used to cross with 35S-*EcGlcDH* and 35S-*CrGlcDH* as a second photorespiratory mutant.

4.2 Chlorophyll fluorescence

Many scientists used chlorophyll fluorescence as an important tool to evaluate changes in the photochemistry of photosystem II (PSII) and to detect the linear electron flux as well as to get hints about the CO_2 assimilation routes in vivo (Ritchie, 2006; Baker, 2008). On the one hand, this method allows to measure photosynthetic performances of plants and algae in a simple, rapid, nondestructive and objective way (Ritchie, 2006; Baker, 2008). On the other hand, it only allows to predict changes of photosynthetic performances under stress situations, because the interpretation of resulting data is complex and controversially discussed (Maxwell and Johnson, 2000; Baker, 2008). The principle of chlorophyll fluorescence is based on the absorbed light energy by chlorophyll a (Chla) molecule of PSII (Maxwell and Johnson, 2000; Ritchie, 2006; Baker, 2008). Absorbed light energy raises one electron from a ground state to a higher energy state. This electron is captured by an electron acceptor pool and tunneled through the electron chain reaction of the photosynthetic light reaction. So the electron transport results in photochemical energy (photochemical quenching) (Ritchie, 2006). Not all excited electrons of Chl a are captured by the electron acceptor pool and the electrons fall back to the ground state (Ritchie, 2006). The redundant energy can be dissipated as heat (non-photochemical quenching) or re-emitted as chlorophyll fluorescence (Maxwell and Johnson, 2000; Baker, 2008). Nevertheless, chlorophyll fluorescence only describes the intactness of photosynthetic potential and the real photosynthetic capacity of a plant. More measurements of the flux through photosynthesis and photorespiration, like gas exchange and labeling experiments, are necessary to get a clear overview about the real performances in plants.

My results of the chlorophyll measurements showed that $\Delta Cat2$ mutants were affected as compared to WT by lowering the CO_2 concentration (Figure 16). The $\Delta Cat2$ mutants were characterized by a reduced F_v/F_m , $Y(II)$ and NPQ during the shift from high CO_2 concentrations to ambient CO_2 condition. These differences became stronger with longer exposure to ambient CO_2 . $\Delta Cat2$ plants were characterized by a clearly visible phenotype after a few days at low CO_2 concentrations. The leaves were bleached and yellow, whereas

younger leaves were light green to yellowish and emerged leaves were light green. The plants even died under longer exposure to low CO₂ concentrations starting at ambient CO₂ (data not shown). A reduced F_v/F_m value was also found in other photorespiratory mutants grown at ambient CO₂ for example glyk1, Shm1 and pglp1. The F_v/F_m of glyk1, Shm1 and pglp1 mutants even declined due to longer exposure to ambient CO₂ concentrations in these mutants similar to the observed behavior of Δ Cat2 mutants (Timm et al., 2012). Plants grown at ambient air are characterized by a photorespiratory rate of around 20-25 % (Sharkey, 2001) due to this Δ Cat2 mutants accumulated H₂O₂ under this situation (Queval et al., 2007). In turn, accumulated H₂O₂ can lead to formation of reactive oxygen species (ROS). Both can react with several biological molecules leading to destroyed proteins, lipids or DNA and reducing the photosynthetic performances in plants due to altering or blocking the biological function of enzymes (Scandalios et al., 1997; Pignocchi et al., 2003; Vandenabeele et al., 2004). The toxic effect of H₂O₂ and ROS also led to a reduced growth rate of Δ Cat2 mutants at ambient CO₂ conditions due to severe perturbation of the antioxidant machinery, which had a negative influence on cell division and cell growth as well as the possibility of inducing cell death (Pignocchi et al., 2003; Vandenabeele et al., 2004). The possibility to induce cell death machinery is an explanation for the chlorotic spots and the yellowish leaves of Δ Cat2 plants compared to WT. WT plants can detoxify H₂O₂ and the toxic effect of H₂O₂ and ROS is missing. Furthermore, H₂O₂ can rapidly diffuse through biological membranes and consequently can cause oxidative stress and damages far away from the site of formation (Scandalios et al., 1997). So H₂O₂ can leave the peroxisome, the site of formation, and enter the chloroplast there H₂O₂ can react with proteins, which are sensitive to H₂O₂ including enzymes from the Calvin cycle, like fructose biphosphate and glyceraldehyde-3-phosphate dehydrogenase. This can negatively influence photosynthesis (quantum efficiency) and plant yield (photosynthetic yield and biomass) (Scandalios et al., 1997). Catalase 2 is not only responsible to remove photorespiratory produced H₂O₂, but also H₂O₂ produced by different oxidases or by the reduction of O₂⁻ formed during the photosynthetic electron chain reaction (Mittler et al., 2004). The production of H₂O₂ and ROS is elevated during photorespiration especially in Δ Cat2 mutants at low CO₂ concentrations or at high light conditions leading to a strongly reduced F_v/F_m and Y(II) value. Δ Cat2 mutants showed a stronger reduction of quantum efficiency and photosynthetic capacity after shifting the plants from high CO₂ to low CO₂ conditions. The F_v/F_m value declined slowly, whereas the Y(II) declined stronger compared to WT or az plants (Figure 16, 18-21). Strong photorespiratory conditions like high light intensities causes over-reduction at the reducing side of the PSI in the chloroplast leading to decreased NADP levels and thereby an increased diversion of electrons to oxygen as well as a boost production of ROS (Scandalios et al., 1997; Allan et al., 2009). Furthermore, the electrons of the PSII system become highly excited by the constant

absorbed high light energy. Photoinhibition takes place due to the permanently excited electrons resulting in damaging the D1 protein, which is necessary at the beginning of the electron transport chain (Allan et al., 2009). The PSII system is not able to absorb more light energy and the F_v/F_m value as well as the $Y(II)$ declined in the $\Delta Cat2$ mutant as well as in the double mutants $\Delta Cat2/35S-EcGlcDH$ and $\Delta Cat2/35S-CrGlcDH$ compared to WT (Figure 16, Figure 18-21). The over-reduction of PSI and the constant activation of PSII system led to a permanently damaged photochemical system so that photooxidation took place resulting in bleached leaves and reduced chlorophyll content as well as declined photosynthetic capacity in $\Delta Cat2$ plants (Allan et al., 2009). Interestingly, the differences in the F_v/F_m value and $Y(II)$ between $\Delta Cat2$ and WT as well as between $\Delta Cat2$ and $\Delta Cat2/35S-EcGlcDH$ or $\Delta Cat2/35S-CrGlcDH$ were only observed for cotyledons and the second and third emerged leaf (old leaves), but not in young leaves (Figure 18-21; Supplemental Figure 32-35). On the one hand, accumulation of photorespiratory H_2O_2 was higher in old leaves than in young leaves. Cotyledons are the first photosynthetically active tissue and photorespiratory H_2O_2 can accumulate. Gene expression of photorespiratory related genes were measured in six days old cotyledons (Zhong et al., 1994). On the other hand, leaf senescence is initialized earlier in older plant tissue than in younger one. It was shown that H_2O_2 influence the initiation of leaf senescence. The gene expression of *Cat2* is reduced and H_2O_2 accumulated resulting in protein degradation and reduced chlorophyll content (Orendi et al., 2001; Mittler et al., 2004; Vanderauwera et al., 2005; Zimmermann et al., 2006; Chang et al., 2009). Due to this, leaf senescence is linked to oxidative stress (Orendi, 2001). The accumulated photorespiratory H_2O_2 led to leaf senescence decreasing the F_v/F_m and $Y(II)$ value under stress situations like low CO_2 concentrations. In conclusion, $\Delta Cat2$ mutants showed a reduced photosynthetic capacity compared to WT or compared to $\Delta Cat2$ mutants combined with transgenic overexpressors of GlcDH due to the accumulation of toxic H_2O_2 and ROS in leaves. The photorespiratory accumulated H_2O_2 had in general a negative influence on enzyme activities, damaged the photosystem and reduced the chlorophyll content leading to a reduced quantum efficiency and photosynthetic capacity in $\Delta Cat2$ mutants compared to WT. The accumulation of H_2O_2 and ROS was higher in older leaves than in younger ones resulting in bleached cotyledons and also to reduced F_v/F_m as well as declined $Y(II)$. The flow through the major photorespiratory pathway was reduced in the $\Delta Cat2/35S-CrGlcDH$, because glycolate was already removed in the chloroplast. Due to this a reduced amount of glycolate was catalyzed to glyoxylate in the peroxisomes and the photorespiratory H_2O_2 content declined. The decreased H_2O_2 content led to a reduced negative impact on the photosynthetic capacity in form of a slightly higher F_v/F_m and $Y(II)$ value in the $\Delta Cat2/35S-CrGlcDH$ plants. Hints for the same effect were also found for $\Delta Cat2/35S-EcGlcDH$, but the impact of 35S-*EcGlcDH* was not stable concluding that the photorespiratory flux was not

reduced in $\Delta\text{Cat}2/35\text{S-}E\text{cGlcDH}$ plants as high as in $\Delta\text{Cat}2/35\text{S-CrGlcDH}$ plants. The effect of both GlcDH transgenes was only minor in the az background, because they did not show a positive influence at photosynthetic performances.

The non-photochemical quenching (NPQ) was also reduced in the $\Delta\text{Cat}2$ mutants as compared to WT or az plants. NPQ is linearly related to heat dissipation, so that redundant energy, which is not used in the photochemical process, is lost in form of heat (Maxwell and Johnson, 2000; Foyer et al., 2012). It was suggested that the NPQ value should be higher in the mutant background, because the light energy was not completely used in the photorespiratory mutant and the redundant energy should be lost in form of heat. But the value was reduced. The lower NPQ value is associated with a change of the ground-fluorescence under stress situations. Early studies detected an increased ground-fluorescence of the leaves after treatment with high temperature (Maxwell and Johnson, 2000). The increased ground-fluorescence was an indication parameter for the photoinhibitory damage in photosynthetic tissue due to high temperature, low temperature or drought (Gamon and Pearcy, 1989; Epron et al., 1992; Maxwell and Johnson, 2000). Such damage can occur in $\Delta\text{Cat}2$ mutants, which are deficient in oxidative stress tolerance resulting in a reduced protection against photoinhibition at ambient as well as at low CO_2 concentrations. The photosynthetic capacity can also be influenced by treatment with chemicals like DCMU (3-(3,4-dichlorophenyl)-1,1-dimethylurea). DCMU was attached to the D1 protein inhibiting the electron transport from Q_A to Q_B in the electron transport chain and increasing the ground-fluorescence of treated plants. Due to the increased ground fluorescence, the maximal quantum yield (F_v/F_m) was declined as well as the photosynthetic capacity ($Y(II)$) (Hipkins and Baker, 1986). The integration of a GlcDH transgene had no impact on NPQ neither in $\Delta\text{Cat}2$ nor in az plants.

4.3 Gene expression of H_2O_2 -inducible genes

The accumulation of H_2O_2 was used to investigate the impact of photorespiratory side pathways on the major photorespiratory cycle at gene expression levels. H_2O_2 plays a dual role in plants. On the one hand, H_2O_2 is a toxic by-product of cell metabolism like photorespiration in plants (Vanderauwera et al., 2005). On the other hand, it is also an important signal molecule in stress protection as well as in signal transduction and has a direct impact on gene expression (Vandenabeele et al., 2004; Vanderauwera et al., 2005). Elevated H_2O_2 levels influence the defense response during biotic and abiotic stresses including genes for acclimation, cross-tolerance, up regulation of heat shock proteins during high light intensities or induction of active cell death processes (Vandenabeele et al., 2004; Vanderauwera et al., 2005). Different H_2O_2 -inducible genes were measured during this thesis

including different oxidases, which can metabolize H_2O_2 , and genes involved in response to ROS, pathogen defense or in common stress response. Plants have different oxidases to detoxify H_2O_2 including catalase (Cat), glutathione S-transferase, glutathione/thioredoxin peroxidase (Gpx) and ascorbate peroxidase (Apx) (Mhamdi et al., 2010). Δ Cat2 mutants are the best background to investigate the impact of perturbation of specific genes influenced by photorespiratory produced H_2O_2 due to the accumulation of H_2O_2 in the mutant plants (Mhamdi et al., 2010). It was shown that the different oxidases or peroxidases were H_2O_2 -inducible genes (*GstF8*, *Gpx6*, *Apx1* and *Oxi1*) and that these genes were much stronger induced in the Δ Cat2 background than in the WT plants due to exposure to low CO_2 and maybe due to the higher accumulation of photorespiratory H_2O_2 in mutant plants (Queval et al. 2007). My results showed that after 6 h exposure to low CO_2 concentrations the gene expression of *GstF8* and *Gpx6* was maximal in the Δ Cat2 mutant background (Figure 17). Also, a positive impact of the transgenic GlcDH was observed. Δ Cat2/35S-*Cr*GlcDH plants were characterized by lower gene expression of H_2O_2 -inducible genes, especially for *GstF8* and *Gpx6*, than Δ Cat2 mutants without a transgenic GlcDH (Figure 24). This was not observed for the combination of Δ Cat2 with 35S-*Ec*GlcDH (Figure 23). 35S-*Cr*GlcDH also showed hints for a positive impact in the az background (WT-like plants) (Figure 24). Here the expression of H_2O_2 -inducible genes was slightly reduced in 35S-*Cr*GlcDH plants as compared to az plants. This reduction in the az background was unstable and was not reproducible during the different replicates. *GstF8* showed the strongest effect to low CO_2 concentration in the Δ Cat2 mutant. GST has a critical role in the response to oxidative stress and detoxifying of xenobiotics in plants as well as for the response to different environmental stress including herbicides and pathogens (Chen et al., 1996). *GstF8* had an alternate promoter, which led to the formation of a small *GstF8* and a large *GstF8* transcript (Thatcher et al., 2007). The small *GstF8* transcript was more expressed in leaves than in roots, whereas the large transcript was higher expressed in roots than in green tissue (Thatcher et al., 2007). It was suggested that the alternative promoter is responsible for the differential tissue-specific and stress-responsive expression pattern as well as for the differential targeting of both proteins (GstF8 small and large protein) (Thatcher et al., 2007). During this study only green tissue of a plant was used for the gene expression measurement excluding the influence of tissue specific expression. *GstF8* was also used as an early stress- response gene, whose expression was induced 45 min after treatment with H_2O_2 , whereas a longer exposure to H_2O_2 led to a decrease of *GstF8* expression (Chen et al., 1996; Sappl et al., 2009; Gleason et al., 2011). This behavior of *GstF8* expression was also observed during this study. The induction already started after 1 h exposure to low CO_2 , but the peak was reached after 6 h treatment and decreased again. Here, *GstF8* showed the highest expression level in the Δ Cat2 compared to the other genotypes (Δ Cat2/35S-*Ec*GlcDH or

Δ Cat2/35S-CrGlcDH, az and 35S-EcGlcDH or 35S-CrGlcDH). Only the 35S-CrGlcDH transgene had a significant effect on *GstF8* expression in the mutant background. The expression was reduced in Δ Cat2/35S-CrGlcDH compared to Δ Cat2 indicating that the flux through photorespiratory H₂O₂ production was reduced in these plants.

Not only the expression of *GstF8* was induced due to oxidative stress, but also several peroxidases were up regulated due to oxidative damage caused by H₂O₂ and ROS (Milla et al., 2003). One of these peroxidase was *Gpx6*. *Gpx6* is a plant peroxidase, which metabolizes H₂O₂ via oxidation of phenolic compounds (Asada, 2006) GPX6 is a key enzyme of the antioxidant network and acts as a scavenging system for H₂O₂, ROS and reactive nitrogen species (RNS) as well as a key enzyme in pathogen response (Dayer et al., 2008; Chang et al., 2009; Noctor et al., 2011). The expression is up regulated by photooxidative stress like treatment with H₂O₂, even with different strength of the induced stress (Milla et al., 2003; Fischer et al., 2009) concluding that *Gpx6* seems to have the same role for response to oxidative stress, pathogen defense and response to abiotic stresses like *GstF8* and is involved in the redox signaling pathway in plants (Noctor et al., 2011). *Gpx6* showed also the strongest expression pattern after 6 h exposure to low CO₂ concentrations in the mutant background (Figure 23-24). The expression of *Gpx6* was lower in Δ Cat2/35S-CrGlcDH than in the Δ Cat2 mutant plants. The combination of Δ Cat2 with 35S-EcGlcDH did not show any stable differences over the three replicates. This indicated that the integration of 35S-EcGlcDH had no impact on the major photorespiratory pathway, whereas the integration of 35S-CrGlcDH had a positive impact in the mutant background reducing the flow through the major pathway and in turn reducing the accumulation of photorespiratory H₂O₂. This positive impact was absent in the azygous background.

Two other genes that were analyzed for their response to the CO₂ shift were *APX1* and *OX1*. The ascorbate peroxidase (APX) is the first enzyme of the ascorbate-glutathione cycle eliminating H₂O₂ by reducing ascorbate to monodehydroascorbate and water (Kang et al., 1998; Cuk et al., 2010). The last step of the regeneration cycle of glutathione is the glutathione reductase (GR), which also represents the rate limiting step of the cycle (Kang et al., 1998). The contents of ascorbate and glutathione play a crucial role in response to oxidative stress and in the defense against it (Foyer and Noctor, 2005). Both genes were up regulated by abiotic and biotic stress as well as during development of seeds (Caverzan et al., 2012). The expression pattern of *Apx1* showed a coregulation with other genes involved in the response to oxidative stress like *Cat2*, *Sod*, *Gr* or *Gpx6* (Kang et al., 1998; Mhamdi et al., 2010; Caverzan et al., 2012) induced by environmental stimuli like salt, drought, high light, high temperatures and H₂O₂ content (Caverzan et al., 2012). *Apx1* knock-out mutants were characterized by reduced growth rate and alternations in the physiology as well as in the metabolism (Caverzan et al., 2012). The reduced growth rate reminds the phenotype of

Δ Cat2 mutants, which showed also reduced growth at photorespiratory conditions. The H_2O_2 content in leaves of *Apx1* knock-out mutants was increased compared to the control and caused the collapse of the H_2O_2 scavenging system at high irritations like high light also reminding the behavior Δ Cat2 mutant (Karpinski et al., 1997; Davletova et al., 2005). An *Apx1* knock-out mutant in rice was characterized by reduced growth, semi-dwarf seedlings, yellow-green leaves and lesions (Zhang et al., 2013). The *Apx1* expression was increased due to exposure to light and even more expressed due to high light intensities, drought or after applying H_2O_2 (Storozhenko et al., 1998; Yoshimura et al., 2000; Panchuk et al., 2002; Rossel et al., 2002; Pignocchi et al., 2003; Qin et al., 2008). A light induced expression and a slightly induced expression due to low CO_2 concentrations was observed in the Δ Cat2 mutant background and azygous background (Figure 17). My hypothesis was that the *Apx1* gene expression would be higher in Δ Cat2 mutants compared to 35S-*EcGlcDH* or 35S-*CrGlcDH*, because the flux through photorespiration should be reduced. No positive influence was detected neither for the integration 35S-*EcGlcDH* nor for 35S-*CrGlcDH* in the Δ Cat2 or az background indicating that *Apx1* expression is not induced via photorespiration. Similar results were observed for the expression pattern of *Oxi1*. The expression of *Oxi1* was near the detection border, so the expression was only measurable after 1 and 6 h exposure to low CO_2 conditions in the Δ Cat2 background. It was shown that the expression of *Oxi1* was induced by H_2O_2 and in response to H_2O_2 -generating stimuli, oxidative stress or ROS produced by plant-pathogen interaction (Rentel et al., 2004; Petersen et al., 2009). *Oxi1* is general responsible for root hair development and basal defense against pathogens (Petersen et al., 2009). GUS staining revealed that *Oxi1* expression appeared around the region of wounding, the same region there the H_2O_2 content was induced (Petersen et al., 2009). So *Oxi1* expression seems to be an important tool for response to oxidative stress as well as for defense against pathogens (Rentel et al., 2004; Petersen et al., 2009). Although *Oxi1* plays an important role in oxidative stress response, the measurement of the expression pattern at low CO_2 concentrations was not suitable due to the low gene expression in the Δ Cat2 background and az background.

Tolerance to oxidative stress involved genes, pathways and mechanism that are unknown up to day (Luhua et al., 2008). Microarray data showed hints that three additional genes were induced by low CO_2 concentrations (Niessen, unpublished). These three additional genes were *Atlea5*, *Atwak1* and *Atwrky33*. *Atlea* encodes the late embryogenesis abundant protein and plays a role in the response to environmental changes (Zhao et al., 2011). *Atlea3-3* and *Atlea3-4* for example were responsible for response to abiotic stress, ABA, high salinity and osmotic stress as well as for cold tolerance (Zhao et al., 2011). Some *Atlea* genes even have an important role in oxidative stress tolerance. Overexpression lines showed a higher tolerance against drought, cold and freezing like *Atlea4* and *Atlea5* (Dalal et al., 2009; Salleh

et al., 2012). Different *Atwak* genes had also a broad range of responsibility. Some were responsible for linking environmental stimuli to physiological responses including oxidative stress and were co-expressed with known pathogen defense related genes (Meier et al., 2010). Former studies revealed that *Atwak1* was involved in early response to pathogens. The gene expression was strongly induced after infection with fungi and bacteria or after wounding (Verica, 2002; Verica, 2003). The last potential gene, expressed due to low CO₂ concentrations was *Atwrky33*. *Atwrky* transcript factors were involved in the regulation of plant processes including pathogen response, senescence, development and interaction with ROS (Euglem et al., 2000; Lippok et al., 2007). Only two of these genes showed an induction due to low CO₂ concentration in the mutant background and in WT plants. *Atwak1* was induced in both genotypes in the same intensity (Figure 17). The expression peak was detected after 6 h exposure to low CO₂. *Atlea5* was strongly induced in the Δ Cat2 mutant as compared to the WT after shifting the plants for 6 h from high CO₂ to low CO₂ conditions. *Atwrky33* did not show any differences between the CO₂ treatment or genotypes. Unfortunately, the expression was not different between Δ Cat2 and Δ Cat2/35S-*EcGlcDH* or Δ Cat2/35S-*CrGlcDH* plants (Supplemental Figure 36+37). The integration of a transgenic GlcDH had no impact on the expression level in the mutant background. The same was observed in the az background, no differences were detected neither between the CO₂ concentrations or the genotypes (Supplemental Figure 36+37).

In conclusion, genes involved in oxidative stress response like *GstF8* and *GPX6* were influenced by photorespiratory accumulated H₂O₂, whereas genes indirectly involved in H₂O₂ removal due to their role for H₂O₂ mediated pathogen response were not influenced by photorespiratory H₂O₂ accumulation. Significant differences were observed for *GstF8* and *Gpx6* in Δ Cat2 plants compared to Δ Cat2/35S-*CrGlcDH* indicating a reduced flux through the major photorespiratory pathway. The difference between az and 35S-*CrGlcDH* was not stable over the three replicates, so that a interpretation was not possible. The integration of 35S-*EcGlcDH* did not show any positive effects neither in Δ Cat2 background nor in az background concluding that the flux in plants combined with 35S-*EcGlcDH* were not characterized by a reduced flux through photorespiration like plants, which were combined with 35S-*CrGlcDH*.

4.4 Metabolites

Metabolite profiles were used to investigate changes in plant metabolism during different stresses like CO₂ or to investigate a mutation of a special enzyme in comparison to the WT. Photorespiration is closely linked to N metabolism and C metabolism in plants, which is needed for an optimal growth and biomass production (Novitskaya et al., 2002). N

metabolism is complicated by photorespiration due to the NH_3 release in the mitochondria resulting from the formation of serine and the refixation of the released NH_3 in the chloroplast by the formation of glutamate from glutamine (Leegood et al., 1995; Novitskaya et al., 2002). Changing the CO_2 concentration has an impact on the rates of the amino acid cycle. Higher photorespiration rates influence contents of glycine, serine and glutamine (Stitt et al., 2002; Foyer et al., 2009). Several studies revealed that the ratio of glycine and serine value directly correlates with the flux through photorespiration (Novitskaya et al., 2002; Allan et al., 2009). Different photorespiratory mutants showed an accumulation of glycine under photorespiratory supporting conditions, whereas the content of serine declined or increased depending of the knock-out (Tolbert, 1981; Novitskaya et al., 2002). The accumulation of glycine was also observed in the $\Delta\text{Cat}2$ as well as in az plants with the same intensity (Figure 26). Other photorespiratory mutants were characterized by a higher glycine accumulation compared to WT after shifting the plants from high CO_2 to ambient CO_2 concentrations. For example, the SGAT knock-out mutant showed a higher glycine accumulation than WT at ambient CO_2 concentrations (Somerville and Ogren, 1980b). A similar pattern was observed for the HPR1/HPR2 double mutant. The glycine level increased after shifting the plants from high CO_2 to ambient CO_2 , whereas the glycine level of the single mutant was not different compared to WT (Timm et al., 2008). Another photorespiratory knock-out mutant accumulated glycine, because of the deficient formation of glycine to serine (Somerville and Ogren, 1981). Due to the fact that the glycine level increased after shifting the plants from high to low CO_2 concentrations, the shifting was successful, but maybe the shift was too hard and led to an equal accumulation in both genotypes (Figure 26). The $\Delta\text{AtGlcDH}$ mutant was also characterized by an accumulation of glycine after shifting the plants from ambient CO_2 to low CO_2 concentrations, but the increase of the glycine value was lower compared to the one of the WT (Niessen et al., 2012). Furthermore, no significant differences for glycine were observed between $\Delta\text{Cat}2$ and $\Delta\text{Cat}2/35\text{S-EcGlcDH}$ or $\Delta\text{Cat}2/35\text{S-CrGlcDH}$ plants as well as for all genotypes of the az background. The serine content also increased due to the treatment. Serine level increased more in the $\Delta\text{Cat}2$ mutant as compared to az plants. The integration of 35S-CrGlcDH had an impact on the serine accumulation in the $\Delta\text{Cat}2$ background as well as in the az background (Figure 26-27). The genotypes combined with 35S-CrGlcDH were characterized by a lower serine accumulation than their corresponding genotype without a transgenic GlcDH concluding that the flux through the glycine-serine conversion was higher in these plants. In contrast, the integration of 35S-EcGlcDH had no influence on the serine level neither in the $\Delta\text{Cat}2$ nor in the az background. Other photorespiratory mutants were also characterized by an accumulation of serine. The SGAT mutant showed a serine accumulation at ambient CO_2 concentration (Somerville and Ogren, 1980b). The same pattern was observed in HPR single

(HPR1 and HPR2) as well as for HPR double mutant, which were characterized by a serine accumulation after transferring the plants from high to ambient CO₂ concentrations (Timm et al., 2008). Contrariwise, the serine content in $\Delta AtGlcDH$ lines did not change after shifting from ambient to low CO₂ concentration like the corresponding WT (Niessen et al., 2012). Other photorespiratory mutants were characterized by decreased serine contents after shifting. $\Delta Ggat$ mutants showed a decrease in serine values, whereas the overexpressor line was characterized by increased serine content after shifting plants from high CO₂ to ambient CO₂ (Igarashi et al., 2003; Igarashi et al., 2006). Glycine:serine ratio showed a positive correlation with photorespiratory flux, whereas aspartate and alanine are negative correlated with photorespiration (Novitskaya et al., 2002). With higher photorespiratory rates the content of alanine declined in both $\Delta Cat2$ and az plants (Figure 25-27). The decreased alanine content was also observed in the $\Delta Cat2$, $\Delta Cat2/35S-EcGlcDH$, $\Delta Cat2/35S-CrGlcDH$, az, $35S-EcGlcDH$ and $35S-CrGlcDH$ plants. No differences between the genotypes were observed. Also no positive impact of the integration of a transgenic GlcDH was observed in form of a weaker declined alanine contents. The activity of alanine aminotransferases are correlated with photorespiration. Higher photorespiration rate resulted in increasing activities of AlaAT leading to alanine accumulation instead of asparagine (Ricoult et al., 2005). Accumulation of alanine as well as the increase gene expression of AlaAT contributed to a higher tolerance to low CO₂ concentration. In contrast, reducing the expression of alanine synthesis resulted in a disturbed germination and development of seedlings at low CO₂ concentrations (Ricoult et al., 2005). A similar pattern was observed in HPR1 mutants. The alanine content decreased with increased photorespiration (Timm et al., 2008). The changes in the content correlated with enhanced levels of aspartate, asparagines and arginine (Timm et al., 2008). The complete role of alanine during photorespiratory conditions is not known, but alanine seemed to have an important role for tolerance against low CO₂ conditions (Tolbert, 1981; Ricoult et al., 2005). Photorespiration negatively influences photorespiration resulting in reduced sugar contents. For example SGAT mutants were characterized by a reduced starch and sucrose content (Somerville and Ogren, 1980b). AlaAT knock-out mutants ($\Delta AlaAT$) were also characterized by a reduced glucose and fructose content after shifting the plants from ambient to low CO₂ conditions, whereas sucrose content did not change due to the shift (Niessen et al., 2012). A different pattern was observed for $\Delta Cat2$ mutant as compared to az plants (Figure 25). The sucrose and glucose content did not decrease in $\Delta Cat2$ plants after shifting the plants from high to low CO₂ concentration. In contrast, sucrose as well as glucose content of az plants clearly decreased due to the treatment. Maybe the shift was not long enough to strongly influence the sucrose content, but long enough to have a negative impact for the glucose content in az plants. The reduction of the glucose content was also observed in $\Delta Cat2$, $\Delta Cat2/35S-EcGlcDH$, $\Delta Cat2/35S-CrGlcDH$,

az, 35S-*EcGlcDH* and 35S-*CrGlcDH* plants (Figure 26-27). No significant differences were observed in the Δ Cat2 background independent of the combination with 35S-*EcGlcDH* or 35S-*CrGlcDH*, but a positive impact was observed in the az background. The combinations with a transgenic GlcDH were characterized by a lower decrease of glucose content compared to the corresponding az plants. As previously described aspartate is also negatively correlated with photorespiration. The aspartate content was reduced in both Δ Cat2 and az plants (Figure 25). The content was more decreased in Δ Cat2 mutants than in az plants. The level of aspartate was also decreased in Δ Cat2, Δ Cat2/35S-*EcGlcDH* and Δ Cat2/35S-*CrGlcDH*, whereas no differences between these genotypes were detected (Figure 26-27). The same was observed for the az background. A negative influence of photorespiration to the aspartate content was observed during this study, but no difference between GlcDH transgene and their corresponding az plant was detected. A significant difference between Δ Cat2 and az plants was observed for the threonic acid value (Figure 25). Threonic acid was significantly increased in Δ Cat2 plants, but not changed in az. No differences were detected between Δ Cat2 and Δ Cat2/35S-*EcGlcDH* or Δ Cat2 and Δ Cat2/35S-*CrGlcDH* (Figure 26). Further, no differences were detected in the az background independent of the genotype (Figure 27). Threonic acid plays a role in the vitamin C metabolism. Vitamin C has an important role for the redox signaling pathway, during response to pathogens, as anti-oxidant, as stress response factor and as enzyme co-factor (Debolt et al., 2007). Due to this the threonic acid signaling pathway is activated in Δ Cat2 mutants, but not in az plants after shifting the plant from high CO₂ to low CO₂ conditions. The photorespiratory fluxes influence the content of different metabolites (Foyer et al., 2009) and also regulated via gene expression and mRNA level of photorespiratory genes. Level of photorespiratory metabolite were regulated in a day/night cycle increasing with onset of the light, were maximal at the end of the day and decreasing after the light is switched off (Murray et al., 1989; McClung, 1997; Timm et al., 2013). Timm suggested that there is a correlation between the influences of photorespiratory fluxes to the metabolite contents and in turn the metabolites influence gene expression of photorespiratory-related genes (Timm et al., 2013). This hypothesis revealed a much more complex regulation of plants gene expression and metabolism related to photorespiration than ever suggested. To investigate such a complex connection, more experiments are needed including a broad range of photorespiratory stresses like CO₂, light, drought and temperature. Unfortunately, the impact of alternative photorespiratory side pathways on the major pathway was not seen in metabolite levels.

4.5 Importance of the mitochondrial side-pathway

Photorespiratory mutants were characterized by a broad range of different phenotypes including “weak”, “intermediate” and “heavy” photorespiratory mutants (Timm and Bauwe, 2013). “Weak” photorespiratory mutants are viable at ambient CO₂ concentrations like Δ Cat2, Δ Ggat, Δ AtGlcDH, Δ AlaAT, HPR1, HPR2, HPR3 as well as SHMT1 knock-out mutants. These “weak” photorespiratory mutants were characterized by a reduced growth and some of them also showed formation of chlorotic spots (Somerville and Ogren, 1981; Igarashi et al., 2003; Queval et al., 2007; Timm et al., 2008; Niessen et al., 2009; Niessen et al., 2012). Mutants of the “intermediate” phenotype were unviable at ambient CO₂ concentration, but viable at high CO₂ indicating on the one hand an important role for photorespiration, but on the other hand that the enzyme was not required for photorespiratory unrelated functions (Somerville and Ogren, 1981; Timm and Bauwe, 2013). Mutants of this category are SGAT, Fd-GOGAT, GS, GLYK and PGLP1 (Somerville and Ogren, 1980a; Somerville and Ogren, 1980b; Murray et al., 1989; Boldt, 2005; Schwarte and Bauwe, 2007). “Heavy” photorespiratory mutants were characterized by a lethal mutation even at high CO₂ concentrations (Timm and Bauwe, 2013). The SHMT1/SHMT2 and the GLDP1/GLDP2 double knock-out mutants were unviable at high CO₂ concentrations (Engel et al., 2007; Engel et al., 2011). Both enzymes represented the close relationship of photorespiration glycine-serine conversion with the C₁ metabolism of plants (Engel et al., 2011; Timm and Bauwe, 2013). The C₁ molecule is essential for plants, because it is the precursor for proteins, nucleic acids, alkaloids and the incorporation of lipids (Bauwe et al., 2010). In this work, a “weak” main photorespiratory mutant (Δ Cat2) was crossed with a second “weak” photorespiratory mutant (Δ AtGlcDH) of the mitochondrial side-pathway. Single mutants were viable at ambient CO₂ concentrations. Δ Cat2 mutants showed a reduced growth, yellowish leaves and the spontaneous formation of chlorotic spots at ambient CO₂ concentrations (Queval et al., 2007). This phenotype was observed in young plants growing at short day conditions (8h light and 16 h darkness), but was no longer detected in eight week old plants. Eight weeks old Δ Cat2 mutants looked like the WT, whereas the differences were found in the chlorophyll content and thickness of the leaves compared to parallel grown WT plants. Growing the plants at high light irradiations led to a strong visible photorespiratory phenotype. Δ Cat2 leaves were bleached and more chlorotic spots were detected compared to Δ Cat2 plants grown at low irradianations. The Δ AtGlcDH mutant did not show any visible photorespiratory phenotype compared to WT plants. The mutant was characterized by a reduced mitochondrial CO₂ release and a reduced PIB as compared to WT (Niessen et al., 2009). The F₂ generation from the crossing of Δ Cat2 with Δ AtGlcDH showed a reduced germination rate. Only five double mutants under about 400 plants were found in the F₂ generation indicating a disturbed segregation in the F₂ generation. The F₂ generation was

grown at ambient CO₂ concentrations and the double mutant died under this condition concluding that the double mutant is not really viable at ambient CO₂ concentration like an “intermediate” photorespiratory mutant. Due to that, the mutants were grown at high CO₂ and two double mutants survived and were used to generate F₃ seeds. The investigation of the F₃ generation confirmed the hypothesis that the double mutant is not viable at ambient CO₂ concentrations. Double mutant plants showed a reduced germination rate, bleached leaves, abnormal development of leaves and died after growing three weeks at ambient CO₂ concentrations. It seems that the main photorespiratory pathway in the double mutant is disturbed and toxic intermediates accumulated influencing photosynthetic performances, germination and development of Δ Cat2/ Δ AtGlcDH plants. Furthermore, the mitochondrial side pathway seems to play a reduced role in a healthy plant, but an important role in a Δ Cat2 mutant background. The natural chloroplastidal side pathway is not strong enough to complement the photorespiratory double knock-out mutation. Both side pathways are necessary to bypass the main pathway and maybe to reduce the accumulation of toxic intermediates in a “weak” photorespiratory mutant like Δ Cat2 leading to the “weak” photorespiratory phenotype and to the possibility to survive at ambient CO₂ concentrations. To investigate the influence of the mitochondrial side pathway in more detail, more experiments were needed. It has to be confirmed that the double mutant really is a “intermediate” photorespiratory mutant and viable at high CO₂ concentrations, but not at ambient CO₂ concentrations. Furthermore, the other way around should be investigated. This means the influence of the overexpression of the mitochondrial side pathway to the main photorespiratory pathway. Δ Cat2 mutants as well as Δ Ggat mutants were dipped with overexpressors of the complete mitochondrial side pathway including the over expression of AtGlcDH and AlaAT1 (35S-AlaAT1/35S-AtGlcDH). These mutants can be used to perform the same experiments as with the genotypes from the crossing of Δ Cat2 with 35S-*Ec*GlcDH and 35S-*Cr*GlcDH. The integration of 35S-*Cr*GlcDH, a transgenic GlcDH, leads to a reduced flow through the main photorespiratory pathway leading to a higher photosynthetic efficiency and reduced expression of H₂O₂-inducible genes. Maybe the overexpression of a natural side pathway also leads to reduced flux through the photorespiratory pathway like the integration of 35S-*Cr*GlcDH.

5 Conclusion

The results of this study revealed that the chloroplastidal side pathway has a minor role in photorespiration and is a rudimental evolutionary side pathway in higher plants. Transgenic plants overexpressing *CrGlcDH* showed reduced flux through the major photorespiratory pathway resulting in a reduced production of photorespiratory H_2O_2 in the mutant background under ambient air and low CO_2 conditions. Interestingly, *EcGlcDH* overexpressors did not show any impact on the major pathway. Possible further experiments are for example genome walking to define the integration site of the transgene, immune blotting to analyze the presence of the enzyme and enzyme activity assays. Moreover, the influence of the transgene was not observed in the azygous background. Due to this, the hypothesis that the chloroplastidal side pathway has an important role in photorespiration was not confirmed. Data from this project indicate that the mitochondrial side pathway may have a significant impact on the major pathway. The double knock-out mutant of the major photorespiratory pathway and the mitochondrial side pathway was not viable at ambient CO_2 concentrations. On the one hand, more experiments are necessary to investigate the influence of the mitochondrial side pathway in detail. The double knock-out mutant has to be characterized under ambient and high CO_2 concentrations using chlorophyll fluorescence measurements, metabolite profiling and growth experiments. On the other hand, the characterization of overexpression lines of the mitochondrial side pathway would help to understand if the mitochondrial side pathway has a significant impact on photorespiration.

6 Appendix

6.1 Supplemental Figures

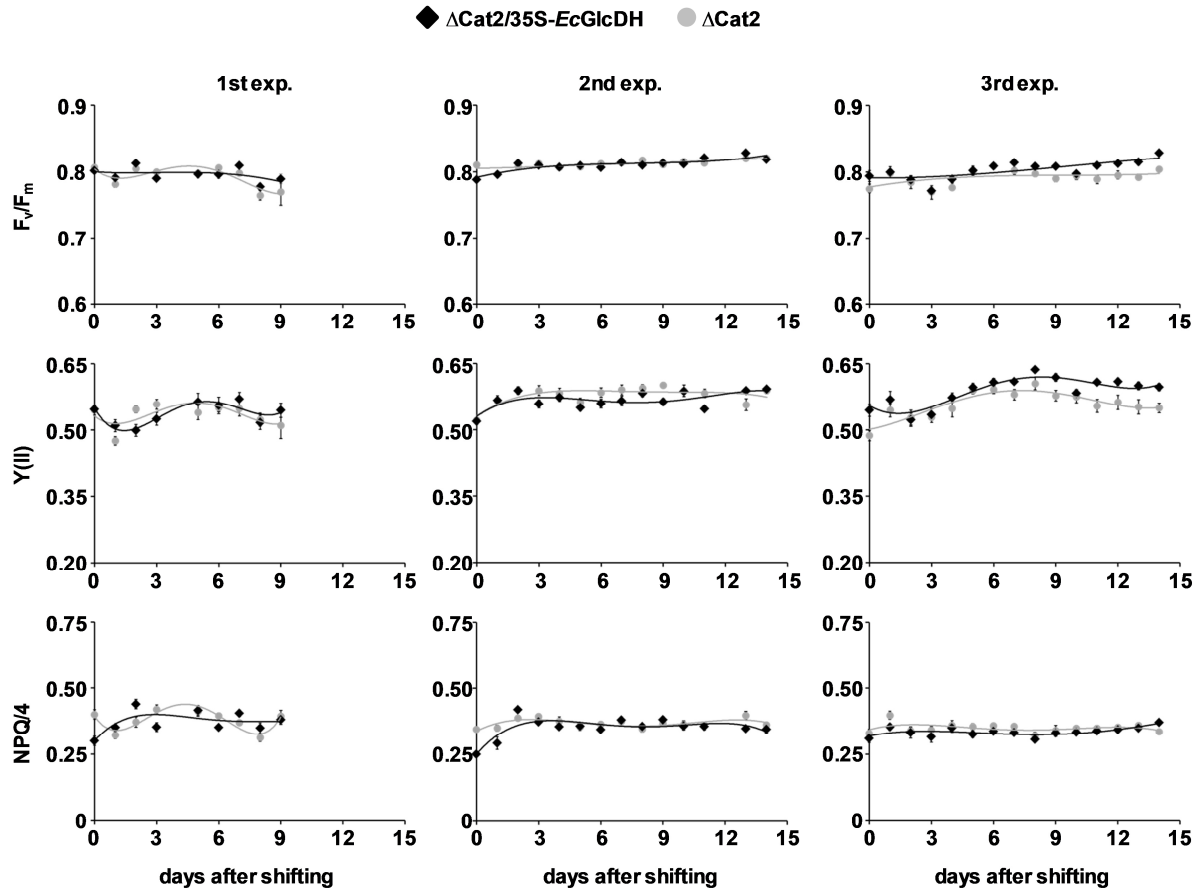


Figure 32: Chlorophyll fluorescence of young of the Δ Cat2 mutant background from the crossing of Δ Cat2 with 35S-*EcGlcDH* during a shift from high CO₂ concentration to low CO₂ concentration. Three weeks old plants were shifted for 14 days from high CO₂ concentration (2000 ppm) to low CO₂ concentrations (150 ppm). Chlorophyll-fluorescence parameters, F_v/F_m (maximal quantum yield), $Y(II)$ (photosynthetic yield) and NPQ (non-photochemical quenching) were recorded every day using Imaging-Pam (2.2.4.2) starting at high CO₂ concentration (0 days after shifting) and ending at 14 days after shifting. The measurement was done for 30 min using a pulse of 20 sec between the saturated light pulses and an actinic light of 120 μ E. Shown are three independent experiments with at least 15 individuals for each genotype. Data points are the means \pm SE.

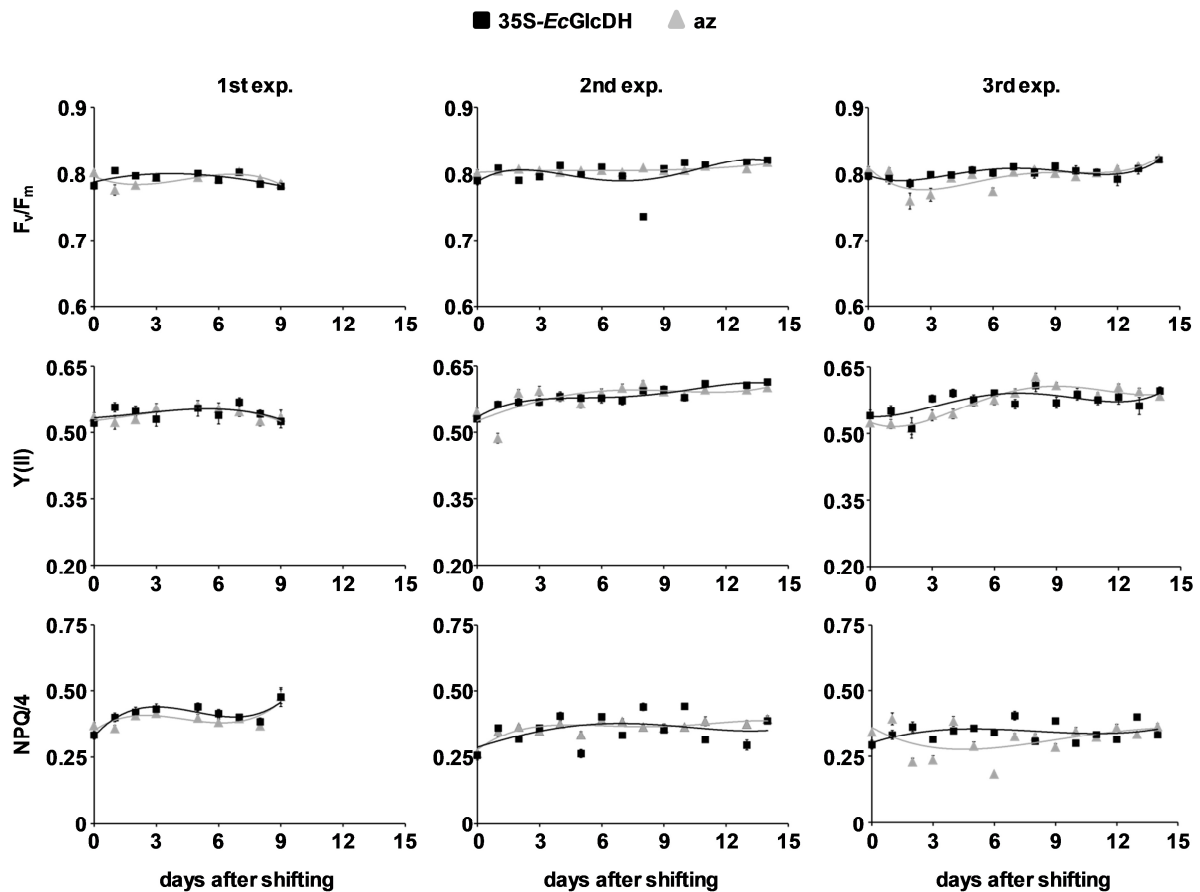


Figure 33: Chlorophyll fluorescence of young of the az background from the crossing of Δ Cat2 with 35S-*EcGlcDH* during a shift from high CO₂ concentration to low CO₂ concentration. Three weeks old plants were shifted for 14 days from high CO₂ concentration (2000 ppm) to low CO₂ concentrations (150 ppm). Chlorophyll-fluorescence parameters, F_v/F_m (maximal quantum yield), $Y(II)$ (photosynthetic yield) and NPQ (non-photochemical quenching) were recorded every day using Imaging-Pam (2.2.4.2) starting at high CO₂ concentration (0 days after shifting) and ending at 14 days after shifting. The measurement was done for 30 min using a pulse of 20 sec between the saturated light pulses and an actinic light of 120 μ E. Shown are three independent experiments with at least 15 individuals for each genotype. Data points are the means \pm SE.

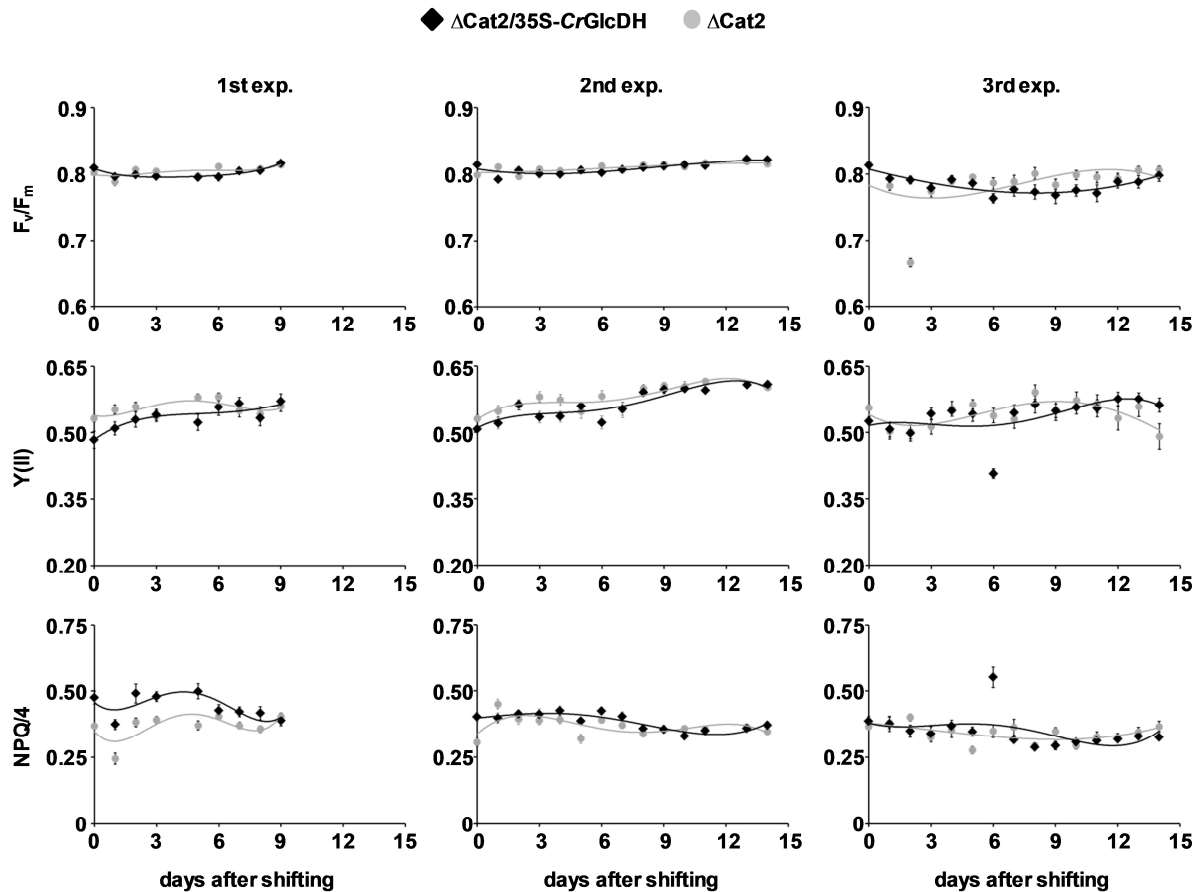


Figure 34: Chlorophyll fluorescence of young of the Δ Cat2 mutant background from the crossing of Δ Cat2 with 35S-CrGlcDH during a shift from high CO₂ concentration to low CO₂ concentration. Three weeks old plants were shifted for 14 days from high CO₂ concentration (2000 ppm) to low CO₂ concentrations (150 ppm). Chlorophyll-fluorescence parameters, F_v/F_m (maximal quantum yield), $Y(II)$ (photosynthetic yield) and NPQ (non-photochemical quenching) were recorded every day using Imaging-Pam (2.2.4.2) starting at high CO₂ concentration (0 days after shifting) and ending at 14 days after shifting. The measurement was done for 30 min using a pulse of 20 sec between the saturated light pulses and an actinic light of 120 μ E. Shown are three independent experiments with at least 15 individuals for each genotype. Data points are the means \pm SE.

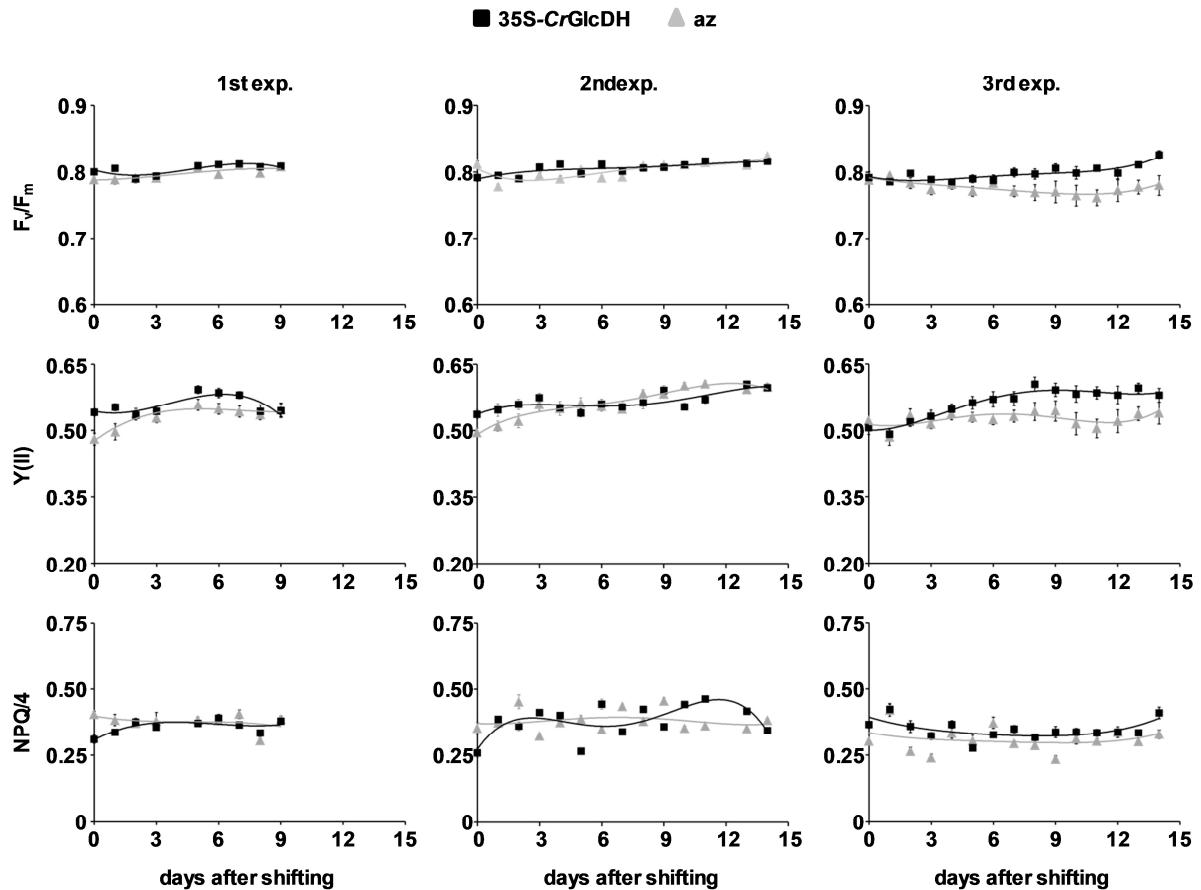


Figure 35: Chlorophyll fluorescence of young of the az background from the crossing of Δ Cat2 with 35S-CrGlcDH during a shift from high CO₂ concentration to low CO₂ concentration. Three weeks old plants were shifted for 14 days from high CO₂ concentration (2000 ppm) to low CO₂ concentrations (150 ppm). Chlorophyll-fluorescence parameters, F_v/F_m (maximal quantum yield), $Y(II)$ (photosynthetic yield) and NPQ (non-photochemical quenching) were recorded every day using Imaging-Pam (2.2.4.2) starting at high CO₂ concentration (0 days after shifting) and ending at 14 days after shifting. The measurement was done for 30 min using a pulse of 20 sec between the saturated light pulses and an actinic light of 120 μ E. Shown are three independent experiments with at least 15 individuals for each genotype. Data points are the means \pm SE.

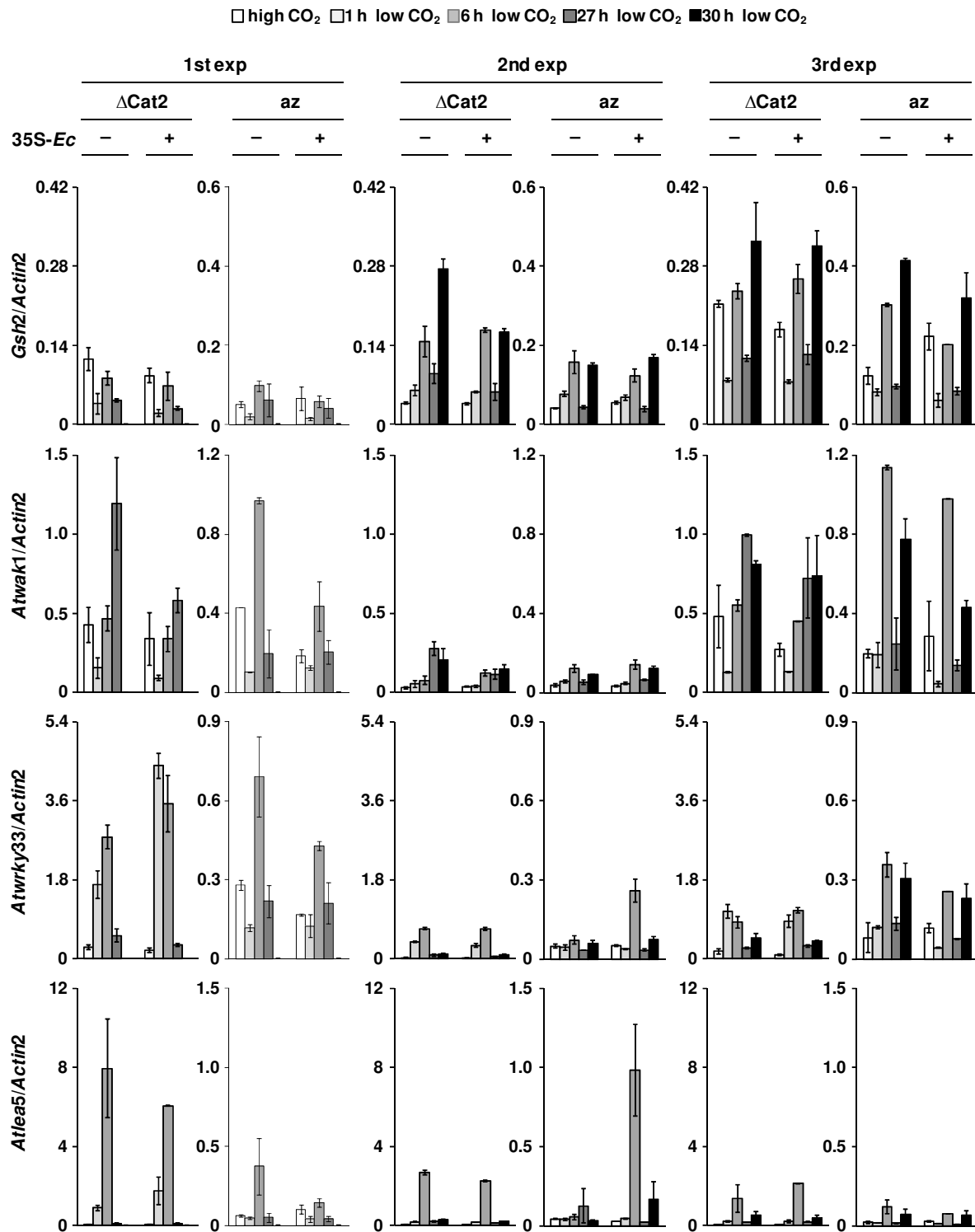


Figure 36: Gene expression of genes involved in response to oxidative stress or pathogen defense in the Δ Cat2 background and azygous background from the crossing of Δ Cat2 with 35S-*Ec*GlcDH at high (0 h) CO₂ conditions and after shifting to low CO₂ concentrations for 1, 6, 27 and 30 h. Plants were grown three weeks at short day conditions (8 h light and 16 h darkness) and high CO₂ (2000 ppm) and were shifted to low CO₂ concentration (150 ppm). Ten plants were harvested for each time point and genotypes were identified via PCR following by pooling twice three plants and cDNA synthesis. This was done for high CO₂ as well as for low CO₂ concentrations. The expression levels were standardized to expression level of *Actin2*. Shown are the means \pm SE from two pools for each experiment. Δ Cat2 represents the Δ Cat2 background and az the azygous background. 35S-*Ec* represents 35S-*Ec*GlcDH, thereby – stands for the absence of 35S-*Ec*GlcDH and + for the presence of 35S-*Ec*GlcDH.

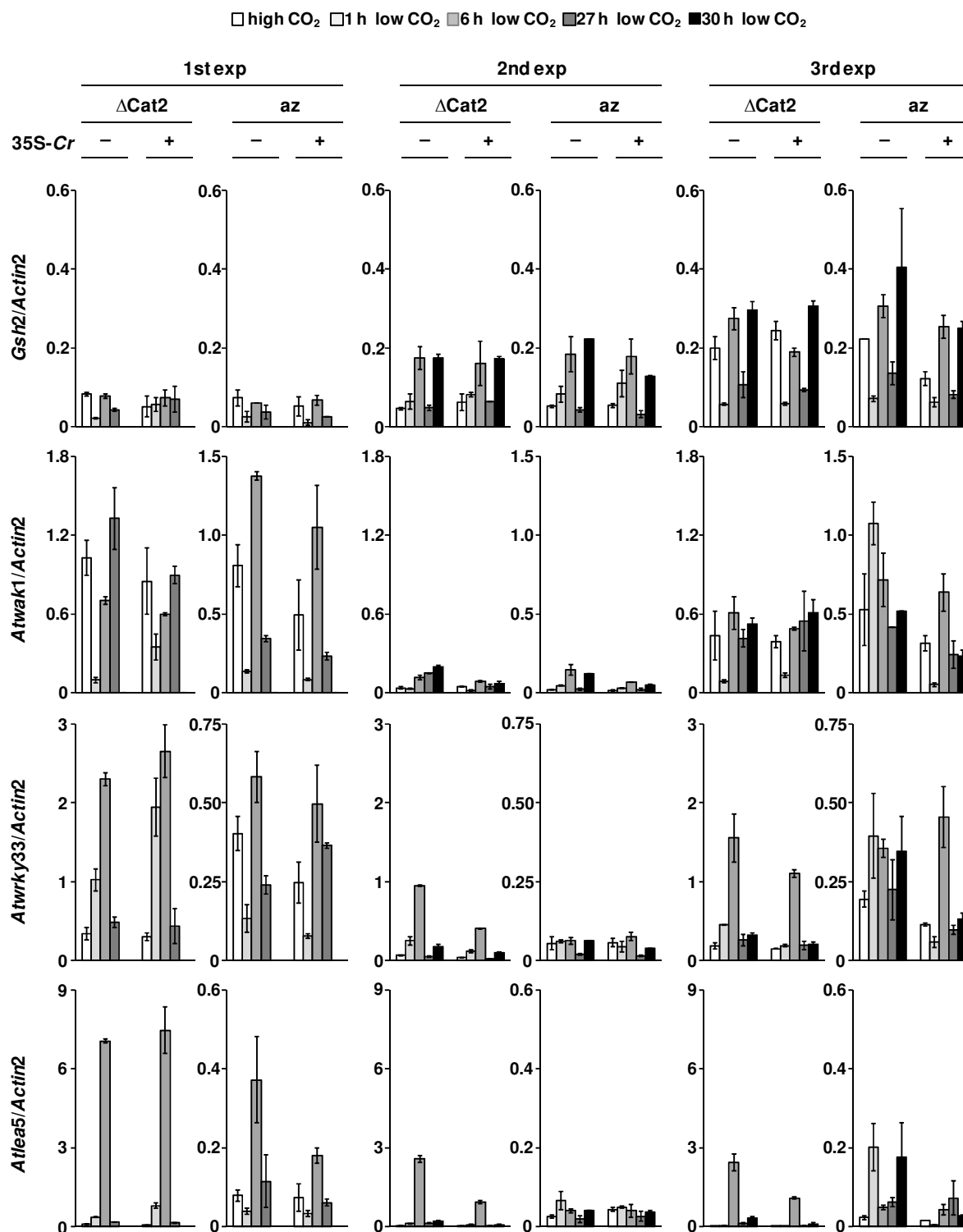


Figure 37: Gene expression of genes involved in response to oxidative stress or pathogen defense in the Δ Cat2 background and azygous background from the crossing of Δ Cat2 with 35S-CrGlcDH at high (0 h) CO₂ conditions and after shifting to low CO₂ concentrations for 1, 6, 27 and 30 h. Plants were grown three weeks at short day conditions (8 h light and 16 h darkness) and high CO₂ (2000 ppm) and were shifted to low CO₂ concentration (150 ppm). Ten plants were harvested for each time point and genotypes were identified via PCR following by pooling twice three plants and cDNA synthesis. This was done for high CO₂ as well as for low CO₂ concentrations. The expression levels were standardized to expression level of *Actin2*. Shown are the means \pm SE from two pools for each experiment. Δ Cat2 represents the Δ Cat2 background and az the azygous background.

6.2 List of figures

Figure 1: Carboxylase- and oxygenase- reaction of RubisCO in green leaves of higher plants, which also contains photorespiration	11
Figure 2: Overview of the major photorespiratory pathway in <i>Arabidopsis thaliana</i>	12
Figure 3: Overview of the major photorespiratory pathway including the known alternative photorespiratory pathways in <i>Arabidopsis thaliana</i>	19
Figure 4: Glycolate metabolism of cyanobacteria including a plant-like glycolate metabolism (outer circle) and a bacterial-like glycolate metabolism (inner circle)	21
Figure 5: The photorespiratory major pathway including transgenic approaches to reduce photorespiration	24
Figure 6: Overview of the glycolate pathway in higher plants up to serine formation in the mitochondria, which includes the unknown chloroplastidal bypass pathway and the known mitochondrial bypass pathway.	26
Figure 7: Markers used throughout this work for gel-electrophoresis.....	30
Figure 8: Structure of pTRAK-AGA6 (A215-142) and pTRAK-AtGDH (A215-182).....	37
Figure 9: Cloning strategy to create an overexpression vector carrying ALAAT1 and AtGlcDH (35S-AlaAT1/35S-AtGlcDH).....	38
Figure 10: „Floral-dip“-transformation of <i>Arabidopsis thaliana</i> plants.	49
Figure 11: Gradient after ultra-centrifugation. Pictured is a 45% percoll gradient after ultra-centrifugation.....	50
Figure 12: Diagram showing the main parts of an ambisexual blossom.....	54
Figure 13: Chlorophyll-fluorescence of photorespiratory mutants and wild type (WT) plants at ambient air conditions (400 ppm CO ₂).....	57
Figure 14: Chlorophyll fluorescence of photorespiratory mutants and WT plants under CO ₂ stress.	58
Figure 15: Relative gene expression of knocked out genes in the mutant background.	59
Figure 16: Chlorophyll-fluorescence of Δ Cat2 and WT plants during a shift from high CO ₂ concentration to ambient CO ₂ concentrations.	61
Figure 17: Gene expression of H ₂ O ₂ -inducible genes in <i>Cat2</i> knock-out mutants (Δ Cat2) and WT plants at high and low CO ₂ concentrations during the day.	62
Figure 18: Chlorophyll fluorescence of old leaves of the Δ Cat2 mutant background from the crossing of Δ Cat2 with 35S- <i>EcGlcDH</i> during a shift from high CO ₂ concentration to low CO ₂ concentration.....	67
Figure 19: Chlorophyll fluorescence of old leaves of the azygous background from the crossing of Δ Cat2 with 35S- <i>EcGlcDH</i> during a shift from high CO ₂ concentration to low CO ₂ concentration.....	68

Figure 20: Chlorophyll fluorescence of old leaves of the Δ Cat2 mutant background from the crossing of Δ Cat2 with 35S- <i>CrGlcDH</i> during a shift from high CO ₂ concentration to low CO ₂ concentration.....	69
Figure 21: Chlorophyll fluorescence of old leaves of the azygous background from the crossing of Δ Cat2 with 35S- <i>CrGlcDH</i> during a shift from high CO ₂ concentration to low CO ₂ concentration.....	70
Figure 22: Harvesting time points during the shifting experiment from high CO ₂ to low CO ₂ concentrations.....	71
Figure 23: Gene expression of H ₂ O ₂ -inducible genes in the Δ Cat2 background and azygous background from the crossing of Δ Cat2 with 35S- <i>EcGlcDH</i> at high (0 h) CO ₂ conditions and after shifting to low CO ₂ concentrations for 1, 6, 27 and 30 h.....	72
Figure 24: Gene expression of H ₂ O ₂ -inducible genes in the Δ Cat2 background and azygous background from the crossing of Δ Cat2 with 35S- <i>CrGlcDH</i> at high (0 h) CO ₂ conditions and after shifting to low CO ₂ concentrations for 1, 6, 27 and 30 h.....	74
Figure 25: Metabolite profiles of Δ Cat2 and az plants were grown for three weeks at high CO ₂ concentrations (2000 ppm) and were then shifted to low CO ₂ (150 ppm) conditions.....	77
Figure 26: Metabolite profiles of the Δ Cat2 background from the crossing of Δ Cat2 with 35S- <i>EcGlcDH</i> and 35S- <i>CrGlcDH</i>	79
Figure 27: Metabolite profiles of the az background from the crossing of Δ Cat2 with 35S- <i>EcGlcDH</i> and 35S- <i>CrGlcDH</i>	81
Figure 28: Identification of the T-DNA insertion and the genomic sequence from the F ₂ generation resulting of the crossing from Δ Cat2 with Δ <i>AtGlcDH</i>	84
Figure 29: Phenotype of the Δ Cat2, Δ <i>AtGlcDH</i> , Δ Cat2/ Δ <i>AtGlcDH</i> and az of the F ₃ generation from the crossing of Δ Cat2 with Δ <i>AtGlcDH</i> mutants	87
Figure 30: ¹⁴ CO ₂ release in transiently transformed tobacco plants over expressing RFP (control), <i>AlaAT1</i> (35S- <i>AlaAT1</i>), <i>AtGlcDH</i> (35S- <i>AtGlcDH</i>) and both in a combination (35S- <i>AlaAT1</i> +35S- <i>AtGlcDH</i>)	88
Figure 31: ¹⁴ CO ₂ release transiently transformed tobacco plant leaves overexpressing a red fluorescent protein (control), <i>AlaAT1</i> in a combination with <i>AtGlcDH</i> (35S- <i>AlaAT1</i> +35S- <i>AtGlcDH</i>) and both overexpressed in one vector (clone I and III) .	89
Figure 32: Chlorophyll fluorescence of young of the Δ Cat2 mutant background from the crossing of Δ Cat2 with 35S- <i>EcGlcDH</i> during a shift from high CO ₂ concentration to low CO ₂ concentration.....	106
Figure 33: Chlorophyll fluorescence of young of the az background from the crossing of Δ Cat2 with 35S- <i>EcGlcDH</i> during a shift from high CO ₂ concentration to low CO ₂ concentration.....	107
Figure 34: Chlorophyll fluorescence of young of the Δ Cat2 mutant background from the crossing of Δ Cat2 with 35S- <i>CrGlcDH</i> during a shift from high CO ₂ concentration to low CO ₂ concentration.....	108

Figure 35: Chlorophyll fluorescence of young of the az background from the crossing of Δ Cat2 with 35S-*CrGlcDH* during a shift from high CO₂ concentration to low CO₂ concentration109

Figure 36: Gene expression of genes involved in response to oxidative stress or pathogen defense in the Δ Cat2 background and azygous background from the crossing of Δ Cat2 with 35S-*EcGlcDH* at high (0 h) CO₂ conditions and after shifting to low CO₂ concentrations for 1, 6, 27 and 30 h.....110

Figure 37: Gene expression of genes involved in response to oxidative stress or pathogen defense in the Δ Cat2 background and azygous background from the crossing of Δ Cat2 with 35S-*CrGlcDH* at high (0 h) CO₂ conditions and after shifting to low CO₂ concentrations for 1, 6, 27 and 30 h.....111

6.3 List of tables

Table 1: Instruments and equipment used throughout this study	27
Table 2: Software and internet-programs used throughout this study.....	29
Table 3: Markers used throughout this study	30
Table 4: Reaction kits used throughout this study	30
Table 5: Enzymes used throughout this study.....	31
Table 6: Specific chemicals used throughout this study	32
Table 7: Material and chemicals for GC-MS analysis used throughout this study.....	32
Table 8: Oligonucleotides used throughout this study	33
Table 9: Medium for <i>E. coli</i> cultivation.....	39
Table 10: Medium for <i>Agrobacterium tumefaciens</i> cultivation	39
Table 11: Medium for plant growth.....	40
Table 12: Buffers and solutions for DNA/RNA isolation.....	41
Table 13: Solutions and buffers needed for agarose gel electrophoresis	42
Table 14: Ligation mixture.....	43
Table 15: Standard PCR mixture	44
Table 16: Standard PCR conditions	44
Table 17: Primer systems for identification of the different genotypes.....	44
Table 18: Multiplex PCR mixture.....	45
Table 19: Digestion of DNA.....	46
Table 20: Reverse transcriptase reaction mix	46
Table 21: Quantitative real-time polymerase chain reaction mix	47
Table 22: Quantitative real-time polymerase chain reaction conditions	47
Table 23: Composition of the 2x infiltration medium.....	48
Table 24: Buffers and solutions needed for mitochondria isolation.....	51
Table 25: Bradford reagent	51
Table 26: Extraction buffer for metabolites.....	53
Table 27: Sorbitol stock solution	53

Table 28: Segregation of the F ₁ and F ₂ generation of crossed Arabidopsis plants	54
Table 29: Overview of the important received genotypes from the crossing of Δ Cat2 and Δ Ggat with 35S- <i>Ec</i> GlcDH and 35S- <i>Cr</i> GlcDH and their intended use.	66
Table 30: Summary of the PCR amplification results of the F ₂ generation from the crossing of Δ Cat2 and Δ AtGlcDH mutants.	83
Table 31: Observed and theoretical segregation rate of the F ₂ generation from the crossing of Δ Cat2 and Δ AtGlcDH.	85
Table 32: The growth phenotypes of three weeks old plantlets are shown below, using the stage-based phenotypic analysis of Boyes.....	86
Table 33: Results of the identification of the T ₁ generation.....	89

6.4 List of abbreviations

Abbreviation	full form
^1O	Singlet oxygen
2-PG	2-phosphoglycolate
3-PGA	3-phosphoglycerate
%	Percent
Acetyl-CoA	Acetyl-coenzyme A
ADP	Adenosine diphosphate
Amp	Ampecillin
AlaAT	Alanine aminotransferase
<i>A. thaliana</i>	<i>Arabidopsis thaliana</i>
AtGlcDH	<i>Arabidopsis thaliana</i> glycolate dehydrogenase
ATP	Adenosine triphosphate
<i>A. tumefaciens</i>	<i>Agrobacterium tumefaciens</i>
<i>Atlea5</i>	<i>A. thaliana</i> late embryogenesis-associated protein 5
<i>Atwak1</i>	<i>A. thaliana</i> wall-associated kinase 1
<i>Atwrky33</i>	<i>A. thaliana</i> wrky transcription factor 33
<i>Apx1</i>	Ascorbate peroxidase 1
bla	b-lactamase gene for selection in bacteria (ampicillin/carbenicillin resistance)
bp	Base pairs
BSA	Bovine serum albumin
°C	Degree Celcius
C ₂ -Cycle	Photorespiratory cycle (2 Carbon cycle)
C ₃ -cycle	Benson calvin cycle (3 Carbon cycle)
CAT	Catalase
Carb	Carbenicillin
cDNA	Complementary deoxyribonucleotide acid
<i>C. r.</i>	<i>Chlamydomonas reinhardtii</i>
<i>CrGlcDH</i>	<i>Chlamydomonas reinhardtii</i> glycolate dehydrogenase
CO ₂	Corbon dioxide
Cpm	Counts per minute
D-LDH	D(+)-lactate dehydrogenase
DMSO	Dimethyl sulfoxide
DNA	Deoxyribonucleotide acid
dNTP	Deoxyribonucleoside triphosphate

DTT	Dithiothreitol
<i>E. c.</i>	<i>Escherichia coli</i>
<i>EcGlcDH</i>	<i>E. coli</i> glycolate dehydrogenase
EDTA	Ethylendiaminetetraacetic acid
Fd	Ferredoxin
Fd-GOGAT	ferredoxin-dependent glutamine:oxoglutarate aminotransferase
F_v/F_m	Maximum quantum efficiency of PSII photochemistry
g	Gramm
G3P	Glyceraldehyde-3-phosphate
GCL	Glyoxylate carboxyligase
GC/MS	Gas Chromatography/Mass Spectrometry
GDC	Glycine decarboxylase
GDC/SHMT	Glycine decarboxylase/serine hydroxymethyl transferase
GGAT	Glutamate:glyoxylate aminotransferase
GK	Glycerate kinase
GlcDH	Glycolate dehydrogenase
Gly	Glycine
GLYK	Glycerate kinase
GOGAT	Glutamine:2-oxoglutarate aminotransferase
GOX	Glycolate oxidase
<i>Gpx6</i>	Glutathione peroxidase 6
GS	Glutamine synthetase
GR	Glycolate reductase
<i>GstF8</i>	Glutathione-S-trans 8
h	Hour
HEPES	N-2-hydroxyethylpiperazine-N'-2-ethanesulfonic acid
HPR	Hydroxypyruvate reductase
H ₂ O	Water
H ₂ O ₂	Hydrogen peroxide
Kan	Kanamycin
kb	Kilobase pair
LB medium	Luria Bertani medium
mg	Milli gramm
min	Minute
ml	Milli liter
mM	Milli mol
M-MLV-RT	Reverse transcriptase (from Moloney Murine Leukemia virus)

mRNA	Messenger RNA
MS medium	Murashige and Skoog Basal medium
NADPH	Nicotinamide adenine dinucleotide phosphate (reduced)
MSTFA	N-Methyl-N-trimethylsilyltrifluoroacetamide
NCBI	National center for biotechnology information
NBT	Nitrotetrazolium blue chloride
NPQ	Non-photochemical quenching
O ₂	Molecular oxygen
O ₂ ⁻	Superoxide
OD	Optical density
Oxi1	Threonine/serine kinase 1
p35SS/pA35S	Promoter (duplication) and Polyadenylation-/Termination sequence from CaMV
PAnos	Polyadenylation promoter of Nopaline synthetase gene from <i>A. tumefaciens</i>
PCR	Polymerase- Chain- reaction
PCR-cycle	Photosynthetic carbon reduction cycle
PG	Phosphoglycolate
PGA	Phosphoglycerate
PGP	Phosphoglycolate phosphatase
PiB	Postillumination burst
PMS	Phenazine methosulfate
Pnos	Promoter of Nopaline synthase gene from <i>A. tumefaciens</i>
Ppm	Parts per minute
PS	Photosystem
PSI	Photosystem I
PSII	Photosystem II
PYR	Pyruvate
qPCR	Quantitative Real-time PCR
Rif	Rifampicin
RNA	Ribonucleic acid
ROS	Reactive oxygen species
rpm	Rotation per minute
RT	Room temperature
RT	Reverse Transcriptase
RT-PCR	Reverse transcriptase-polymerase chain reaction
RubisCO	Ribulose-1,5-bisphosphate carboxylase/oxygenase

RuBP	Ribulose 1, 5 bisphosphate
SAR	Scaffold Attachment Region from the tobacco RB7 gene (giU67919)
SE	Standard error
sec	Second
Ser	Serine
SGAT	Serine:glutamate aminotransferase
SHMT	Serine hydroxymethyl transferase
sul	The coding sequence, which confers resistance to sulfadiazine
TAE	Tris-Acetate-EDTA-buffer
Tris	Tris-Acetate-EDTA-buffer
TSR	Tatronate semialdehyde reductase
u	Unit
UV	Ultra violet
vol	Volume
v/v	Volume/volume
w/v	Weight/volume
x	Times
xg	Apparent gravity
Y(II)	Photosynthetic yield
µg	Micro gramm
µM	Micro mol
µl	Micro liter

6.5 References

- Ainsworth E. A., Davey P. A., Bernacchi C. J., Dermody O. C., Heaton E. A., Moore D. J., Morgan P. B., Naidu S. L., Yoo Ra H.-S., Zhu X.-G., Curtis P. S., and Long S. P.** (2002). A meta-analysis of elevated [CO₂] effects on soybean (glycine max) physiology, growth and yield. *Global Change Biology*, 8 (8): 695–709.
- Allan W. L., Clark S. M., Hoover G. J., and Shelp B. J.** (2009). Role of plant glyoxylate reductases during stress: a hypothesis. *Biochem. J.*, 423 (1): 15–22.
- Andersson, I.** (2007). Catalysis and regulation in Rubisco. *Journal of Experimental Botany*, 59 (7): 1555–1568.
- Asada, K.** (2006). Production and scavenging of reactive Oxygen species in chloroplasts and their functions. *Plant Physiol.*, 141 (2): 391-396.
- Baker N. R.** (2008). Chlorophyll fluorescence: a probe of photosynthesis in vivo. *Annu. Rev. Plant Biol.*, 59 (1): 89–113.
- Bari R., KebeishR., Rainer Kalamajka R., Rademacher T., and Peterhänsel C.** (2004). A glycolate dehydrogenase in the mitochondria of *Arabidopsis thaliana*. *J. Exp. Bot.*, 55 (397): 623-630.
- Bauwe, H., Hagemann, M., and Fernie, A. R.** (2010). Photorespiration: Players, partners and origin. *Trends in Plant Science*, 15 (6): 330–336.
- Betsche T.** (1983). Aminotransfer from alanine and glutamate to glycine and serine during photorespiration in oat leaves. *Plant Physiol.*, 71 (4): 961–965.
- Blume, C.** (2013) Glycolate and glyoxylate metabolism in higher plants: How natural and artificial pathways contribute to plant metabolism. Dissertation. Gottfried Wilhelm Leibniz University of Hannover.
- Björkman O., and Demmig B.** (1987). Photon yield of O₂ evolution and chlorophyll fluorescence characteristics at 77 K among vascular plants of diverse origins. *Planta*, 170 (4): 489-504.
- Boldt, R.** (2005). D-glycerate 3-kinase, the last unknown enzyme in the photorespiratory cycle in *Arabidopsis*, belongs to a novel kinase family. *The Plant Cell Online*, 17 (8): 2413–2420.

- Boyes D. C., Zayed A. M., Ascenzi R., McCaskill A. J., Hoffman N. E., Davis K. R., and Gorlach J.** (2001). Growth stage-based phenotypic analysis of *Arabidopsis*: a model for high throughput functional genomics in plants. *Plant Cell*, 13 (7): 1499–1510.
- Bradford M. M.** (1976). A rapid and sensitive method for the quantitation of microgram quantities of protein utilizing the principle of protein-dye binding. *Anal Biochem.*, 72 (1-2): 248–254.
- Brooks A. and Farquhar G. D.** (1985). Effect of temperature on the CO₂/O₂ specificity of ribulose-1,5-bisphosphate carboxylase/oxygenase and the rate of respiration in the light: Estimates from gas-exchange measurements on spinach. *Planta*, 165 (3): 397–406.
- Carvalho, J. D. F. C., Madgwick, P. J., Powers, S. J., Keys, A. J., Lea, P. J., and Parry, M. A. J.** (2011). An engineered pathway for glyoxylate metabolism in tobacco plants aimed to avoid the release of ammonia in photorespiration. *BMC Biotechnol.*, 11 (1): 111-117.
- Caverzan A., Passaia G., Rosa S. B., Ribeiro C. W., Lazzarotto F., and Margis-Pinheiro M.** (2012). Plant responses to stresses: Role of ascorbate peroxidase in the antioxidant protection. *Genetics and Molecular Biology*, 35 (4): 1011–1019.
- Chang C. C., Slesak I., Jorda L., Sotnikov A., Melzer M., Miszalski Z., Mullineaux P. M., Parker J. E., Karpinska B., and Karpinski S.** (2009). *Arabidopsis* chloroplastic glutathione peroxidases play a role in cross talk between photooxidative stress and immune responses. *Plant Physiol.*, 150 (2): 670–683.
- Chang Y.-Y., Wang A.-Y., and Cronan J. E. JR.** (1993). Molecular cloning, DNA sequencing, and biochemical analyses of *Escherichia coli* glyoxylate carboligase: AN Enzyme of the acetohydroxy acid synthase-pyruvate oxidase family. *The Journal of Biological Chemistry*, 268 (6): 3911–3919.
- Chauvin L., Tural B., and Moroney J. V.** (2008). *Chlamydomonas reinhardtii* has genes for both glycolate oxidase and glycolate dehydrogenase. Springer; Photosynthesis. Energy from the Sun: 14th International Congress on Photosynthesis: 823–827.
- Chen W. and Singh K. B.** (1999). The auxin, hydrogen peroxide and salicylic acid induced expression of the *Arabidopsis* GST6 promoter is mediated in part by an ocs element. *The Plant Journal*, 19 (6): 667–677.

- Chen W., Chao G., and Singh K. B.** (1996). The promoter of a H₂O₂-inducible, *Arabidopsis* glutathione S-transferase gene contains closely linked OBF- and OBP1-binding sites. *The Plant Journal*, 10 (6): 955–966.
- Cheng K. H., and Colman B.** (1974). Measurements of photorespiration in some microscopic algae. *Planta*, 115 (3): 207-212.
- Chevalier D., Yamaguchi J., and McCourt P.** (1992). Nucleotide sequence of a cDNA for catalase from *Arabidopsis thaliana*. *Plant Physiol.*, 99 (4): 1726-1728.
- Clough S. J. and Bent A. F.** (1998). Floral dip: a simplified method for *Agrobacterium*-mediated transformation of *Arabidopsis thaliana*. *Plant J.*, 16 (6): 735-743
- Cuk K., Gogala M., Tkalec M., Vidakovic-Cifrek Z.** (2010). Transgenerational stress memory in *Arabidopsis thaliana* (L.) Heynh.: antioxidative enzymes and HSP70. *Acta Bot. Croat.*, 69 (2): 183-197.
- Dalal M., Tayal D., Chinnusamy V., and Bansal K. C.** (2009). Abiotic stress and ABA-inducible Group 4 LEA from *Brassica napus* plays a key role in salt and drought tolerance. *Journal of Biotechnology*, 139 (2): 137–145.
- Davletova S., Rizhsky L., Liang H., Shengqiang Z., Oliver D. J., Coutu J., Shulaev V., Schlauch K., and Mittler R.** (2005). Cytosolic ascorbate peroxidase 1 is a central component of the reactive oxygen gene network of *Arabidopsis*. *The Plant Cell Online*, 17 (1): 268–281.
- Dayer R., Fischer B. B., Eggen R. I. L., and Lemaire S. D.** (2008). The peroxiredoxin and glutathione peroxidase families in *Chlamydomonas reinhardtii*. *Genetics*, 179 (1): 41–57.
- Debolt S., Melino V., and Ford C. M.** (2007). Ascorbate as a biosynthetic precursor in plants. *Annals of Botany*, 99 (1): 3–8.
- Dixon D. P. and Edwards R.** (2010). *The Arabidopsis book: Glutathione transferases.*
- Duysens, L. N. M., Amesz, J., and Kamp, B. M.** (1961). Two photochemical systems in photosynthesis. *Nature*, 190 (4775): 510–511.
- Eisenhut M., Ruth W., Haimovich M., Bauwe H., Kaplan A., and Hagemann M.** (2006). The plant-like C₂ glycolate cycle and the bacterial-like glycerate pathway cooperate in phosphoglycolate metabolism in *Cyanobacteria*. *Plant Physiol.*, 142 (1): 333–342.

- Ellis, R.J.** (1979). The most abundant protein in the world. *Trends in Biochemical Sciences*, 4 (11): 241–244.
- Engel N., Ewald, R., Gupta K. J., Zrenner R., Hagemann M., and Bauwe H.** (2011). The presequence of Arabidopsis serine hydroxymethyltransferase SHM2 selectively prevents import into mesophyll mitochondria. *Plant Physiol.*, 157 (4): 1711–1720.
- Engel N., van den Daele K., Kolukisaoglu U., Morgenthal K., Weckwerth W., Parnik T., Keerberg O., and Bauwe H.** (2007). Deletion of glycine decarboxylase in *Arabidopsis* is lethal under nonphotorespiratory conditions. *Plant Physiol.*, 144 (3): 1328–1335.
- Epron D., Dreyer E., and Bréda N.** (1992). Photosynthesis of oak trees [*Quercus petraea* (Matt.) Liebl.] during drought under field conditions: Diurnal course of net CO₂ assimilation and photochemical efficiency of photosystem II. *Plant, Cell & Environment*, 15 (7): 809–820.
- Euglem T., Rushton P. J., Robatzek S., and Somssich I. E.** (2000). The WRKY superfamily of plant transcription factors. *Trends in Plant Science*, 5 (5): 199–206.
- Fahnenstich H., Flügge U.-I., and Maurino V. G.** (2008). *Arabidopsis thaliana* overexpressing glycolate oxidase in chloroplasts: H₂O₂-induced changes in primary metabolic pathways. *Plant Signaling & Behavior*, 3 (12): 1122–1125.
- Fahnenstich H., Scarpeci T. E., Valle E. M., Flügge U.-I., and Maurino V. G.** (2008). Generation of hydrogen peroxide in chloroplasts of *Arabidopsis* overexpressing glycolate oxidase as an inducible system to study oxidative stress. *Plant Physiol.*, 148 (2): 719–729.
- Fischer B. B., Dayer R., Schwarzenbach Y., Lemaire S. D., Behra R., Liedtke A., and Eggen R. I. L.** (2009). Function and regulation of the glutathione peroxidase homologous gene GPXH/GPX5 in *Chlamydomonas reinhardtii*. *Plant Mol. Biol.*, 71 (6): 569–583.
- Foyer C. H., Bloom A. J., Queval G., and Noctor G.** (2009). Photorespiratory metabolism: genes, mutants, energetics, and redox signaling. *Annu. Rev. Plant Biol.*, 60 (1): 455–484.
- Foyer C. H., Neukermans J., Queval G., Noctor G., and Harbinson J.** (2012). Photosynthetic control of electron transport and the regulation of gene expression. *Journal of Experimental Botany*, 63 (4): 1637–1661.
- Foyer C. H., and Noctor G.** (2000). Oxygen processing in photosynthesis regulation and signaling. *New Phytologist*, 146 (3): 359–388.

- Foyer C. H., and Noctor G.** (2005). Oxidant and antioxidant signaling in plants: a re-evaluation of the concept of oxidative stress in a physiological context. *Plant, Cell & Environment*, 28 (8): 1056–1071.
- Foyer C. H., Souriau N., Lelandais M., Kunert K. J., Pruvost C., and Jouanin L.** (1995). Overexpression of glutathione reductase but not glutathione synthetase leads to increases in antioxidant capacity and resistance to photoinhibition in poplar trees. *Plant Physiol.*, 109 (3): 1047–1057.
- Frugoli J. A., Zhong H. H., Nuccio M. L., McCourt P., McPeck M. A., Thomas T. L., and McClung C. R.** (1996). Catalase is encoded by a multigene family in *Arabidopsis thaliana* (L.) Heynh. *Plant Physiol.*, 112 (1): 327–336.
- Furuya A. and Hayashi J. A.** (1962). Glycolic acid oxidation by *Escherichia coli* adapted to glycolate. *J. Bacteriol.*, 85 (5): 1124–1131.
- Gamon J. A., and Pearcy R. W.** (1989). Leaf movement, stress avoidance and photosynthesis in *Vitis californica*. *Oecologia*, 79 (4): 475-481.
- Giuliano G., Hoffman N. E., Ko K., Scolnik P. A., and Cashmore A. R.** (1988). A light-entrained circadian clock controls transcription of several plant genes. *The EMBO Journal*, 7 (12): 3635–3642.
- Gleason C., Huang S., Thatcher L. F., Foley R. C., Anderson C. R., Carroll A. J., Millar A. H., and Singh K. B.** (2011). Mitochondrial complex II has a key role in mitochondrial-derived reactive oxygen species influence on plant stress gene regulation and defense. *Proceedings of the National Academy of Sciences*, 108 (26): 10768–10773.
- Gotto A. M. and Kornberg H. I.** (1961). The metabolism of C₂ compounds in microorganisms. Preparation and properties of crystalline tartronic semialdehyde reductase. *Biochem. J.*, 81 (2): 273–284.
- Goyal A. and Tolbert N. E.** (1996). Association of glycolate oxidation with photosynthetic electron transport in plant and algal chloroplasts. *Proc. Natl. Acad. Sci. U.S.A.*, 93 (8): 3319–3324.
- Griffin J. J., Ranney T. G., and Pharr D. M.** (2004). Photosynthesis, chlorophyll fluorescence, and carbohydrate content of *Illicium* taxa grown under varied irradiance. *J. AMER. SOC. HORT. SCI.*, 129 (1): 46–53.

- Guan L., Polidoros A. N., and Scandalios J. G.** (1996). Isolation, characterization and expression of the maize Cat2 catalase gene. *Plant Mol. Biol.*, 30 (5): 913-924.
- Hansen R. W. and Hayashi J. A.** (1962). Glycolate metabolism in *Escherichia coli*. *J. Bacteriol.*, 83 (3): 679–687.
- Harbinson J., Genty B. and Baker N. R.** (1989). Relationship between the quantum efficiencies of photosystem I and II in pea leaves. *Plant Physiol.*, 90 (3): 1029–1034.
- Havir E. A.** (1986). Inactivation of serine:glyoxylate and glutamate:glyoxylate aminotransferases from tobacco leaves by glyoxylate in the presence of ammonium ion. *Plant Physiol.*, 80 (2): 473-478.
- Heber U., Bligny R., Streb P., and Douce R.** (1996). Photorespiration is essential for the protection of the photosynthetic apparatus of C₃ plants against photoinactivation under sunlight. *Bot. Acta*, 109 (1): 307–315.
- Hipkins M. F., & Baker N. R.** (1986). Photosynthesis, energy transduction: A practical approach. IRL Press; Book, Edited (ISBN 0947946632).
- Igarashi D., Miwa T., Seki M., Kobayashi M., Kato T., Tabata S., Shinozaki K. and Ohsumi C.** (2003). Identification of photorespiratory glutamate:glyoxylate aminotransferase (GGAT) gene in *Arabidopsis*. *Plant J.*, 33 (6): 975-987
- Igarashi D., Tsuchida H., Miyao M., and Ohsumi C.** (2006). Glutamate:Glyoxylate aminotransferase modulates amino acid content during photorespiration. *Plant Physiol.*, 142 (3): 901–910.
- Jordan, D., and Ogren, W.** (1984). The CO₂/O₂ specificity of ribulose 1,5-bisphosphate carboxylase/oxygenase. *Planta*, 161 (4): 308-313.
- Kang K.-S., Lim C.-J., Han T.-J., Kim J.-C., and Jin C.-D.** (1998). Activation of ascorbate-glutathione cycle in *Arabidopsis* leaves in response to aminotriazole. *J. Plant Biol.*, 41 (3): 155–161.
- Karpinski S., Escobar C., Karpinska B., Creissen G., and Mullineaux P. M.** (1997). Photosynthetic electron transport regulates the expression of cytosolic ascorbate peroxidase genes in *Arabidopsis* during excess light stress. *Plant Cell*, 9 (4): 627-640.

- Kebeish R., Niessen M., Thiruveedhi K., Bari R., Hirsch H.-J., Rosenkranz R., Stähler N., Schönfeld B., Kreuzaler F., and Peterhänsel, C.** (2007). Chloroplastic photorespiratory bypass increases photosynthesis and biomass production in *Arabidopsis thaliana*. *Nat Biotechnol*, 25 (5): 593–599.
- Kendall A. C., Keys A. J., Turner J. C., Lea P. J., Mifflin B. J.** (1983). The isolation and characterisation of a catalase-deficient mutant in barley. *Planta*, 159 (6): 505–511.
- Keys A. J.** (2006). The re-assimilation of ammonia produced by photorespiration and the nitrogen economy of C₃ higher plants. *Photosynthesis Research*, 87 (2): 165–175.
- Keys A. J., Bird I. F., Cornelius M. J., Lea P. J., Wallsgrave R. M. & Milfin B. J.** (1978). Photorespiratory nitrogen cycle. *Nature Biotechnology*, 275 (1): 471–743.
- Kisaki T., and Tolbert N. E.** (1969). Glycolate and glyoxylate metabolism by isolated peroxisomes or chloroplasts. *Plant Physiol.*, 44 (2): 242–250.
- Koncz C. and Schell J.** (1986). The promotor of TL-DNA gene 5 controls the tissue-specific expression of chimaeric genes carried by a novel type of *Agrobacterium* binary vector. *Mol Gen Genet.*, 204 (3): 383-396.
- Kozaki A. and Takeba G. O.** (1996). Photorespiration protects C₃ plants from photooxidation. *Nature*, 384 (6609): 557-560.
- Ku M. S., Kano-Murakami Y., and Matsuoka M.** (1996). Evolution and expression of C₄ photosynthesis genes. *Plant Physiol.*, 111 (4): 949–957.
- Kun E** (1952). A study on the metabolism of glyoxal in vitro. *J. Biol. Chem.*, 194 (2): 603–611.
- Kun E., Dechary J. M., Pitot H. C.** (1954). The oxidation of glycolic acid by a liver enzyme. *J. Biol. Chem.*, 210 (1): 269–280.
- Laing W. A., Ogren W. L., Hageman R. H.** (1974). Regulation of soybean net photosynthetic CO₂ fixation by the interaction of CO₂, O₂ and ribulose 1, 5-diphosphate carboxylase. *Plant Physiol.*, 54 (5): 678–685.
- Lawlor D. W.** (2001). *Photosynthesis: 3rd edition*. BIOS scientific published Ltd.
- Lee C. P., Eubel H., O'Tool, N., and Millar A. H.** (2008). Heterogeneity of the mitochondrial proteome for photosynthetic and non-photosynthetic *Arabidopsis* metabolism. *Mol Cell Proteomics*, 7 (7): 1297–1316.

- Leegood R. C., Lea P. J., Adcock M.D., and Häusler R.E.** (1995). The regulation and control of photorespiration. *Journal of Experimental Botany*, 46 (special issue): 1397-1414.
- Liepman A. H. and Olsen L. J.** (2001). Peroxisomal alanine:glyoxylate aminotransferase (AGT1) is a photorespiratory enzyme with multiple substrates in *Arabidopsis thaliana*. *Plant J.*, 25 (5): 487-498.
- Liepman A. H. and Olsen L. J.** (2003). Alanine aminotransferase homologs catalyze the glutamate:glyoxylate aminotransferase reaction in peroxisomes of *Arabidopsis*. *Plant Physiol.*, 131 (1): 215–227.
- Lippok B., Birkenbihl R. P., Rivory G., Brummer J., Schmelzer E., Logemann E., and Somssich I. E.** (2007). Expression of AtWRKY33 encoding a pathogen- or PAMP-responsive WRKY transcription factor is regulated by a composite DNA motif containing W box elements. *Mol Plant Microbe Interact.*, 20 (4): 420–429.
- Lord J. M.** (1972). Glycolate oxidoreductase in *Escherichia coli*. *Biochemica et Biophysica Acta*, 267 (2): 227–237.
- Luhua S., Ciftci-Yilmaz S., Harper J., Cushman J., and Mittler R.** (2008). Enhanced tolerance to oxidative stress in transgenic *Arabidopsis* plants expressing proteins of unknown function. *Plant Physiol.*, 148 (1): 280–292.
- Maier A., Fahnenstich H., Caemmerer S. von, Engqvist M. K. M., Weber A. P. M., Flügge U.-I., and Maurino, V. G.** (2012). Transgenic introduction of a glycolate oxidative cycle into *A. thaliana* chloroplasts leads to growth improvement. *Front. Plant Sci.*, 3 (38): 1-12
- Maxwell K. and Johnson G. N.** (2000). Chlorophyll fluorescence- a practical guide. *Journal of Experimental Botany*, 51 (345): 659–668.
- McClung C. R.** (1997). Regulation of catalases in *Arabidopsis*. *Free Radical Biology & Medicine* Vol., 23 (3): 489-496.
- McElrone A. J., Hamilton J. G., Krafnick A. J., Aldea M., Knepp R. G., and DeLucia E. H.** (2010). Combined effects of elevated CO₂ and natural climatic variation on leaf spot diseases of redbud and sweetgum trees. *Environmental Pollution*, 158 (1): 108–114.

- Meier S., Ruzvidzo O., Morse M., Donaldson L., Kwezi L., Gehring C., and Newbiggin E.** (2010). The *Arabidopsis* aall associated linase-like 10 gene encodes a functional guanylyl cyclase and is co-expressed with pathogen defense related genes. PLoS ONE, 5 (1): e8904.
- Mhamdi A., Queval G., Chaouch S., Vanderauwera S., van Breusegem F., and Noctor G.** (2010). Catalase function in plants: a focus on *Arabidopsis* mutants as stress-mimic models. Journal of Experimental Botany, 61 (15): 4197–4220.
- Milla M. A. R., Maurer A., Rodriguez Huete A., and Gustafson J. P.** (2003). Glutathione peroxidase genes in *Arabidopsis* are ubiquitous and regulated by abiotic stresses through diverse signaling pathways. The Plant Journal, 36 (5): 602–615.
- Miller G., Suzuki N., Rizhsky L., Hegie A., Koussevitzky S., and Mittler R.** (2007). Double mutants deficient in cytosolic and thylakoid ascorbate peroxidase reveal a complex mode of interaction between reactive oxygen species, plant development, and response to abiotic stresses. Plant Physiol., 144 (4): 1777–1785.
- Mittler R., Vanderauwera S., Gollery M., and van Breusegem F.** (2004). Reactive oxygen gene network of plants. Trends in Plant Science, 9 (10): 490–498.
- Murray A. J., Blackwell R. D., and Lea P. J.** (1989). Metabolism of hydroxypyruvate in a mutant of barley lacking NADH-dependent hydroxypyruvate reductase, an important photorespiratory enzyme activity. Plant Physiol., 91 (1): 395–400.
- Nakamura Y. and Tolbert N. E.** (1983). Serine:glyoxylate, alanine:glyoxylate, and glutamate:glyoxylate aminotransferase reactions in peroxisomes from spinach leaves. J. Biol. Chem., 258 (12): 7631-7638.
- Nakamura Y., Kanakagiri S., Van K., He W., and Spalding M. H.** (2005). Distribution of the glycolate dehydrogenase gene in the high-CO₂-requiring mutant HCR89 of *Chlamydomonas reinhardtii*. Can. J. Bot., 83 (7): 820–833.
- Nelson E. B. and Tolbert N. E.** (1970). Glycolate dehydrogenase in green algae. Archives of Biochemistry and Biophysics, 141 (1): 102–110.
- Niessen M.** (2008). Photorespiration in *Arabidopsis thaliana*: Natürliche Evolution und gentechnologische Modifikation. Dissertation. RWTH Aachen University.

- Niessen M., Krause K., Horst I., Staebler N., Klaus S., Gaertner S., Kebeish R., Araujo W. L., Fernie A. R., and Peterhänsel C.** (2012). Two alanine aminotranferases link mitochondrial glycolate oxidation to the major photorespiratory pathway in *Arabidopsis* and rice. *Journal of Experimental Botany*, 63 (7): 2705–2716.
- Niessen M., Thiruveedhi K., Rosenkranz R., Kebeish R., Hirsch H.-J., Kreuzaler F., and Peterhansel C.** (2007). Mitochondrial glycolate oxidation contributes to photorespiration in higher plants. *Journal of Experimental Botany*, 58 (10): 2709–2715.
- Noctor G., and Foyer C.H.** (1998). Ascorbate and glutathione: Keeping active oxygen under control. *Annu. Rev. Plant Physiol. Plant Mol. Biol.*, 49 (1): 249–279.
- Noctor G., Queval G., Mhamdi A., Chaouch S., and Foyer C. H.** (2011). The *Arabidopsis* book: Glutathione.
- Novitskaya L., Trevanion S. J., Driscoll S., Foyer C. H., & Noctor G.** (2002). How does photorespiration modulate leaf amino acid contents? A dual approach through modelling and metabolite analysis. *Plant, Cell & Environment*, 25 (7): 821–835.
- Oliver D. J.** (1981). Role of glycine and glyoxylate decarboxylation in photorespiratory CO₂ release. *Plant Physiol.*, 68 (5): 1031–1034.
- Oliver D. J.** (1979). Mechanism of decarboxylation of glycine and glycolate by isolated soybean cells. *Plant Physiol.*, 64 (6): 1048–1052.
- Orendi G., Zimmermann P., Baar C., Zentgraf U.** (2001). Loss of stress-induced expression of catalase3 during leaf senescence in *Arabidopsis thaliana* is restricted to oxidative stress. *Plant Science*, 161 (2): 301–314.
- Panchuk I. I., Volkov R. A., and Schöffl F.** (2002). Heat stress- and heat shock transcription factor-dependent expression and activity of ascorbate peroxidase in *Arabidopsis*. *Plant Physiol.*, 129 (2): 838–853.
- Papageorgiou G. C., and Govindjee (Eds)** (2005). Chlorophyll a fluorescence a signature of photosynthesis. Series: Advances in Photosynthesis and Respiration. 19. Springer ISBN 978-1-4020-3218-9.
- Pellicer M.-T., Badia J., Aquilar J., Baldomà L.** (1996). Glc locus of *Escherichia coli*: Characterization of genes encoding the subunits of glycolate oxidase and the glc regulator protein. *Journal of Bacteriology*, 178 (7): 2051–2059.

- Peterhänsel C., Blume C. and Offermann S.** (2012). Photorespiratory bypasses: how can they work?: Opinion paper. *Journal of Experimental Botany*, 63 (2): 695–709.
- Peterhänsel C., Horst I., Niessen M., Blume C., Kebeish R., Kürkcüoglu S., Kreuzaler F.** (2010). *The Arabidopsis book: Photorespiration*.
- Peterhänsel C., Krause K., Braun H.-P., Espie G.S., Fernie A.R., Hanson D.T., Keech O., Maurino V.G., Mielewczik M., and Sage R.F.** (2012). Engineering photorespiration: current state and future possibilities. *Plant Biol J*, 15 (4): 754-758.
- Petersen L. N., Ingle R. A., Knight M. R., and Denby K. J.** (2009). OX11 protein kinase is required for plant immunity against *Pseudomonas syringae* in *Arabidopsis*. *Journal of Experimental Botany*, 60 (13): 3727–3735.
- Pignocchi C., Fletscher J. M., Wilkinson J. E., Barnes J. D., and Foyer C. H.** (2003). The function of ascorbate oxidase in tobacco. *Plant Physiol.*, 132 (3): 1631–1641.
- Polodoros A. N. and Scandalios J. G.** (1997). Response of the maize catalases to light. *Free Radical Biology & Medicine*, 23 (3): 497-504.
- Portis A. R. J., Salvucci M. E. and Ogren W. L.** (1986). Activation of ribulosebisphosphate carboxylase/oxygenase at physiological CO₂ and ribulosebisphosphate concentrations by rubisco activase. *Plant Physiol.*, 82 (4): 967–971.
- Prabhu V., Chatson K. B., Abrams G. D., and King J.** (1996). ¹³C nuclear magnetic resonance detection of interactions of serine hydroxymethyltransferase with C₁ - tetrahydrofolate synthase and glycine decarboxylase complex activities in *Arabidopsis*. *Plant Physiol.*, 112 (1): 207–216.
- Qin Y.-M., Hu C.-H. and Zhu Y.-Z.** (2008). The ascorbate peroxidase regulated by H₂O₂ and ethylene is involved in cotton fiber cell elongation by modulating ROS homeostasis. *Plant Signal Behav.*, 3 (3): 194-196.
- Queval, G., Issakidis-Bourguet, E., Hoerberichts, F.A., Vandorpe, M., Gakière, B., Vanacker, H., Miginiac-Maslow, M., van Breusegem, F., and Noctor, G.** (2007). Conditional oxidative stress responses in the *Arabidopsis* photorespiratory mutant *cat2* demonstrate that redox state is a key modulator of daylength-dependent gene expression, and define photoperiod as a crucial factor in the regulation of H₂O₂-induced cell death. *The Plant Journal*, 52 (4): 640–657.

- Queval, G., Neukermans J., Vanderauwera S., van Breusegem F., and Noctor G.** (2012). Day length is a key regulator of transcriptomic responses to both CO₂ and H₂O₂ in *Arabidopsis*. *Plant, Cell & Environment*, 35 (2): 374–387.
- Raines, C.A.** (2011). Increasing photosynthetic carbon assimilation in C₃ plants to improve crop yield: Current and future strategies. *Plant Physiol.*, 155 (1): 136-142.
- Raines, C.A.** (2006). Transgenic approaches to manipulate the environmental responses of the C₃ carbon fixation cycle. *Plant, Cell and Environment*, 29 (3): 331-339.
- Raven, J.A.** (2013). Rubisco: still the most abundant protein of Earth? *New Phytol*, 198 (1): 1–3.
- Rehfeld D. W. and Tolbert N. E.** (1972). Aminotransferases in peroxisomes from spinach leaves. *J. Biol. Chem.*, 247 (15): 4803–4811.
- Rentel M. C., Lecourieux D., Ouaked F., Usher S. L., Petersen L., Okamoto H., Knight H., Peck S. C., Grierson C. S., Hirt H., and Knight M.R.** (2004). OXI1 kinase is necessary for oxidative burst-mediated signalling in *Arabidopsis*. *Nature*, 427 (6977): 858–861.
- Ricoult C., Cliquet J.-B., and Limami A. M.** (2005). Stimulation of alanine aminotransferase (AlaAT) gene expression and alanine accumulation in embryo axis of the model legume *Medicago truncatula* contribute to anoxia stress tolerance. *Physiologia Plantarum*, 123 (1): 30–39.
- Ritchie G. A.** (2006). Chlorophyll fluorescence: What is it and what do the numbers mean? USDA Forest Service Proceedings, P-RMRS-043: 34–43.
- Rossel J.B., Wilson I. W., and Pogson B. J.** (2002). Global changes in gene Expression in response to high light in *Arabidopsis*. *Plant Physiol.*, 130 (3): 1109–1120.
- Saiki R. K., Gelfand D. H., Stoffel S., Scharf S. J., Higuchi R., Horn G. T., Mullis K. B., and Erlich H. A.** (1988). Primer-directed enzymatic amplification of DNA with a thermostable DNA polymerase. *Science*, 239 (4839): 487–491.
- Salleh F. M., Evans K., Goodall B., Machin H., Mowla S. B., Mur L. A. J., Runions J., Theodoulou F. L., Foyer C .H., and Rogers H. J.** (2012). A novel function for a redox-related LEA protein (SAG21/AtLEA5) in root development and biotic stress responses. *Plant, Cell & Environment*, 35 (2): 418–429.

- Salvucci M., and Ogren W.** (1996). The mechanism of rubisco activase: Insights from studies of the properties and structure of the enzyme. *Photosynth Res*, 47 (1): 1-11..
- Sappl P. G., Carroll A. J., Clifton R., Lister R., Whelan J., Harvey Millar A., and Singh K. B.** (2009). The *Arabidopsis* glutathione transferase gene family displays complex stress regulation and co-silencing multiple genes results in altered metabolic sensitivity to oxidative stress. *The Plant Journal*, 58 (1): 53–68.
- Scandalios J. G., Guan L. and Polidoros A. N.** (1997). Catalases in plants: Gene structure, properties, regulation, and expression. *Oxidative Stress and the Molecular Biology of Antioxidant Defenses*. Cold Spring Harbor Laboratory Press: 343-406. ISBN 0-87969-502-1/97.
- Schwarte S., and Bauwe H.** (2007). Identification of the photorespiratory 2-phosphoglycolate phosphatase, PGLP1, in *Arabidopsis*. *Plant Physiol.*, 144 (3): 1580–1586.
- Sharkey T. D.** (2001). Photorespiration. (In Photorespiration, Thomas D Sharkey, ed (John Wiley & Sons, Ltd). *Encyclopedia of Life Sciences*: 1-5.
- Sharkey T. D.** (1988). Estimating the rate of photorespiration in leaves. *Physiologia Plantarum*, 73 (1): 174-152.
- Soitamo A. J., Piippo M., Allahverdiyeva Y., Battchikova N., and Aro E.-M.** (2008). Light has a specific role in modulating *Arabidopsis* gene expression at low temperature. *BMC Plant Biol*, 8 (1): 13.
- Sommerville C. R.** (2001). An early *Arabidopsis* demonstration. Resolving a few issues concerning photorespiration. *Plant Physiol.*, 125 (1): 20–24.
- Sommerville C. R. & Ogren W. L.** (1979). A phosphoglycolate phosphatase-deficient mutant of *Arabidopsis*. *Nature*, 280 (5725): 833–836.
- Sommerville C. R. and Ogren W. L.** (1980a). Inhibition of photosynthesis in *Arabidopsis* mutants lacking leaf glutamate synthase activity. *Nature*, 286: 257-259.
- Sommerville C. R. and Ogren W. L.** (1980b). Photorespiration mutants of *Arabidopsis thaliana* deficient in serine-glyoxylate aminotransferase activity. *Proc Natl Acad Sci U S A.*, 77 (5): 2684–2687.

- Sommerville C. R. and Ogren W. L.** (1981). Photorespiration-deficient mutants of *Arabidopsis thaliana* lacking mitochondrial serine transhydroxymethylase activity. *Plant Physiol.*, 67 (4): 666-671.
- Sparkes I. A., Runions J., Kearns A., and Hawes C.** (2006). Rapid, transient expression of fluorescent fusion proteins in tobacco plants and generation of stably transformed plants. *Nat Protoc*, 1 (4): 2019–2025.
- Stabenau H. and Winkler U.** (2005). Glycolate metabolism in green algae. *Physiologia Plantarum*, 123 (3): 235–245
- Stitt M., Muller C., Matt P., Gibon Y., Carillo P., Morcuende R., Scheible W.-R., and Krapp A.** (2002). Steps towards an integrated view of nitrogen metabolism. *J Exp Bot*, 53 (370): 959–970.
- Storozhenko S., De Pauw P., Van Montagu M., Inzé D. and Kushnir S.** (1998). The heat-shock element is a functional component of the *Arabidopsis* APX1 gene promoter. *Plant Physiol.*, 118 (3): 1005-1014.
- Thatcher L.F., Carrie C., Andersson C. R., Sivasithamparam K., Whelan J., and Singh K. B.** (2007). Differential gene expression and subcellular targeting of *Arabidopsis* glutathione S-transferase F8 is achieved through alternative transcription start sites. *Journal of Biological Chemistry*, 282 (39): 28915–28928.
- Timm S., and Bauwe H.** (2013). The variety of photorespiratory phenotypes - employing the current status for future research directions on photorespiration. *Plant Biol (Stuttg)*, 15 (4): 737–747.
- Timm S., Florian A., Jahnke K., Nunes-Nesi A., Fernie A.R., and Bauwe H.** (2011). The hydroxypyruvate-reducing system in *Arabidopsis*: Multiple enzymes for the same end. *Plant Physiol.*, 155 (2): 694–705.
- Timm S., Florian A., Wittmiß M., Jahnke K., Hageman M., Fernie A.R., and Bauwe H.** (2013). Serine acts as a metabolic signal for the transcriptional control of photorespiration-related genes in *Arabidopsis*. *Plant Physiol.*, 162 (1): 379–389.
- Timm S., Mielewczik M., Florian A., Frankenbach S., Dreissen A., Hocken N., Fernie A.R., Walter A., Bauwe H., and Yang H.** (2012). High-to-low CO₂ acclimation reveals plasticity of the photorespiratory pathway and indicates regulatory links to cellular metabolism of *Arabidopsis*. *PLoS ONE*, 7 (8): 1-15

- Timm S., Nunes-Nesi A., Parnik T., Morgenthal K., Wienkoop S., Keerberg O., Weckwerth W., Kleczkowski L.A., Fernie A.R., and Bauwe H.** (2008). A cytosolic pathway for the conversion of hydroxypyruvate to glycerate during photorespiration in *Arabidopsis*. *The Plant Cell Online*, 20 (10): 2848–2859
- Tolbert N. E.** (1981). Metabolic pathways in peroxisomes and glyoxysomes. *Ann. Rev. Biochem.*, 50 (1): 133-157.
- Tolbert N. E., Clagett C.O., and Burris R.H.** (1949). Products of the oxidation of glycolic acid and L-lactic acid by enzymes from tobacco leaves. *J. Biol. Chem.*, 181 (2): 905–914.
- Tolbert N. E., Oeser A., Kisaki T., Hageman R. H., Yamazaki R. K.** (1968). Peroxisomes from spinach leaves containing enzymes related to glycolate metabolism. *The Journal of Biological Chemistry*, 243 (19): 5179–5184.
- Tural B., and Moroney J.V.** (2005). Regulation of the expression of photorespiratory genes in *Chlamydomonas reinhardtii*. *Canadian Journal of Botany*, 83 (7): 810–819.
- Vandenabeele S., Vanderauwera S., Vuylsteke M., Rombauts S., Langebartels C., Seidlitz H. K., Zabeau M., Van Montagu M., Inzé D., and Van Breusegem F.** (2004). Catalase deficiency drastically affects gene expression induced by high light in *Arabidopsis thaliana*. *The Plant Journal*, 39 (1): 45–58.
- Vanderauwera S., Zimmermann P., Rombauts S., Vandenabeele S., Langebartels C., Gruissem W., Inzé D., and Van Breusegem F.** (2005). Genome-wide analysis of hydrogen peroxide-regulated gene expression in *Arabidopsis* reveals a high light-induced transcriptional cluster involved in anthocyanin biosynthesis. *Plant Physiol.*, 139 (2): 806–821.
- Verica, J.A.** (2002). The cell wall-associated kinase (WAK) and WAK-like kinase gene family. *Plant Physiol.*, 129 (2): 455–459.
- Verica, J.A.** (2003). Tissue-specific and developmentally regulated expression of a cluster of tandemly arrayed cell wall-associated kinase-like kinase genes in *Arabidopsis*. *Plant Physiol.*, 133 (4): 1732–1746.
- Wang Z. Y., and Portis A. R.** (1992). Dissociation of ribulose-1,5-bisphosphate bound to ribulose-1,5-bisphosphate carboxylase/oxygenase and its enhancement by ribulose-1,5-bisphosphate carboxylase/oxygenase activase-mediated hydrolysis of ATP. *Plant Physiol.*, 99 (4): 1348–1353.

- Wingler A., Lea P.J., Quick W.P., and Leegood R.C.** (2000). Photorespiration: metabolic pathways and their role in stress protection. *Philosophical Transactions of the Royal Society B: Biological Sciences*, 355 (1402): 1517–1529.
- Wingler A., Quick W. P., Bungard R. A., Bailey K. J., Lea P. J. & Leegood R. C.** (1999). The role of photorespiration during drought stress: an analysis utilizing barley mutants with reduced activities of photorespiratory enzymes. *Plant, Cell and Environment*, 22 (4): 361-373.
- Woo N. S., Badger M. R., and Pogson B. J.** (2008). A rapid, non-invasive procedure for quantitative assessment of drought survival using chlorophyll fluorescence. *Plant Methods*, 4 (1): 27.
- Yoshimura K., Yabuta Y., Ishikawa T., and Shigeoka S.** (2000). Expression of spinach ascorbate peroxidase isoenzymes in response to oxidative stresses. *Plant Physiol.*, 123 (1): 223-234.
- Yu C., Liang Z., Huang A. H.** (1984). Glyoxylate transamination in intact leaf peroxisomes. *Plant Physiol.*, 75 (1): 7-12.
- Zelitch I. and Day P. R.** (1973). The effect on net photosynthesis of pedigree selection for low and high rates of photorespiration in tobacco. *Plant Physiol.*, 52 (1): 33–37.
- Zhang Z., Zhang Q., Wu J., Zheng X., Zheng S., Sun X., Qiu Q., and Lu T.** (2013). Gene knockout study reveals that cytosolic ascorbate peroxidase 2(OsAPX2) plays a critical role in growth and reproduction in rice under drought, salt and cold stresses. *PLoS ONE*, 8 (2): e57472.
- Zhao P., Liu F., Ma M., Gong J., Wang Q., Jia P., Zheng G., and Liu H.** (2011). Overexpression of AtLEA3-3 confers resistance to cold stress in *Escherichia coli* and provides enhanced osmotic stress tolerance and ABA sensitivity in *Arabidopsis thaliana*. *Mol Biol*, 45 (5): 785–796.
- Zhong H. H., McClung C.R.** (1996). The circadian clock gates expression of two *Arabidopsis* catalase genes to distinct and opposite circadian phases. *Mol Gen Genet*, 251 (2): 196–203.
- Zhong H. H., Young J. C., Pease E. A., Hangarter R. P., and McClung C. R.** (1994). Interactions between light and the circadian clock in the regulation of CAT2 expression in *Arabidopsis*. *Plant Physiol.*, 104 (3): 889–898.

Zelitch, I. (1972). The photooxidation of glyoxylate by envelope-free spinach chloroplasts and its relation to photorespiration. *Arch Biochem Biophys*, 150 (2): 698–70.

Zimmermann P., Heinlein C., Orendi G., and Zentgraf U. (2006). Senescence-specific regulation of catalases in *Arabidopsis thaliana* (L.) Heynh. *Plant Cell Environ*, 29 (6): 1049–1060.

6.6 Lebenslauf

Persönliche Daten	
Name	Katrin Krause
Geburtstag	24.02.1984
Geburtsort	Rostock
Familienstand	ledig
Hochschulausbildung	
seit 12 / 2009	Wissenschaftliche Angestellte am Institut für Botanik der Leibniz Universität Hannover
10 / 2008 - 09 / 2009	Diplomarbeit am Institut für Biochemie der Universität Rostock
07 / 2003 - 09 / 2009	Studium Diplom-Biologie an der Universität Rostock
Schulbildung	
1994 - 2003	Gymnasium "Große Stadt Schule" Rostock
1990 - 1994	Grundschule "Warnowschule" Rostock

6.7 Publikationen

Niessen M., Krause K., Horst I., Staebler N., Klaus S., Gaertner S., Kebeish R., Araujo W. L., Fernie A. R., and Peterhänsel C. (2012). Two alanine aminotransferases link mitochondrial glycolate oxidation to the major photorespiratory pathway in *Arabidopsis* and rice. *Journal of Experimental Botany* 63 (7): 2705–2716.

Peterhänsel C., Krause K., Braun H.-P., Espie G.S., Fernie A.R., Hanson D.T., Keech O., Maurino V.G., Mielewczik M., and Sage R.F. (2012). Engineering photorespiration: current state and future possibilities. *Plant Biol J* (15): 754-758.

6.9 Eidstattliche Erklärung

Hiermit erkläre ich, Katrin Krause, dass ich meine Dissertation mit den Titel „The functional significance of alternative photorespiratory pathways in Arabidopsis thaliana“ selbstständig verfasst, die benutzen Hilfsmittel und Quellen sowie gegebenenfalls die zu Hilfeleistung herangezogenen Institutionen vollständig angegeben habe. Diese Dissertation wurde nicht schon als Masterarbeit, Diplomarbeit oder andere Prüfungsarbeit verwendet.

Hannover, den

Katrin Krause

Danksagung

Zunächst möchte ich Prof. Dr. Christoph Peterhänsel dafür danken, dass ich meine Doktorarbeit an seinem Institut anfertigen konnte. Auch bedanke ich mich bei ihm für das Korrekturlesen der Arbeit und seiner Geduld mit mir.

Herrn Prof. Dr. Huchzermeyer möchte ich dafür danken, dass er mein Koreferat angenommen hat und auch immer für ein Gespräch zu Verfügung stand.

Prof. Dr. Hans-Peter Braun, danke ich für die Übernahme des Prüfungsvorsitzes.

Der AG Peterhänsel, AG Huchzermeyer und AG Offermann danke ich für die nette Arbeitsatmosphäre und auch für die „Mädels“-Abende, die wir zu spät eingeführt haben und einfach zu selten gemacht haben. Danke, dass ihr meine Launen im Labor ausgehalten habt und für die Aufmunterungen, wenn es mal nicht voran ging.

Meinem „Büro“ danke ich für die anregenden Diskussionen und die netten Gespräche, die gegenseitige Aufmunterungen, wenn alles schief ging und man nur noch schwarz gesehen hat. Ihr habt immer ein offenes Ohr gehabt, danke dafür.

Meiner Familie danke ich, dass sie mich in die „weite Welt“ hinaus gelassen haben um meinen eigenen Weg zu finden. Und dennoch war ich nie allein, da sie mir immer zur Seite standen, mir Mut gegeben haben, wenn ich ihn verloren hatte, und immer ein offenes Ohr hatten, wenn ich von Heimweh geplagt war oder die Hoffnung auf Ergebnisse verloren habe.

Danke für alles.